Development of Optical Synthesizers

Dissertation

zur Erlangung des akademischen Grades
doctor rerum naturalium (Dr. rer. nat.),

an der Universität Konstanz
Fachbereich Physik

vorgelegt von

Ulrich Strößner

Tag der mündlichen Prüfung: 14. November 2001

Referent: Prof. Dr. J. Mlynek
Referent: Prof. S. Schiller, Ph.D.

Für Klaus

Deutschsprachige Zusammenfassung

Eine der Erfindungen der letzten Jahrzehnte, die die Wissenschaft am meisten vorangebracht hat, ist der Laser. Seine Anwendungen reichen von der Materialbearbeitung in Industrie und Medizin über breitbandige Telekommunikation bis hin zum Test fundamentaler Gesetze der Physik, um nur ein paar Beispiele zu nennen. Weitere wichtige Schritte waren die Entwicklung schmalbandiger Festkörperlaser, der Femtosekunden-Ti:Sapphir-Laser, der Erbiumdotierte Faserverstärker und der Frequenzkammgenerator, die jeweils völlig neue Forschungsgebiet eröffneten. Doch auch heute noch leiden viele Anwendungen darunter, daß nur bestimmte Teile des optischen Spektrums durch schmalbandige Festkörperlaser abgedeckt werden.

Wir wollen die begrenzte Verfügbarkeit von Wellenlängen durch die Entwicklung eines **Optischen Synthesizers** überwinden. Das ist eine Laserquelle, die das gesamte optische Spektrum überdeckt und alle Eigenschaften aufweist, die man optimalerweise von einem Festkörperlaser erwartet: Hohe Ausgangsleistung, beugungsbegrenzte Strahlqualität, sehr schmale Linienbreite, hohe Frequenzstabilität und einfache und zuverlässige Handhabung.

Um dieses Ziel zu erreichen, haben wir einen einfach resonanten **optisch parametrischen Oszillator (OPO)** aufgebaut. Er besteht aus einem Ringresonator in Bow-Tie-Konfiguration. Wir erreichen eine weite Abstimmbarkeit durch die Verwendung von perodisch gepolten Multigitterkristallen von zwei verschiedenen Materialklassen, die wir durch Kooperationen mit der Universität Kaiserslautern (PPLN) und der Tel Aviv University (PPKTP) erhalten. Ein Etalon regelt die Signalwellenlänge und zwei Piezos die Resonatorlänge. Ein kommerzieller 532 nm Laser (Coherent Verdi) pumpt den OPO im einfachen Durchgang. Um den Emissionsbereich in den roten bis grünen Spektralbereich zu erweitern, verdoppeln wir die Idlerstrahlung effizient in einem externen Resonator mit breitbandiger Phasenanpassung.

Das OPO-System weist einen Emissionsbereich vom Grünen bis ins Mittlere Infrarot (550 – 2830 nm, fast 2,5 Oktaven des optischen Spektrums) auf. Das ist, soweit uns bekannt ist, der weiteste Emissionsbereich, der bislang von einer single-frequency Laserquelle erreicht wurde.

Das System hat eine Ausgangsleistung von typischerweise 30 – 500 mW über den größten Teil des Emissionsbereiches, eine nahezu beugungsbegrenzte Strahlqualität und exzellente spektrale Eigenschaften: Es läuft mehrere Stunden lang ohne Modensprünge und mit einer hohen absoluten Frequenzstabilität mit einer Drift von weniger als 50 MHz pro Stunde. Die Linienbreite beträgt 20 kHz, eine der schmalsten Linienbreiten, die jemals an einem OPO gemessen wurden. Eine neue Eigenschaft ist ein weiter kontinuierlicher Abstimmbereich von bis zu 38 GHz ($>1\,\mathrm{cm}^{-1}$) ohne daß dazu die Pumpe abgestimmt werden müßte.

Somit ist dieser OPO eine universelle Lichtquelle für ein weites Spektrum von Anwendungen wie hochauflösende Spektroskopie, Präzionsmeßtechnik, Laserfallen, Laserkühlen, Charakterisierung optischer Komponenten und vielem anderen. Um seine Leistungsfähigkeit, Flexibilität und Zuverlässigkeit zu demonstrieren, wurde damit das Doppler-freie Hyperfeinspektrum von molekularem Jod im Gelben Spektralbereich gemessen, einem Bereich, der bislang mit Farbstofflasern erzeugt werden mußte.

Als Vorarbeiten zu diesem OPO-System bauten wir zwei weitere single-frequency OPOs, die, als sie entwickelt wurden, einen erheblichen Fortschritt in der wissenschaftlichen Forschung darstellten sowie eine Reihe von schmalbandigen Hochleistungs-Pumplasern im Grünen und Infraroten.

Zum erstenmal sind cw OPOs im kurzwelligen Bereich für Anwendungen geeignet, die hohe Anforderungen an die spektralen Eigenschaften der Laserquelle stellen. Mit dieser Arbeit haben wir kurzwellige OPOs so weit entwickelt, daß sie den Übergang von den Forschungslabors zu Anwendungen sowie der Möglichkeit der kommerziellen Nutzung machen können.

Contents

If you want to build a ship, don't drum up the men to gather wood, divide the work and give orders.
Instead, teach them to yearn for the vast and endless sea.

A. de Saint-Exupery

Chapter 1

Introduction

The laser is one of the inventions that brought science very much ahead in the last decades. Its has various applications ranging from industrial and medical material treatment to high bandwidth telecommunication to testing of fundamental laws of physics to mention only a few. For example, it increased the resolution of spectroscopy by many orders of magnitude within a few years.

Further important steps were the development of reliable diode-pumped narrow-linewidth solid state lasers which allowed for ultra-high resolution spectroscopy, the femtosecond Ti:sapphire laser, opening the door to ultra short time physics, the erbium-doped fiber amplifier which was the key to repeater-less long haul optical telecommunication, and the frequency comb generator which made simple absolute optical frequency measurement possible.

But today still only parts of the optical spectrum are covered by narrow linewidth solid state lasers such as the Ti:sapphire laser, the second harmonic of the Ti:sapphire and external cavity diode lasers. The region from 475 to 630 nm must be reached with dye lasers, which are difficult to operate single-frequency with a narrow linewidth and frequency stable. In the infrared region beyond 1.6 μm, only discrete wavelengths can be obtained from solid state and gas lasers.

Many applications suffer from the limited availability of wavelengths. For example, the well-known methane frequency standard at 3.39 μm is based on the accidental coincidence of a methane absorption line with the emission wavelength of the He-Ne laser. The rest of the methane spectrum has not been measured with high resolution due to the lack of a narrow linewidth laser source. The same holds true for the infrared spectrum of any molecule. Also it is very demanding to realize a Bose-Einstein-condensate with sodium, which is otherwise an ideal candidate for condensation, because there are no diode lasers available at the yellow Na D-lines at 589 nm, so that dye lasers have to be used. For specific applications in the UV and IR spectral region people make do with sum or difference frequency generation of diode or solid state lasers.

We want to overcome the limitations in the choice of wavelength by developing what we call an **optical synthesizer**. That is, a continuous-wave laser source with complete spectral coverage and having all properties that can be expected from a solid state laser: high output power, diffraction limited beam quality, narrow linewidth, and high frequency stability. Furthermore, it should be reliable and sufficiently easy to operate, so that it can be used for scientific as well as industrial applications.

One promising approach towards this goal is frequency down conversion using an **optical parametric oscillator (OPO)**. In recent years the increased availability of novel nonlinear materials and high-power solid-state single frequency pump sources has enabled enormous advances in the development of cw OPOs. For emission wavelengths between 1.5 and 4 μm such devices are now relatively mature [1, 2, 3, 4, 5] and are starting to become commercially available. Single-frequency operation without mode-hops, a very wide emission range and first spectroscopic experiments have been reported [6, 7, 8, 9].

In order to reach shorter wavelengths, first developments of single-frequency cw OPOs pumped by visible radiation have been initiated [10, 11, 12, 13]. Early developments used birefringently phasematched crystals [14, 15, 16, 17, 18]. Batchko et al. first used a periodically poled crystal (PPLN) in a 532 nm pumped cw OPO emitting over 917 – 1267 nm [19]. Neither device had stable single-frequency operation, which is crucial for many applications. A stable, widely tunable single-frequency cw OPO pumped in the visible and emitting in the near-IR has not yet been demonstrated except for those presented in this thesis.

Our approach is shown in fig. 1.1. We use a commercial, fixed-frequency narrow-

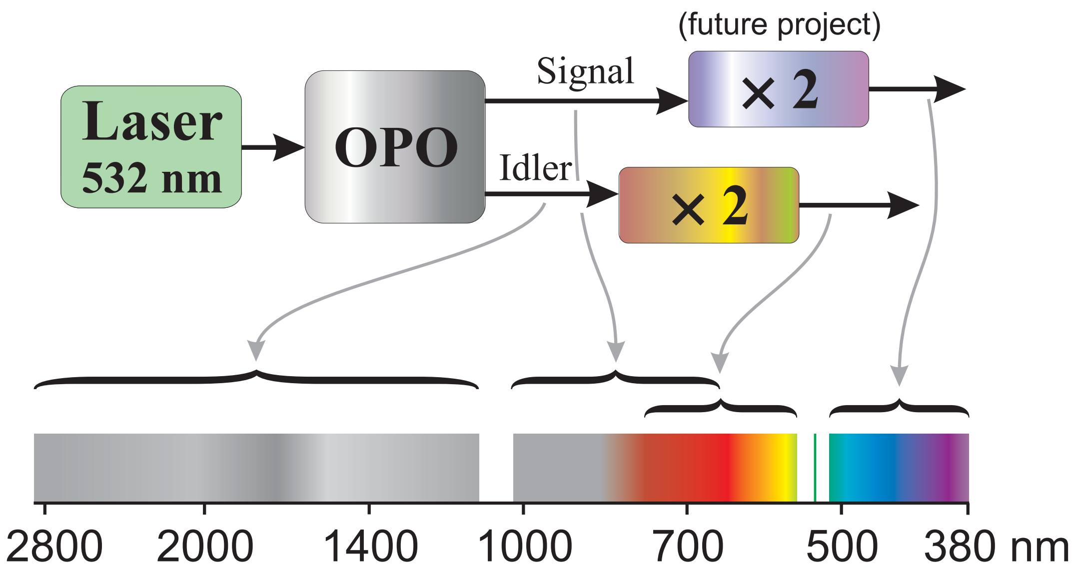

Figure 1.1: Concept of the tunable light source.

linewidth solid-state laser to pump a widely tunable OPO. It emits a signal ranging from the red to the near IR and an idler from the near to the mid IR. To extend the emission range further into the visible we frequency double the idler to generate red, orange, yellow and green. One could also frequency double the signal (this will be a future project for us) to generate green, blue, purple and near UV.

In this thesis we present a cw OPO system according to this concept with an exceptionally large emission range from 550 to 2830 nm, which to our knowledge is the largest emission range of any single-frequency source so far. In addition, it exhibits a high output power and excellent spectral properties: ultra-narrow linewidth, high absolute frequency stability, and large continuous tuning range.

As prior work to this project we developed two more single frequency OPOs which have been a significant step in scientific research at the time they were developed. They also allowed us to gain experience about optic parametric oscillation as well as different nonlinear materials and resonator configurations. Additionally we developed a series of high-power narrow-linewidth pump lasers in the visible and infrared as pump sources for high power OPOs. As the performance of the earlier OPOs has been excelled by the one described above they will be treated in a separate chapter at the end of this thesis.

For the first time, short wavelength OPOs are suitable for applications that require a light source of high spectral purity. This was demonstrated by performing Doppler-free spectroscopy on molecular iodine in the yellow spectral region. With this work we have developed short wavelength OPOs to a stage that they can be transferred from basic research into application as well as possible commercial use.

This thesis is organized as follows:

Chapter 2 gives an introduction into nonlinear optics and optical parametric oscillation.

Chapter 3 describes the setup of the OPO and the frequency doubler with special attention to its design considerations.

Chapter 4 is devoted to the performance of both OPO and frequency doubler as obtained experimentally and its application for Doppler-free spectroscopy of iodine.

Chapter 5 describes two earlier single frequency OPOs as well as a series of narrow linewidth pump lasers.

Chapter 2

Theory

Summary

This chapter gives an introduction into the physical principle of optic parametric oscillation. Phase matching and quasi-phase matching, which determine the output wavelengths, the oscillation threshold, linewidth, mode structure, and transverse beam profile are discussed. A more general introduction into nonlinear optics can be found in [20]. A detailed discussion of quasi-phase matching is given in in [21]. A detailed theory of the OPO with resonant pump and signal is described in [22].

An optical parametric oscillator (OPO) can be interpreted as a photon splitter. It converts the optical energy contained in a "pump" laser beam into two longer wavelength beams called the "signal" and the "idler" (fig. 2.1). It is the inverse of a frequency doubler (or sum frequency generator) but the two generated waves of an OPO do not have to be equal.

Figure 2.1: Principle of an OPO

The main parts of an OPO are a nonlinear optical crystal in an optical cavity resonating either the signal or idler (singly resonant OPO, SRO) or both (doubly resonant OPO, DRO), see fig. 2.2. A pump laser is aligned to match the cavity mode and may also be resonated. A DRO is overconstrained because signal and idler simultaneously have to fulfil the resonance condition of the cavity. So stable operation is only possible with active control of the cavity length.

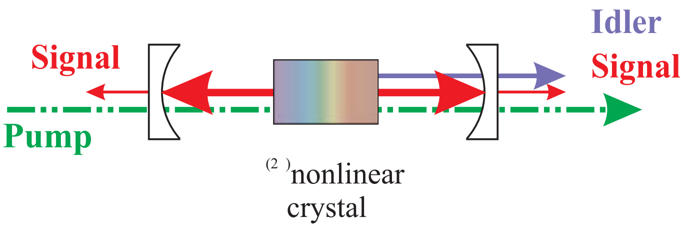

Figure 2.2: Schematic setup of a singly resonant OPO with standing wave cavity.

2.1 Nonlinear interaction

In any real atomic system, polarization induced in the medium is not proportional to the optical electric field but can be expressed in a Taylor series expansion as

$$P_i = \varepsilon_0 \left(\chi^{(1)}_{ij} E_j \ + \ \chi^{(2)}_{ijk} E_j E_k \ + \ \chi^{(3)}_{ijkl} E_j E_k E_l \ + \ \ldots \right) \quad , \tag{2.1}$$

where P_i is the i th component of the instantaneous polarisation and E_i is the i th component of the instantaneous field. Summations over repeated indices are assumed. $\chi^{(1)}_{ij}$ is the linear susceptibility, which gives rise to the index of refraction. $\chi^{(2)}_{ijk}$ is the second order nonlinear susceptibility and is responsible for second harmonic generation, sum and difference frequency generation, and optic parametric amplification and oscillation. $\chi^{(3)}_{ijkl}$ is the third order nonlinear susceptibility and gives rise to four wave mixing processes like third harmonic generation, Raman and Brillouin scattering, self focusing and optical self phase modulation. For symmetry reasons only non centrosymmetric crystals can possess a nonvanishing $\chi^{(2)}_{ijk}$ tensor. [20]

An OPO is based on frequency down conversion via the $\chi^{(2)}$ interaction. To understand the frequency conversion, we investigate a true singly resonant OPO, in which only the signal wave is resonated. Assume some signal field is already present in the cavity. Then the nonlinear crystal acts as a difference frequency generator, splitting pump photons into signal and idler photons. Thus, the idler is generated and the signal is amplified at the expense of the pump which is partially depleted. If the nonlinear gain for the signal exceeds the linear losses in the resonator the signal will increase or — if no signal is present — it will start building up, like in a laser resonator.

2.2 Phase matching

What determines the signal and idler frequencies? On one hand, the energy conservation condition

$$\hbar\omega_p = \hbar\omega_s + \hbar\omega_i \quad , \tag{2.2}$$

which is trivial, and on the other hand the momentum conservation or phase matching condition

$$\hbar k_p = \hbar k_s + \hbar k_i \quad , \tag{2.3}$$

where $\omega_{p,s,i}$, $k_{p,s,i} = n_{p,s,i}\, 2\pi/\lambda$, and $n_{p,s,i}$ are the frequencies, wave-vectors, and refractive indices of the pump, signal and idler beams. As the crystal has dispersion the latter only can be fulfilled if the crystal is birefringent and different polarisation directions are employed. For a given pump wavelength, crystal orientation, and crystal temperature there are generally only one or two signal–idler pairs that fulfill both conditions simultaneously.

Consider phase matching in a bit more detail. In the plane wave approximation the efficiency of the nonlinear interaction is proportional to

$$\Big(\int_0^L d_{nl} \cos\phi \, dz\Big)^2 \quad , \tag{2.4}$$

where L is the crystal length, $d_{nl} = \frac{1}{2}\chi^{(2)}$ is the nonlinear coefficient, and ϕ is the phase between the pump and the sum frequency of signal and idler. If the phase-matching condition is fulfilled $\cos\phi = 1$ and the integral is $L\, d_{nl}$. Without phase-matching $\cos\phi$ changes sign and the integral almost vanishes (it becomes $\mathrm{sinc}\Delta k L$ with $\Delta k = k_p - k_s - k_i$).

2.3 Quasi-phase matching

An alternative is quasi-phase matching (QPM), see fig. 2.3. It was invented nearly 40 years ago independently by Bloembergen et al. [23] and Franken and Ward [24], but practically usable crystals could not be manufactured until about 1993. A domain engineered (periodically poled) nonlinear crystal is used. It is artificially structured by the methods described in the references below so that the ferroelectric domains are spatially inverted with the same periodicity as $\cos\phi$ changes sign (coherence length). For most practical cases this period is between 2 and 40 μm. Inversion of the ferroelectric domain changes the sign of d_{nl}. Then $d_{nl} \cdot \cos\phi$ is always positive and the integral becomes nonzero. Relation 2.3 becomes

$$k_p - k_s - k_i = \pm\frac{2\pi}{\Lambda} \quad , \tag{2.5}$$

where Λ is the poling period. QPM reduces the effective nonlinearity by a factor of $\pi/2$ compared to birefringent phase matching. However, the polarisation of the interacting beams can be chosen freely and thus the largest element of the nonlinear tensor of the crystal can be used. Usually this overcompensates the reduction in efficiency. For example for second harmonic generation of 1064 nm in $LiNbO_3$ $d_{13} = -4.7\,\mathrm{pm/V}$ (phase matching) while $d_{\mathrm{eff}} = d_{33}/(\pi/2) = -17.2\,\mathrm{pm/V}$ (QPM). Furthermore it is in principle possible to phase match any wavelengths within the transparency range of the crystal. Amongst the crystals that have been periodically poled by different processes are $LiNbO_3$ [25, 26, 27, 28], MgO:$LiNbO_3$ [29], $LiTaO_3$ [30, 31], $KNbO_3$ [32], $KTiOPO_4$ (KTP) and isomorphs (KTA, RTP, RTA) [33, 34, 35, 36], GaAs [37, 38], and $BaMgF_4$ [39].

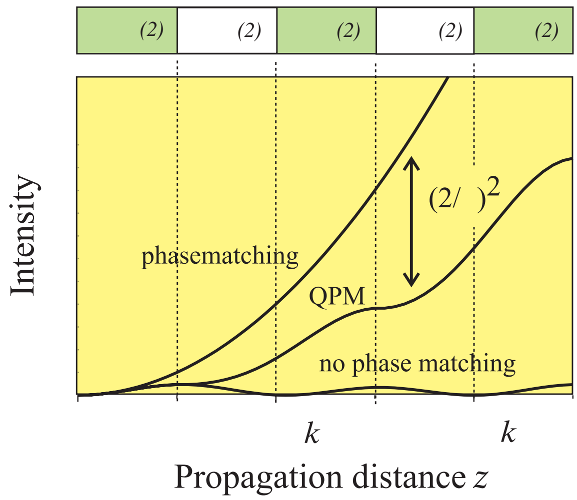

Figure 2.3: Principle of quasi-phase matching

Often periodically poled multigrating crystals containing several channels with different poling periods (see fig. 2.4, 2.5) are used. For tuning the output wavelengths of the OPO it is sufficient to move the appropriate poling period into the beam path. Fine tuning is achieved by adjusting the crystal temperature (the refractive indices are temperature-dependent and thus another signal–idler pair is phasematched). The wavelength and temperature-dependent refractive index is given by a so called Sellmeier equation. From this together with equation 2.5 the output wavelengths can be calculated as shown in fig. 4.2 and 4.3. For various crystal materials published Sellmeier equations with different degree of accuracy can be found in the literature (see section 4.1).

2.4 Threshold

As mentioned above, the OPO will start oscillating if the gain for the signal exceeds the losses. This gives the condition for the threshold pump power

$$P_{th} = L_s/E \quad , \tag{2.6}$$

where L_s are the round trip losses for the signal in the resonator (absorption in the crystal and losses from the antireflection coatings, mirrors including an output coupler if present, and other intracavity elements) and E is the effective nonlinearity

$$E = \frac{4\mu_0 d_{\mathrm{eff}}^2 \omega_s^2 \omega_i^2}{\pi c^2 n_p^2 \omega_p} Lh \quad , \tag{2.7}$$

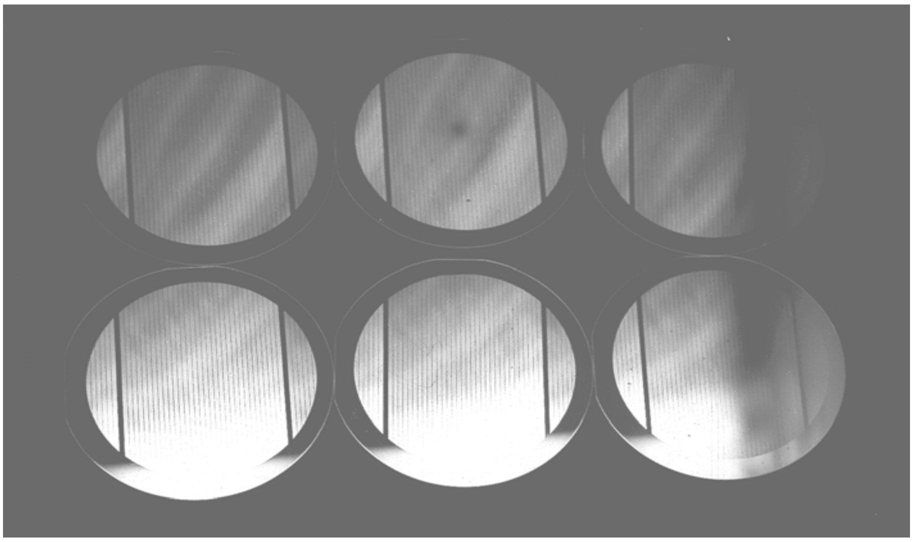

Figure 2.4: Six 3-inch periodically poled $LiNbO_3$ wafers before cutting, polishing, and anti-reflection coating. Clearly visible are 32 channels with different poling periods separated from further channels on both sides by an unpoled region on each crystal. Photo: J.-P. Meyn

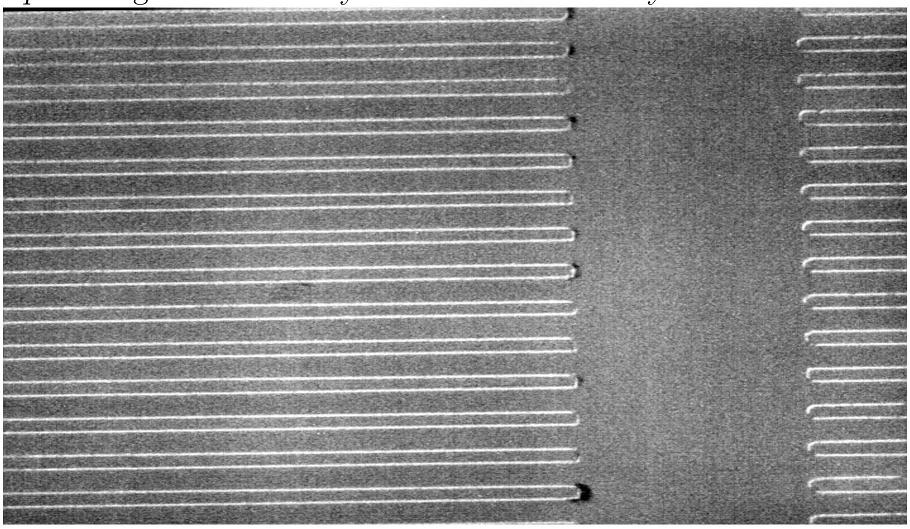

Figure 2.5: Domains in PPLN with a period of 20 μm. Photo: J.-P. Meyn

where μ_0 is the permeability of vacuum, c is the speed of light, L is the crystal length and h is a focusing parameter which is approximately 1 for nearly optimal focusing of $L/z_R \approx 3 - 10$ (z_R: Rayleigh range) [22, 40].

If the pump is also resonated, the extracavity pump threshold is given by

$$P_{th\,ext} = \frac{(T_p + V_p)^2}{4\,T_p} P_{th} \tag{2.8}$$

where T_p is the pump input coupler transmission and V_p are the linear round trip losses for the pump excluding the input coupler transmission. Further calculations regarding the output power and efficiency can be found in [22]. For a cw OPO the gain is usually much smaller than for a laser and therefore an OPO is much more sensitive to signal losses.

2.5 Mode structure and linewidth

A singly resonant OPO behaves like a laser with a homogeneously broadened linewidth. The resonator mode that experiences the highest gain will start oscillating. It uses up the pump power and thus prevents oscillation of other modes. In practice, however the OPO can exhibit frequent hops between different longitudinal resonator modes. Usually there are more than 100 resonator modes within the gain profile. Useful techniques to prevent mode-hops include increasing the free spectral range of the resonator or adding wavelength selecting elements such as an etalon.

The signal linewidth is determined by the stability of the OPO resonator and can be smaller than the linewidth of the pump laser. It follows from energy conservation that the frequency content of the idler (which is the difference frequency of the pump and the signal) is the convolution of the linewidth of the pump and the signal. Even if the OPO is pumped by a multi-mode laser the signal runs on a single mode and the idler images the mode structure of the pump (convoluted with the signal linewidth) [19].

The transverse mode profile of the signal is also determined by the resonator geometry and usually should be a TEM_{00} mode. The mode profile of the idler has to be calculated as the overlap integral between the pump and the signal. As they have different wavelengths the idler mode cannot be a pure TEM_{00} mode. But if the pump is TEM_{00} and the OPO does not run very far from degeneracy,[1] more than 90 % of the idler power is in the TEM_{00} mode [22].

[1] degeneracy: $\nu_{\text{signal}} = \nu_{\text{idler}}$

Chapter 3

Setup

Summary

Our goal was to implement an OPO with an extremely wide tuning range from the visible to the infrared, providing high output power and excellent spectral properties.
To approach this goal we constructed an OPO with a singly resonant bow-tie shaped ring cavity to extract the beam at a single output port. This also provides the flexibility to add an intra-cavity etalon at the second beam waist to control the signal frequency and to use two piezoelectric transducers to control the cavity length. Broad tunability is achieved by the use of periodically poled multigrating crystals of two different families which were provided by the University of Kaiserslautern (PPLN) and Tel Aviv University (PPKTP). The OPO is pumped single pass by a commercial 532 nm laser (Coherent Verdi) which runs reliable, single frequency and frequency stable. In the resonator design special attention was given to thermal lensing effects in the nonlinear crystal and high mechanical and thermal stability.
To extend the emission range into the red to green spectral region, the idler output is efficiently frequency doubled in an external resonator with broadband phase matching.

Prior to this project we set up two more OPOs. They are described in chapter 5.

3.1 Pump source

As a pump source for the OPO a widely available commercial continuous-wave single-frequency 532 nm laser (Coherent Verdi V10) is used. It consists of a Nd:YVO_4 ring laser end-pumped by two fiber coupled diode bars and with an intra-cavity LBO frequency doubler. It has a near diffraction limited output power of 10 W and is non-tunable. We measured an earlier model 5 W Verdi laser to have a 20 kHz linewidth, 500 kHz jitter over 1 ms and a low frequency drift of less than 50 MHz/h (see section 5.3.5).

With a halfwaveplate and a polarizing beam splitter the laser power is distributed between two experiments. A 2:1 telescope reduces the beam size and a subsequent optical isolator prevents back-reflections into the laser. A confocal scanning Fabry-Perot interferometer monitors the laser to ensure single-frequency operation. A single lens focuses the laser into the OPO. The waist position and size can be adjusted independently by moving the incoupling lens and one of the telescope lenses respectively.

3.2 Nonlinear crystals

To get a direct material comparison we use nonlinear periodically poled multigrating crystals of two different families, periodically poled $KTiO_4$ (PPKTP) and periodically poled $LiNbO_3$ (PPLN).

Two PPKTP multigrating crystals, 24 x 19 x 0.3 and 24 x 19 x 0.5 mm in size with a total of 19 different poling periods from 8.96 – 12.194 μm, were fabricated at Tel Aviv University using the low temperature poling method [35] combined with the recently developed pyroelectric monitoring technique [36].

The PPLN multigrating crystal, 25 x 35 x 0.5 mm in size with 23 different poling periods from 6.51 – 9.59 μm, was fabricated at the University of Kaiserslautern according to the method described in reference [28]. Hard baked photoresist was used as an insulator and LiCl solution was used for electrical contacting. The electrode width was chosen to be 1.3 – 2.3 μm to obtain a uniform domain duty cycle of 50 % for all periods.

The poling periods were designed to provide quasi-phase matching from degeneracy to 660 nm (PPKTP) and 645 nm (PPLN). The gap between the wavelengths obtained from two adjacent poling periods is covered by varying the crystal temperature over a range of 70 °C (PPLN) and 105 °C (PPKTP). The poling periods and output wavelengths calculated according to published Sellmeier equations are listed in appendix A.1.

To avoid undesired etalon effects caused by residual reflections from the crystal end faces all crystals were polished at an angle of 0.5°.

3.3 OPO resonator

Fig. 3.1 shows the OPO schematic. It is set up as a singly resonant OPO pumped in a single pass and resonating the signal in a bow tie shaped ring cavity.

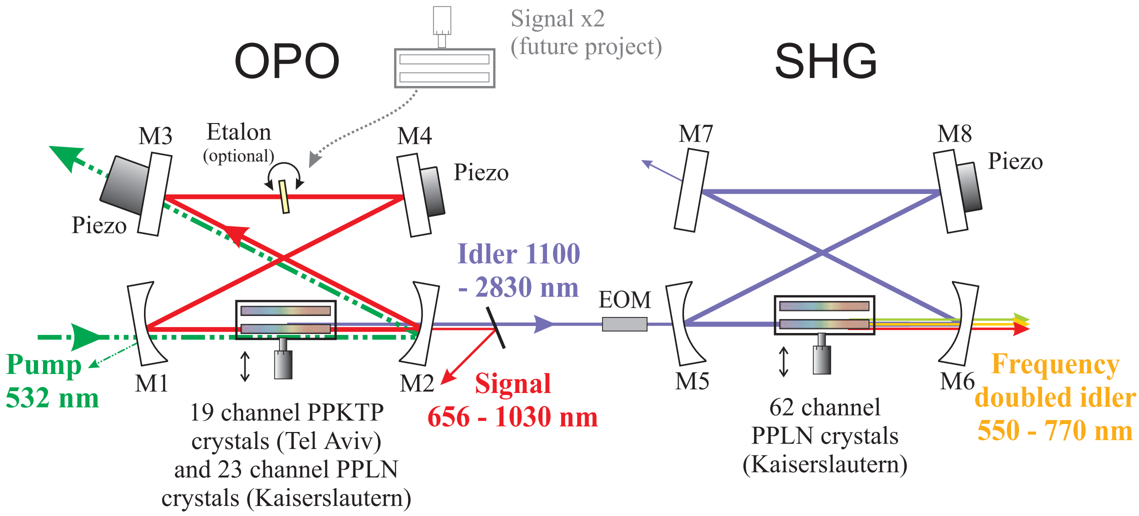

Figure 3.1: OPO and SHG setup. Pump laser, optical isolator, modematching optics, ovens, and lock electronics are not shown. Total size including pump laser and auxiliary optics: 1.1 m^2.

3.3.1 Resonator mirrors

The mirrors were manufactured by Layertec GmbH. Mirror M2 has a reflectivity of 99 % for the pump (532 nm), > 99.8 % for the signal (690 – 1030 nm), and < 5 % for the idler (1100 – 2300 nm); mirrors M1, M3, and M4 have a reflectivity of 1 % for the pump, > 99.8 % for the signal, and < 5 % for the idler. The crystal end faces carry broadband antireflection coatings, made by Tafelmeier GmbH, with a residual reflectivity of 0.5 % for the pump, < 0.2 % (PPKTP) and < 0.4 % (PPLN) for the signal, and < 15 % for the idler (all values as specified by the manufacturers).

The reflectivity of the mirrors for the signal is much higher than specified over most of the tuning range, so that only a tiny leakage through the mirrors serves as signal output.

The total idler power feed back into the crystal after one round trip is smaller than $1.8 \cdot 10^{-5}$. Thus the OPO is really a singly resonant device.

Residual reflections at mirrors M1, M3, and M4 cause the pump wave to be weakly resonated (total round trip loss: 99.9999 %). If the resonator length is varied with a piezo, this results in an intra-cavity pump power modulation of 0.4 % which is negligible for this device.[1] However, the 1 % pump power reflected off the incoupling mirror M1 has a modulation of 33 %. It can thus be used as an error signal for locking the OPO to the pump laser. This allows to compensate for thermal expansion of the cavity length.

[1] Remember that the amplitudes of the interfering beams have to be added and subtracted, not the intensities. So even a weak beam can generate a relatively strong interference signal.

3.3.2 Thermal lenses

Nearly all of the generated signal power and a few percent of the pump power is dissipated in the crystal while all of the idler power leaves the resonator through mirror M2. This dissipation heats the crystal in the center of the beam path and thus creates a thermal lens which can have a focal length down to a few mm. The power of the lens p in Diopters (or inverse meters) is given by [41]

$$p = \frac{1}{f} = \frac{\alpha(\mathrm{d}n/\mathrm{d}T)P^c}{\pi K_c} \int\limits_{\text{crystal length}} \frac{\mathrm{d}z}{w^2(z)} \quad , \tag{3.1}$$

where α is the power absorption coefficient, $\mathrm{d}n/\mathrm{d}T$ the change of the refractive index with temperature, P^c the intra-cavity power, K_c the thermal conductivity and $w(z)$ the $1/\mathrm{e}^2$ beam radius along the crystal length. With an equal dissipated power, the thermal lens is 5 times stronger in PPLN ($\mathrm{d}n/\mathrm{d}T = 99.5 \cdot 10^{-6}/°\mathrm{C}$ at $T = 150°\mathrm{C}$ [42], $K_c = 4.6\mathrm{W}/(\mathrm{m}\,°\mathrm{C})$ [43]) than in PPKTP ($\mathrm{d}n/\mathrm{d}T = 14.5 \cdot 10^{-6}/°\mathrm{C}$ [44], $K_c = 3\mathrm{W}/(\mathrm{m}\,°\mathrm{C})$ [45]).

At the time the resonator was designed the intensities of the intra-cavity waves, absorption coefficients, effective nonlinearity, and thus the strength of the thermal lens were not known precisely. However, it was estimated that the focal length was on the order of a few mm and thus a resonator design taking the thermal lens into account is crucial for obtaining stable oscillation. The following conditions were to be fulfilled:
1. The resonator must be stable with a thermal lens as strong as possible.
2. The resonator also must be stable without a thermal lens. Otherwise the OPO operates fine once it is operating, but it would be impossible to turn it on.
3. The thermal lens shall not affect the mode matching of the pump significantly so that the alignment can be done at low power and without the signal wave present in the cavity.
4. The resonator should approach the optimum focusing condition of $L/z_R \approx 3$ – 10.
5. The astigmatism should be low to optimize the efficiency and to enable good mode matching without the use of cylindrical lenses.

3.3.3 Resonator design

In a simulation the thermal lens of power $p = 1/f$ was approximated as 8 ideal thin lenses each of power $p\,/\,8 = 1\,/\,8f$ distributed evenly over the crystal length. This approximation does neither account for the pump intensity variation due to focusing, nor for spherical aberration.

For the simulation the variables as defined in fig. 3.2 were used. The propagation through half the crystal length is described by the beam propagation matrix

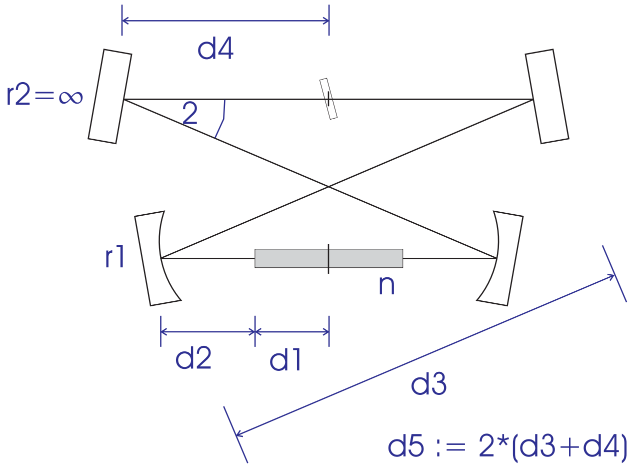

Figure 3.2: Definition of the resonator geometry.

(notation according to [20])

$$\mathbf{M}_{\text{half crystal}} = \left[\begin{pmatrix} 1 & d_1/8 \\ 0 & 1 \end{pmatrix} \begin{pmatrix} 1 & 0 \\ -(8f)^{-1} & 1 \end{pmatrix} \begin{pmatrix} 1 & d_1/8 \\ 0 & 1 \end{pmatrix} \right]^4 \tag{3.2}$$

and propagation around the resonator, starting in the middle of the crystal is described by

$$\begin{aligned} \mathbf{M} \;=\; & \mathbf{M}_{\text{half crystal}} \cdot \begin{pmatrix} 1 & 0 \\ 0 & 1/n \end{pmatrix} \begin{pmatrix} 1 & d_2 \\ 0 & 1 \end{pmatrix} \begin{pmatrix} 1 & 0 \\ \frac{-2}{r_1 \cos^{\pm 1} \phi} & 1 \end{pmatrix} \cdot \\ & \cdot \begin{pmatrix} 1 & d_5 \\ 0 & 1 \end{pmatrix} \begin{pmatrix} 1 & 0 \\ \frac{-2}{r_1 \cos^{\pm 1} \phi} & 1 \end{pmatrix} \begin{pmatrix} 1 & d_2 \\ 0 & 1 \end{pmatrix} \begin{pmatrix} 1 & 0 \\ 0 & n/1 \end{pmatrix} \cdot \mathbf{M}_{\text{half crystal}} \,, \end{aligned} \tag{3.3}$$

where n is the refractive index of the nonlinear crystal (1.847 for KTP and 2.186 for PPLN). The factor $\cos^{+1}\phi$ in the matrices for the curved mirrors accounts for the tangential and $\cos^{-1}\phi$ for the sagittal plane of incidence.

A set of parameters fulfilling the conditions outlined above was found: $r1 = 100\,\text{mm}$, $\phi = 14°$, $d1 = 12.5\,\text{mm}$, $d2 = 47\,\text{mm}$, $d3 = 108.6\,\text{mm}$, $d4 = 36.4\,\text{mm}$, $d5 = 290\,\text{mm}$. The beam radius along the resonator is shown in fig. 3.3. The resonator is stable with a thermal lens focal length varying from infinity down to 4 mm, only slightly influencing the beam radius outside the crystal. Without thermal lens the focusing is slightly less tight than optimum with an $1/\text{e}^2$ beam radius of 48 μm and 13 % astigmatism only (for a wavelength of 800 nm). With thermal lenses the focusing is even tighter than that of an optimally focused Gaussian beam. The second waist has a radius of 250 μm. The resonator has a free spectral range of 700 MHz (PPKTP) and 680 MHz (PPLN).

Additional advantageous features of this design are: the PPLN and PPKTP crystal can be exchanged without the need for changing the mirror positions despite

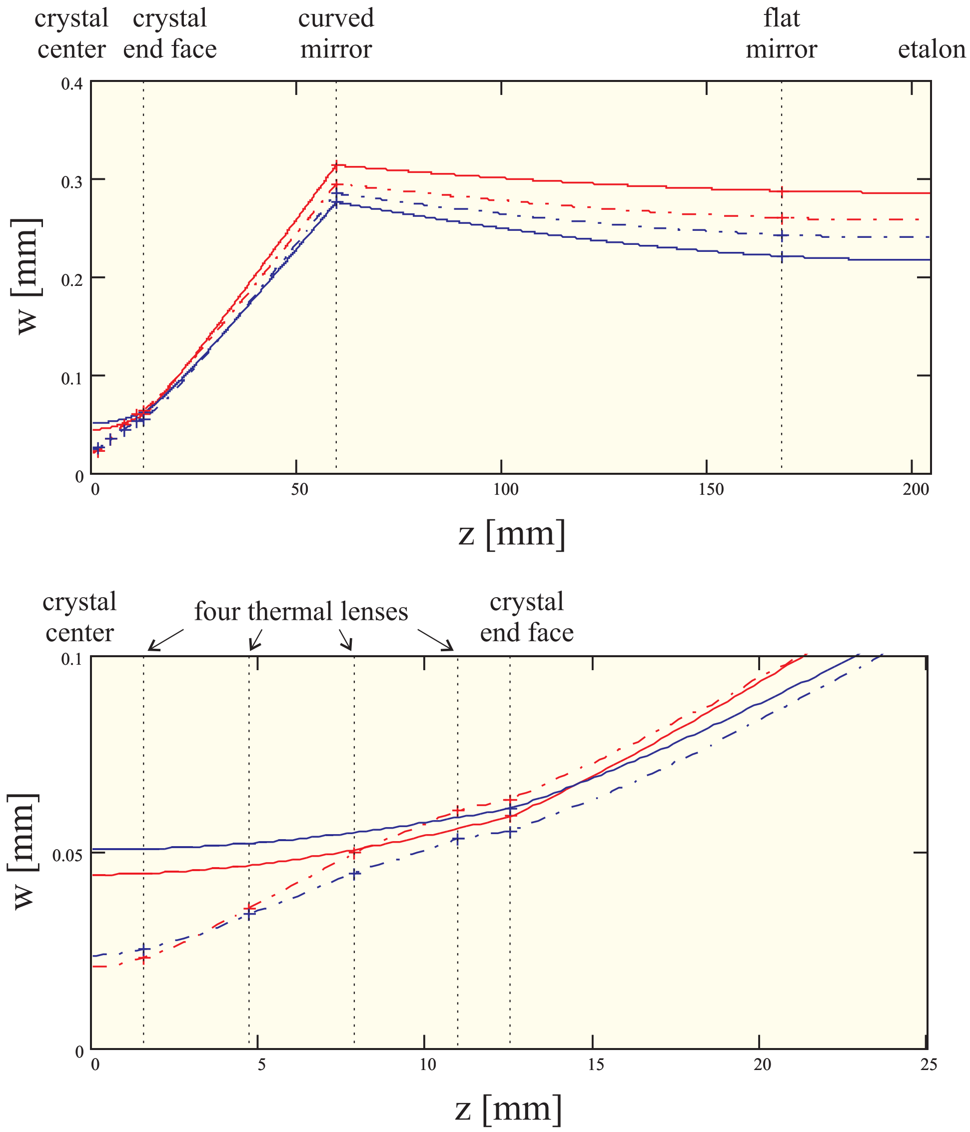

Figure 3.3: Top: $1/e^2$ beam radius along the OPO resonator calculated for the PPKTP crystal and a wavelength of 800 nm. Solid lines: without thermal lenses; dashed lines: with eight thermal lenses of 32 mm focal length each; red: tangential plane; blue: sagittal plane. Bottom: enlargement.

the substantial difference in the refractive indices. A deviation from the calculated lengths of more than 1 mm can be tolerated. Because the crystal end faces are polished at an angle of 0.5° and the crystals show dispersion, the pump, signal and idler beams are separated by about 0.3 mm on the mirrors but coincide almost perfectly inside the crystal.

3.4 Etalon

An etalon is inserted into the second beam waist to control the signal frequency and prevent modehops.

An etalon is a thin Fabry-Perot interferometer consisting from two plane mirrors of equal reflectivity. Most often the etalon consists from a glass plate with the mirrors coated onto the surfaces. Only frequencies that are integer multiples of the free spectral range of the etalon are transmitted. To ensure efficient frequency selection the free spectral range of the etalon should be in the order of the gain profile of the OPO or larger. The width of the transmission peak of the etalon is determined by the reflectivity of the coatings and should be sufficiently narrow to select one resonator mode of the OPO within the gain profile. If very high reflectivities are employed they have to be equal with high accuracy so that the transmission losses remain small.

Two fused silica etalons, $d = 0.25$ and $0.5\,\mathrm{mm}$ thick with a reflectivity of $20-60\,\%$ per surface for the signal and $0.2\,\%$ for the pump are used. They are mounted via an invar adaptor[2] on a galvo drive (tilt angle $\pm 4°$, possible control bandwidth up to $\approx 100\,\mathrm{Hz}$). For small tilt angles φ the free spectral range of the etalon is

$$\mathrm{FSR}_{\mathrm{et}} = \frac{c}{2nd} \cdot \left(1 - \frac{\varphi^2}{2n^2}\right) \simeq 200 \text{ or } 400\,\mathrm{GHz} \quad , \tag{3.4}$$

for $d = 0.5\,\mathrm{mm}$ and $0.25\,\mathrm{mm}$ respectively, where $n = 1.45$ is the refractive index of fused silica. The free spectral range varies quadratically with the tilt angle.

To operate the OPO the frequency transmitted by the etalon has to match the gain profile of the nonlinear crystal. This can be achieved either by tilting the

[2] the thermal expansion coefficient of invar is close to that of fused silica

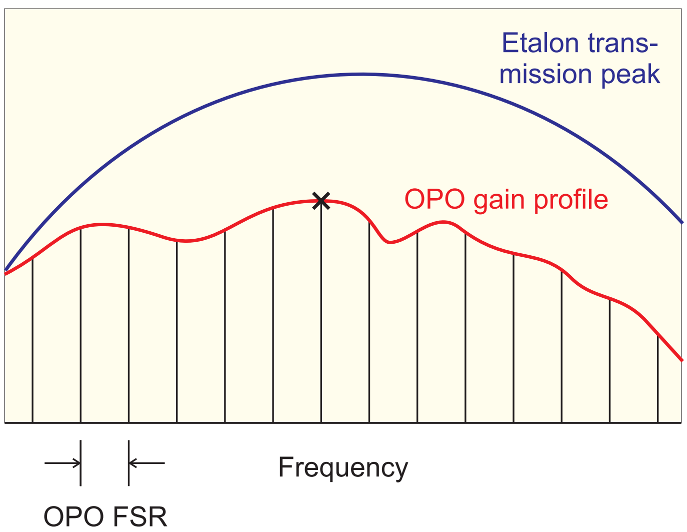

Figure 3.4: Selection of an OPO resonator mode using the etalon.

etalon or changing the crystal temperature. The width of the transmission peak of the etalon (defined as full width at 99 % of the transmission maximum) is 3 – 11 GHz (FWHM = 33 – 70 GHz) for the thick etalon and twice that for the thin one. Compared to this the gain profile of the parametric interaction has a width (defined as full width at 99 % of the gain maximum) between 4.5 GHz (at 650 nm signal wavelength) and 34 GHz (at 1000 nm) (FWHM = 40 – 280 GHz). The etalon narrows the total gain profile and thus helps to select one resonator mode and prevent modehops. Furthermore its transmission profile is smooth while the gain profile of the crystal may have ripples (see fig. 3.4). So the etalon enables access of any desired wavelength, stable operation, and continuous tuning of the OPO.

If the etalon is tilted to an angle φ the beams reflected off the front and the back of the etalon do not overlap completely. As long as the reflectivity R of each etalon surface is $\leq 90\,\%$ and φ is small, this causes additional losses of

$$4\,\frac{R}{1-R}\left(\frac{d}{nw}\right)^2 \sin^2\varphi \quad , \tag{3.5}$$

where w is the $1/\mathrm{e}^2$ beam radius. For our OPO this gives $0.06 - 0.35\,\% \cdot (\varphi/1^\circ)^2$ for the thick etalon and 1/4 of that for the thin one. Note that the losses scale quadratically with tilt angle but linearly with change of the free spectral range and thus of the transmitted wavelength. These walk-off losses could be avoided using an air spaced etalon which can be tuned piezoelectrically without the need for tilting it.

3.5 Mechanical setup

The crystals are mounted in a gold-coated copper oven formed from two copper plates with gaps fitting the crystal dimensions. The oven is mounted via two marcor (machinable glass) rods on two parallel translation stages moving the crystal vertically through the beam path.

The oven is electrically heated by four heating rods (Watlow Firerod) and the temperature is controlled using two PT100 thermoresistors and a PID controller. The copper plate mounted to the translation stages suffers from additional thermal losses induced by the marcor rods. To compensate for them a resistor is connected in series with the heating rods at the other copper plate. To homogenize the temperature the oven is surrounded by an aluminum box. The oven has a temperature stability of better than 5 mK with a temperature difference between the two copper plates below 0.1 K over the temperature range from 30 – 250 °C.

To achieve high mechanical stability the whole OPO is mounted on a massive aluminum block, $261.0 \times 220.5 \times 70.0$ mm in size. The mirrors are held by commercial adjustable mirror mounts (Bill Lees). The position of the mounting holes for these are placed so that the mirror spacings are as calculated without further alignment.

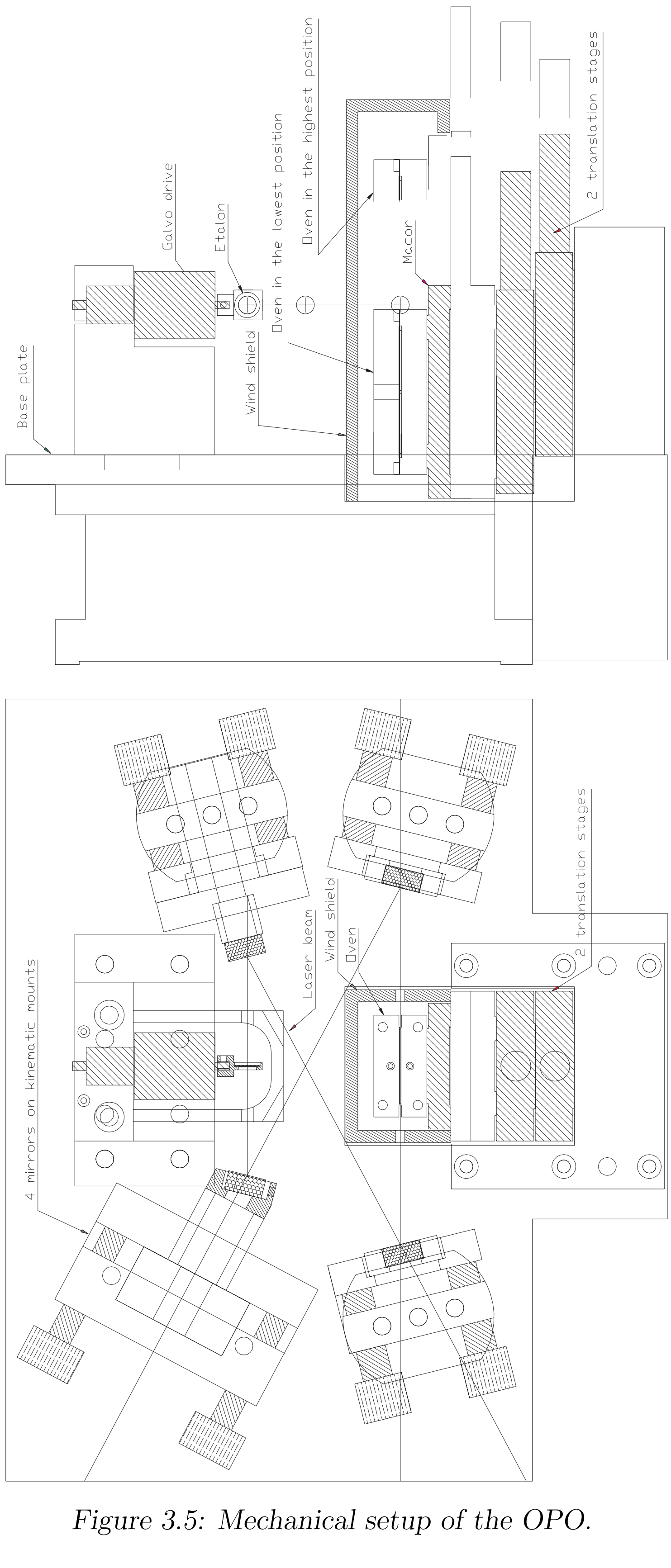

Figure 3.5: Mechanical setup of the OPO.

The two flat mirrors are glued onto low voltage piezoelectric transducers of different sizes and frequency responses each on a massive steel counter weight that is screwed onto the adjustable mirror mount. The smaller one of the two piezos has a resonance frequency of 38 kHz thus allowing for a control bandwidth of 10 – 15 kHz.

To protect the OPO from air turbulences and dust it is covered by an acrylic glass box. The whole setup is shown in fig. 3.5 and fig. 3.6.

The device is aligned by first setting it up as a pump resonant OPO with a 5 %-input coupler and 3 mirrors reflecting the pump. By scanning one of the two piezos the transversal and longitudinal modematching of the pump laser into the cavity is aligned precisely before subsequently mirrors M1, M3 and M4 are exchanged against mirrors that are transmitting the pump. The order is important and after each mirror change the OPO cavity is realigned to maximize the interference signal in the back reflected pump beam (section 3.3.1) and the output power.

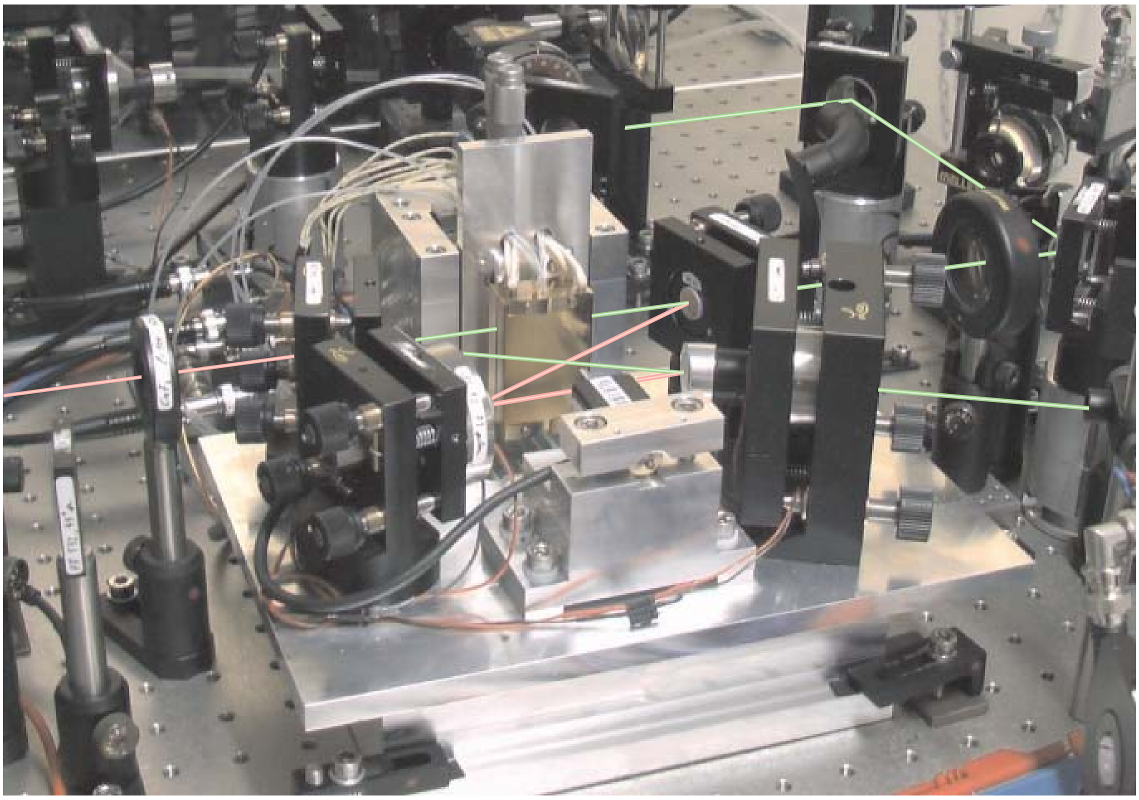

Figure 3.6: OPO resonator with the thermal shielding removed. The etalon is in the front and the crystal oven in the back.

3.6 Frequency Doubler

It is difficult to obtain short wavelength radiation directly from an OPO. If the pump wavelength is kept constant at 532 nm, signal and idler both run into a regime of increasing absorption for all periodically poled materials available at present. If a pump wavelength shorter than 532 nm is used, pump absorption will become an issue and an appropriate pump laser has to be found. An alternative for generating tunable visible light is frequency doubling the signal or idler of a green-pumped OPO.

As long as there is no optimized output coupler implemented in the OPO the emitted signal power is too weak to be frequency doubled efficiently. However, there are several watts of signal resonating in the OPO cavity, so it should be easy to implement an intra-cavity frequency doubler. It is important though that the phasematching bandwidth of the frequency doubler exceeds the total gain bandwidth of the OPO. Otherwise the nonlinear losses induced by the doubler will cause the OPO to run at a wavelength that is not phase matched for the doubling process. This condition can be achieved by using a very short doubler crystal (at the expense of efficiency), an aperiodically or chirped poled crystal, or additional wavelength-selective elements like an etalon.

The situation for the idler is different. There is plenty of idler power emitted which can be frequency doubled efficiently in an external resonator. The only difficulty is that broadband phase matching is required.

As of 2001 we left the doubler for the signal as a future project and set up an external resonant doubling cavity for the idler from 1100 – 1540 nm, producing 550 – 770 nm (green to red). The doubler is set up as a bow-tie shaped ring cavity to get the visible light from a single output port and to avoid back reflections into the OPO. This is necessary because there is no broadband optical isolator available for the wavelength range to be doubled. The setup schematic is shown in fig. 3.1.

3.6.1 Nonlinear crystals

In a frequency doubler, the crystal temperature has a much weaker effect on the phase matched wavelength than in an OPO. Therefore many more different poling periods are required. We use two PPLN multigrating crystals, each 43 x 47 x 0.5 mm in size, with a total of 62 different poling periods from 6.51 – 20.93 μm. By varying the crystal temperature between 150 and 220 °C they provide quasi-phase matching for frequency doubling of any wavelength between 1060 and 1650 nm. Note that the OPO produces this wavelength range with 5 gratings only.

The crystals were fabricated at the University of Kaiserslautern by the method described in section 3.2 and are among the largest (in area) ever used. They are shown in fig. 2.4 and 2.5. The OPO crystal is identical to the first 23 gratings of the doubler crystals. The poling periods and phasematching wavelengths calculated according to the Sellmeier equation by [42] are listed in appendix A.1. To avoid back reflections of the idler into the OPO the crystal entrance and exit faces are polished at an angle of 0.5° and 0.75° respectively.

3.6.2 Resonator

The resonator geometry is given by $r1 = 75\,\mathrm{mm}$, $\phi = 14.3°$, $d1 = 21\,\mathrm{mm}$, $d2 = 32.4\,\mathrm{mm}$, $d3 = 106.2\,\mathrm{mm}$, $d4 = 39.8\,\mathrm{mm}$, $d5 = 292\,\mathrm{mm}$ (definitions according to fig. 3.2). The beam radius along the resonator is shown in fig. 3.7. The resonator, which

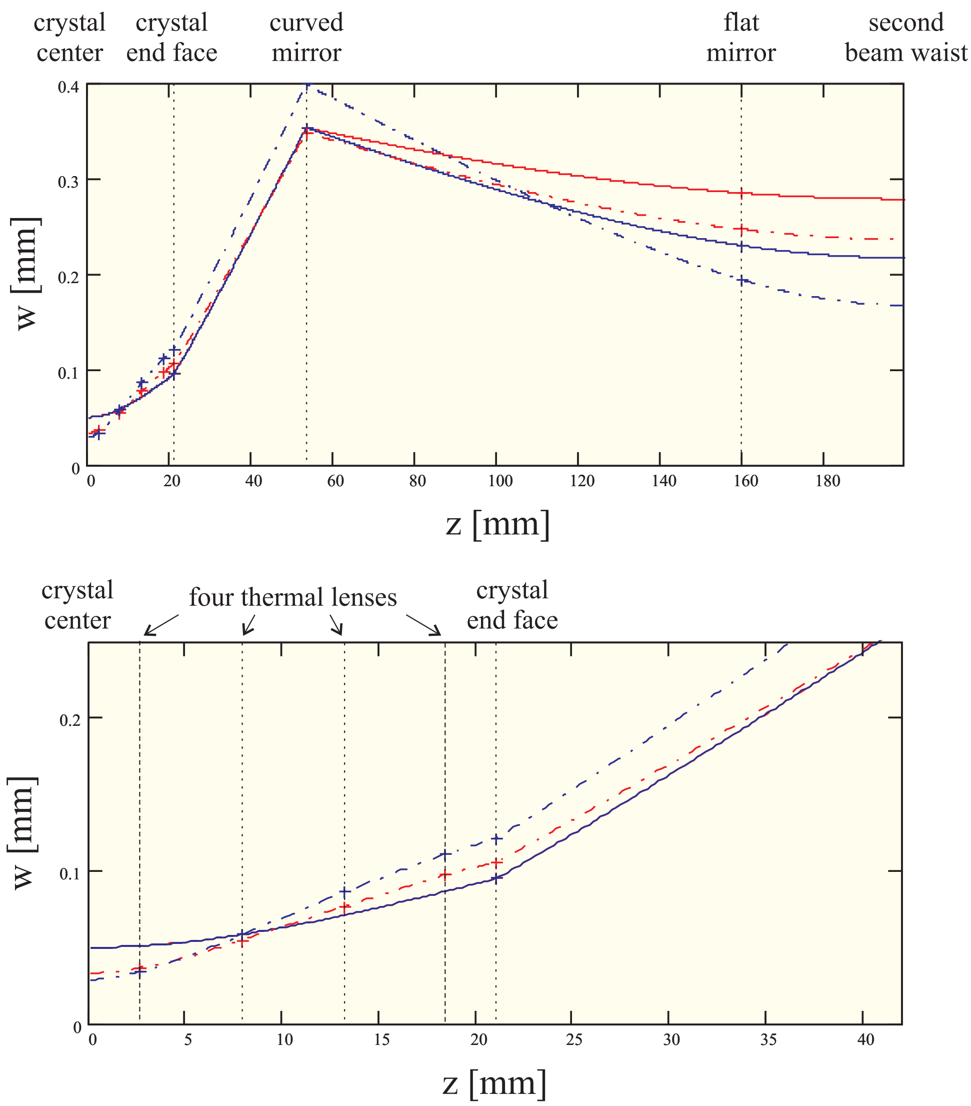

Figure 3.7: Top: $1/e^2$ beam radius along the SHG resonator calculated for a wavelength of 1300 nm. Solid lines: without thermal lenses; dashed lines: with eight thermal lenses of 96 mm focal length each; red: tangential plane; blue: sagittal plane. Bottom: enlargement.

was not optimized for stability against thermal lenses, is stable with a thermal lens from infinity down to 12 mm. The focusing is near optimum with a non-astigmatic $1/e^2$ beam waist of 50 μm (for a wavelength of 1300 nm).

The resonator mirrors M6, M7, and M8 reflect the idler power with R> 99.8 % from 1064 – 1540 nm and transmit the doubled idler with T> 90 %. Mirror M5 acts as an input coupler with a reflectivity of 98.3 ± 0.2 % for the idler. Mirror M8 is mounted on a piezoelectric transducer. The crystal end faces carry broadband antireflection coatings with a reflectivity of < 0.5 % for the idler and < 6.5 % for the doubled idler.

The expected efficiency will be discussed in section 4.7.2.

The idler is coupled into the SHG resonator via two anti-reflection coated lenses and an electro-optical modulator (EOM). The latter is built from a MgO:$LiNbO_3$ crystal, $20.0 \times 2.25 \times 1.75$ mm in size with gold coated +c and -c faces and anti reflection coated end faces. It is driven via a passive enhancement circuit with a resonance frequency of 12.7 MHz.

The cavity length is locked to the idler with a control bandwidth of 6 kHz using a standard Pound-Drever-Hall [46] method and a piezo. The error signal is obtained

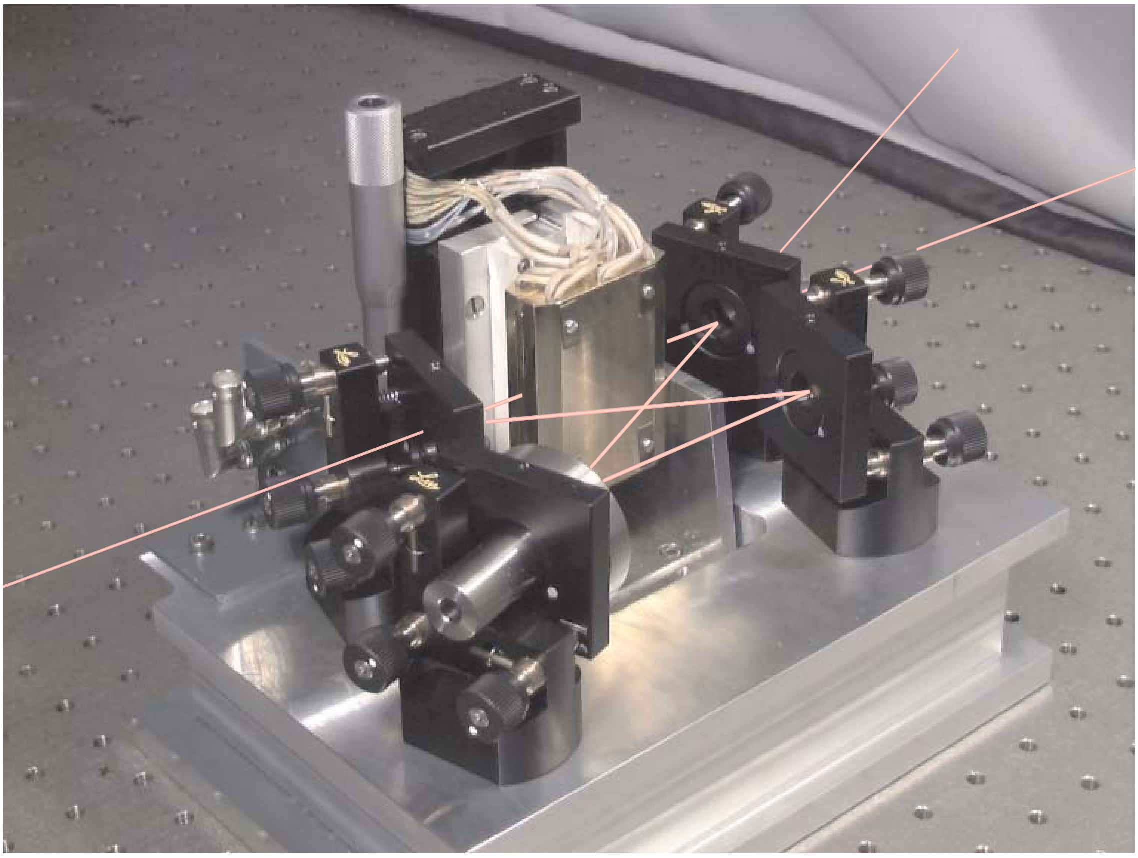

Figure 3.8: SHG resonator with the thermal shielding removed. The crystals are mounted in the gold-coated copper oven.

using the EOM and the idler wave transmitted through one of the high reflecting mirrors.

The mechanical setup is very similar to that of the OPO. However, the crystals are too large to be mounted beside another. They are stacked on top of each other with a 3 mm copper plate between them. Two translation stages move the crystals horizontally and vertically through the beam path. The setup is shown in fig. 3.8.

Chapter 4

Experimental Results

Summary

The OPO system shows an emission range from the green to the mid infrared (550 – 2830 nm) which, to our knowledge, is the broadest tuning range of any single-frequency source so far.

The output power is up to 800 mW in the idler, 60 mW in the signal, and 70 mW in the frequency-doubled idler. Both signal and idler power are expected to increase to well above 100 mW with optimized out- and incoupling mirrors. In addition, 160 mW of yellow light at 580 nm and up to 1.25 mW of blue light generated by non-phasematched frequency doubling of the signal were obtained.

The OPO shows mode-hop-free oscillation for several hours and high absolute frequency stability with a drift of less than 50 MHz per hour. The linewidth has been measured to be 20 kHz, which is one of the narrowest ever reported for an OPO. Up to 38 GHz continuous tuning for both signal and idler have been demonstrated without tuning the pump laser.

Both PPLN and PPKTP are used as nonlinear materials and their performance is compared.

The OPO including frequency doubler runs reliably and is relatively easy to use. To demonstrate its versatility and reliability it was used to perform Doppler-free iodine spectroscopy in the yellow wavelength region. Previously this spectral range had to be obtained with dye lasers.

The OPO was tuned changing the poling periods and crystal temperature for both crystal materials. The output power was maximized by optimizing the pump power for each individual wavelength. To summarize the most important result first the total emission range and output powers obtained with the OPO and frequency doubler are shown in fig. 4.1. The details will be discussed below.

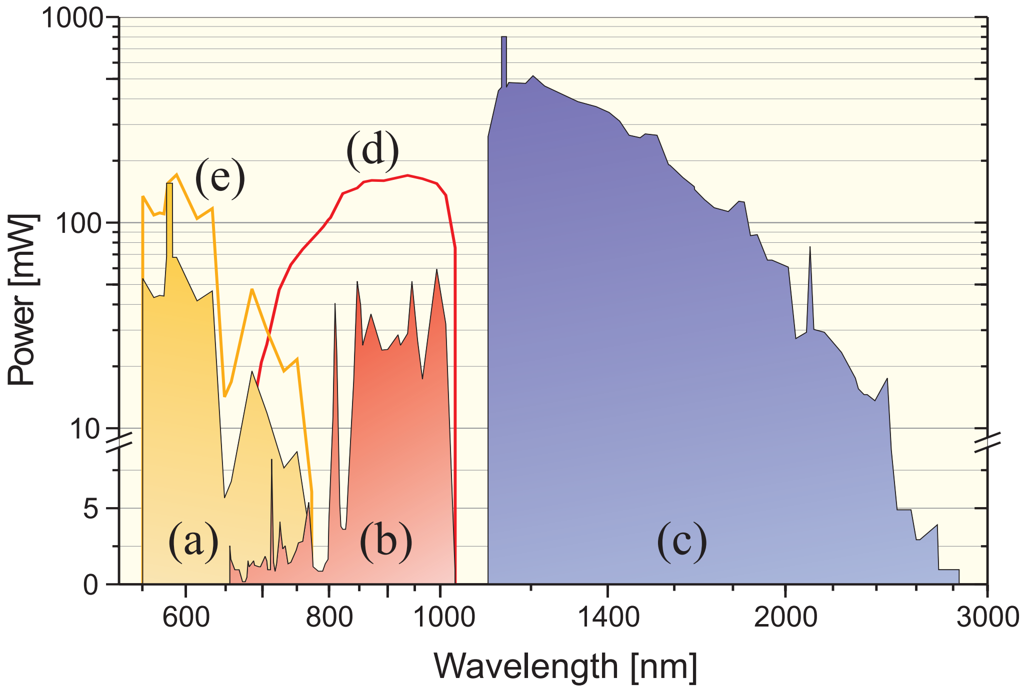

Figure 4.1: Frequency doubled idler (a), signal (b), and idler power (c), versus wavelength. Shaded areas: measured powers. Data combined from the PPLN and PPKTP OPO with and without etalon. Lines: conservative estimate of the signal (d) and doubled idler power (e) expected for optimized out- and incoupling mirrors.

4.1 Emission range

The wavelength of the signal was measured using a fiber-coupled high resolution wavemeter (Burleigh WA 1500, 50 MHz resolution). The pump wavelength was also measured with the wavemeter to be 532.2556 nm. Thus, the idler wavelength could be calculated precisely and there was no need for measuring it directly.

For both crystal materials the output wavelengths were measured for different poling periods and for different temperatures without an etalon. The measured wavelengths are shown together with the tuning curves calculated from equation 2.5 and the Sellmeier equations by [42, 47, 44, 43] in fig. 4.2 and fig. 4.3. For PPLN the emission range extends from 656 – 1035 nm (signal) and from 1096 – 2830 nm (idler). This is by far the broadest emission range ever reported for an OPO or for a cw laser source (covering more than two octaves). For PPKTP the emission range is almost the same, extending from 669 – 1034 nm (signal) and from 1097 – 2600 nm (idler). The emission range actually is broader than the specified bandwidth of the mirrors. The etalon induces additional losses and thus reduces the emission range slightly to 665 – 2666 nm (PPLN) and to 870 – 1400 nm (PPKTP).

The small gap at degeneracy is a basic feature of the singly resonant device: both signal and idler are resonated. There is oscillation but the OPO shows the tuning behavior of a doubly resonant OPO and no stable emission could be obtained.

Between 752 and 776 nm no measurements could be obtained for PPKTP because the crystal input face of two samples had been destroyed over a width of four gratings when the OPO was operating at a temperature of 150 °C. It could not be determined whether the damage was due to the crystals or the coatings.

Comparison with published Sellmeier equations

For both materials the wavelengths predicted by published Sellmeier equations deviate from the measured wavelengths by up to 30 nm. For PPLN the equation by Jundt [42] is more accurate than the equation by Edwards and Lawrence [43] for signal wavelengths above 760 nm and temperatures below 200 °C, while the opposite is true below 760 nm and above 200 °C.

For PPKTP the temperature-independent Sellmeier equation by Fradkin et al. [47] combined with the temperature derivatives by Wiechmann et al. [44] is quite accurate at room temperature as well as far from degeneracy while it deviates substantially above 120 °C and near degeneracy. The equations by Kato [48] and especially that by Boulanger et al. [49] are less accurate.

Alexander Fisher from Tel Aviv University is currently working on a more accurate temperature dependent Sellmeier equation for PPKTP based on our data and additional interferometric measurements of the first and second temperature derivatives of the refractive index for extraordinary polarisation n at different wavelengths [50].

4.2 Output power

The signal and idler output powers were measured behind mirror M2 using dichroic mirrors to separate the different beams. Commercial thermal and semiconductor power meters were used. The powers were corrected for the losses induced by the dichroic mirrors, but they were not corrected for the losses induced by the crystal coating or the outcoupling mirror. The output powers are summarized in fig. 4.1. They reach up to 800 mW for the idler and up to 60 mW for the signal. In addition up to 1.25 mW of blue light is generated by non-phasematched frequency doubling of the signal in the OPO crystal. For the frequency doubled idler power see section 4.6. The measured power, efficiency, pump depletion, and oscillation threshold are shown in more detail in fig. 4.4, fig. 4.5, and fig. 4.6. The pump power was varied between 0.8 – 3.3 W to maximize the output power for each individual wavelength and OPO configuration. Data with lower power are also plotted in the figures.

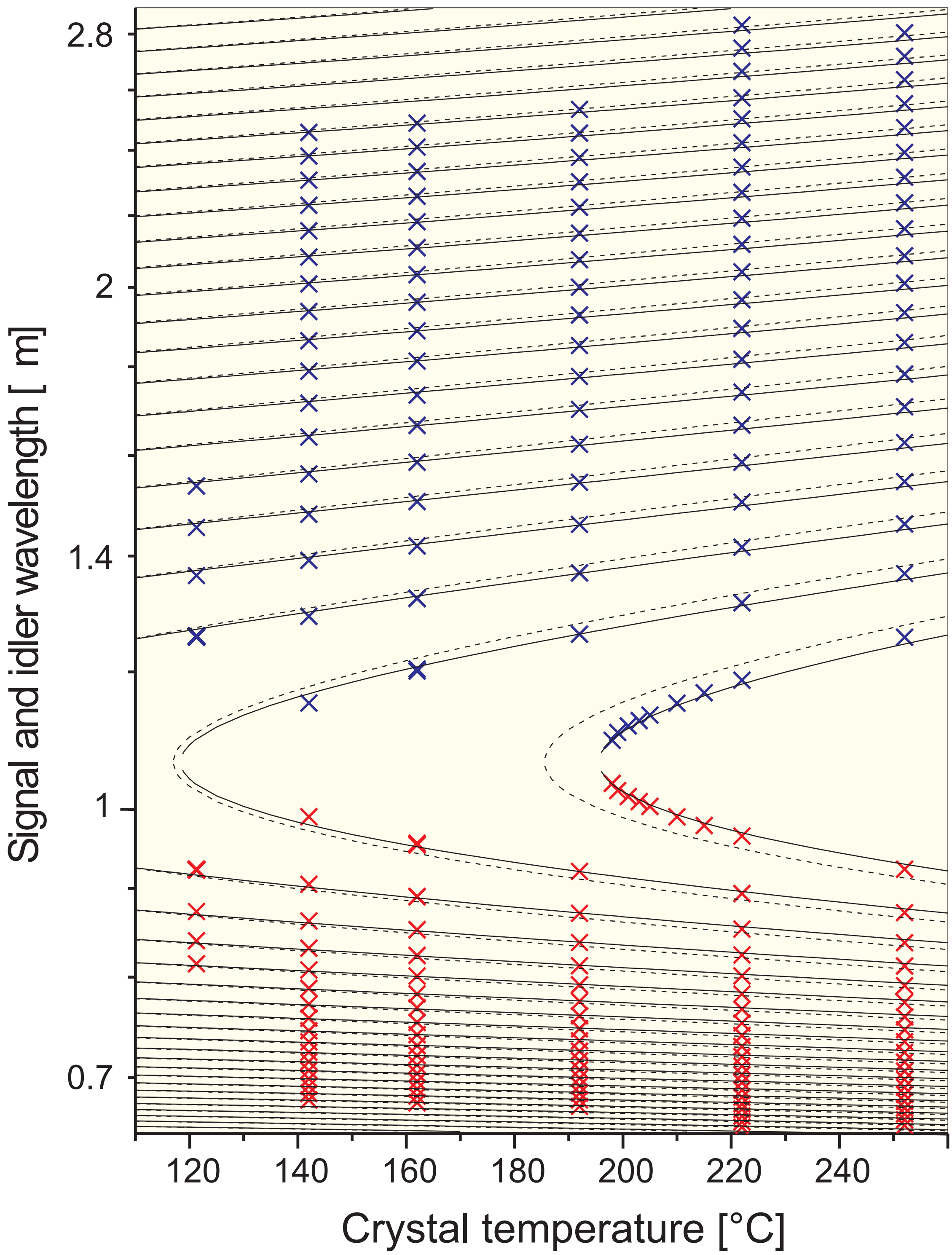

Figure 4.2: Output wavelengths of the PPLN OPO. Crosses: measured wavelengths; lines: tuning curves calculated from the Sellmeier equations by Jundt [42] (straight); and Edwards and Lawrence [43] (dashed).

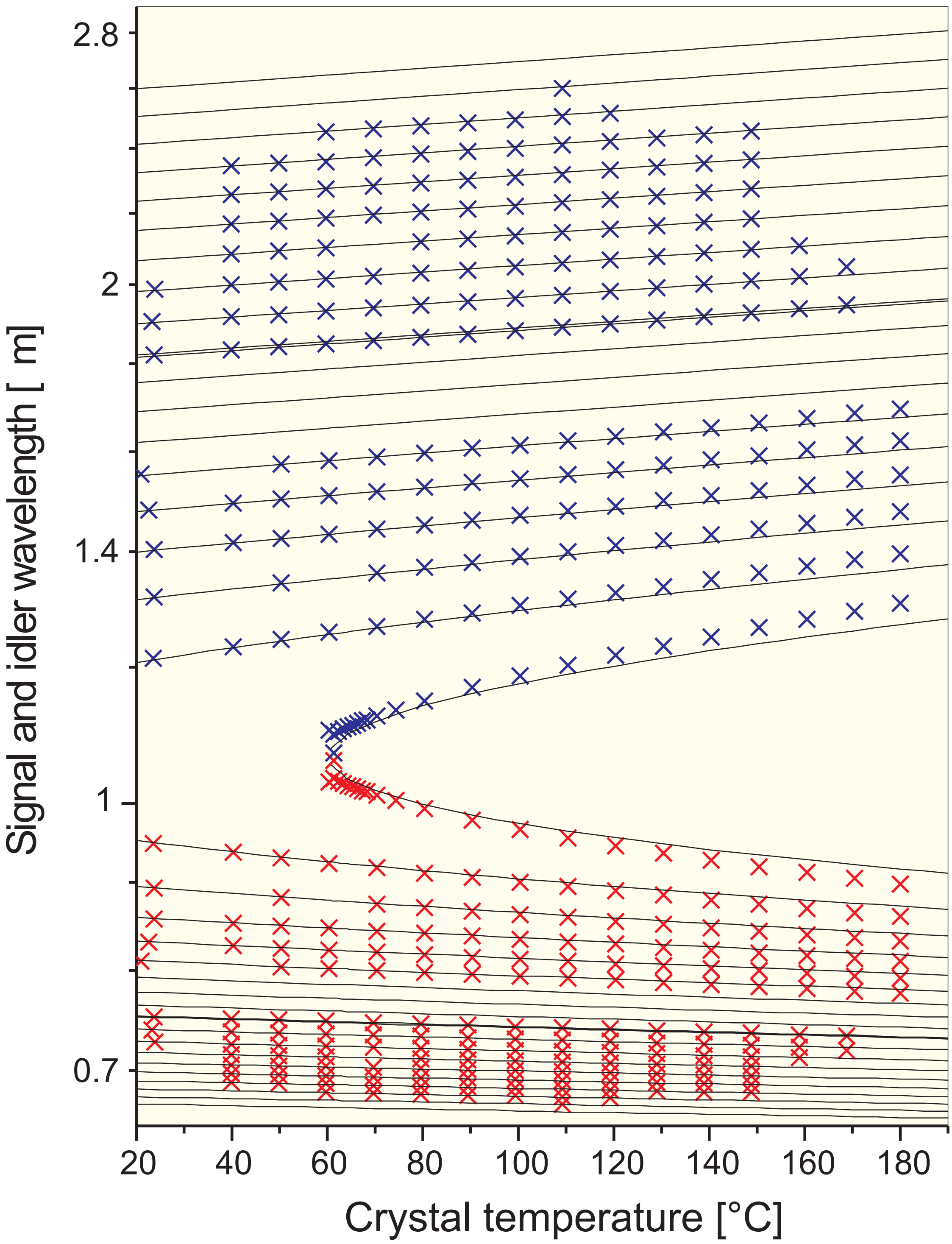

Figure 4.3: Output wavelengths of the PPKTP OPO. Crosses: measured wavelengths; lines: tuning curves calculated from the Sellmeier equation by Fradkin et al. [47] and Wiechmann et al. [44].

Idler

The idler power versus pump power is shown in fig. 4.6. 500 mW of idler power could be reproduced reliably for different wavelengths with both crystals. In contrast an idler power of 800 mW was obtained with the PPKTP crystal only once for a few seconds and could not be reproduced. At the spot used the crystal was darkened afterwards and the OPO did not oscillate any more.

Since there was a BK7 lens, which is transparent up to $2\,\mu$m only, in the beam path between the OPO and the power meter, the idler power is expected to be much higher for wavelengths longer than $2\,\mu$m than measured here.

In contrast to many other OPOs the output power is not limited by the available pump power.

For PPKTP, the damage threshold is a limiting factor. We did not want to risk damage to the crystal because at 2.4 W of pump power we had seen some crystal damage already and only for one of the two crystals a spare was available. The resonating signal power is two orders of magnitude below damage threshold of $1\,\mathrm{MW/cm^2}$ reported by Jacco et al. for ns pulses at 1064 nm [51].

The limiting factor for the PPLN crystal are thermal effects, especially thermal lenses, mainly originating from absorption of the signal in the crystal. They can bring the resonator out of the stability region and scramble up the beam profile and the mode overlap between pump and signal. The output power saturates at a certain power level. Furthermore if the OPO is operated with the PPLN crystal, without etalon, near degeneracy, and far above threshold, the emitted beam profile is not round any more.

Signal

The signal is emitted only as a tiny leakage (0.001 – 0.2 %) through the four high reflecting resonator mirrors. However the transmission through mirror M2 is 3 – 100 times higher over most of the wavelength range than through the other mirrors. Therefore only the signal emitted from this port is measured here. The losses induced by the etalon (about 1 %, in approximate agreement with what is expected from equation 3.5) act as an additional output port emitting up to 100 mW signal (near degeneracy) which in principle could be used for applications if the beam steering induced by the etalon is compensated by external optics.

Compared to PPLN the signal power for PPKTP is about twice as high. From the measured mirror transmission it can be concluded that the signal power resonating in the cavity is on the order of 10 W (PPLN) and 20 W (PPKTP) near degeneracy.

The number of generated signal and idler photons are equal. Thus the signal power that is generated in the crystal can be calculated from the measured idler power as $P_i \cdot \omega_s/\omega_i$. From this and the resonating power the intra cavity round trip losses for the signal without etalon can be determined to be approximately 4 %

(PPLN) and 2 % (PPKTP) near degeneracy, corresponding to a finesse of 150 and 300 respectively. About 0.5 – 1 % of the loss can be attributed to the mirrors and the antireflection coatings. So the crystal losses are 3 % and 1 % respectively. The losses for the pump have been measured directly to be 4 % (PPLN) and 17 % (PPKTP) per single pass through the crystal including losses from the anti-reflection coatings.

The difference in the signal losses can be understood by a phenomenon called green induced infrared absorption (GRIIRA) or excited state absorption: While the infrared absorption in the ground state is low, the green light excites the atoms to a state in which they can absorb the infrared light. GRIIRA of about 0.75 %/cm has been measured in $LiNbO_3$ [52] but it has never been reported in KTP.

An output coupler with a signal transmission of 1.3 % (PPLN) or 0.7 % (PPKTP) would couple one-fourth of the generated signal power, which is more than 100 mW over most of the signal range, out of the resonator. This should affect the overall performance of the OPO only very little. The expected signal power is shown as line in fig. 4.1. With higher transmission it might be possible to extract even more signal power. This would also reduce the thermal load to the crystal and the strength of the thermal lens, and possibly also increases the achievable idler power.

Efficiency

A power conversion efficiency from pump (as measured in front of the OPO) to idler (behind the outcoupling mirror) of up to 30 % was obtained for both materials. This corresponds to a quantum efficiency (counted in photon numbers) internal to the crystal of up to 69 % as shown in fig. 4.4. The pump depletion (without the linear losses) reaches up to 69 % for PPLN and 93 % for PPKTP as shown in fig. 4.4 and 4.6.

Threshold

The threshold strongly depends on the wavelength, crystal temperature and etalon used. It varies from 290 to more than 2000 mW for PPKTP and from 340 to more than 1500 mW for PPLN (see fig. 4.5). The threshold with etalon was measured for a small tilt angle and is higher if larger tilt angles are employed.

PPKTP has both lower losses and lower gain than PPLN and thus it is much more sensitive to additional losses induced by the etalon. So the etalon affects the threshold, output power and emission range much stronger for PPKTP.

Using signal round trip losses of 4 % and 2 % as determined above, a nonlinear coefficient of $d_{\text{eff}} = d_{33} \cdot 2/\pi,\ d_{33} = -27\text{pm/V}$ (PPLN [20]) and 14.9 pm/V (PPKTP [53]) and near optimum focusing ($h \simeq 1$), equation 2.6 gives a theoretical oscillation threshold of 570 and 660 mW respectively. This is a factor of 2 higher (!) than the lowest measured threshold. One possible reason for this deviation are thermal lenses which reduce the beam radius inside the crystal relative to a Gaussian beam.

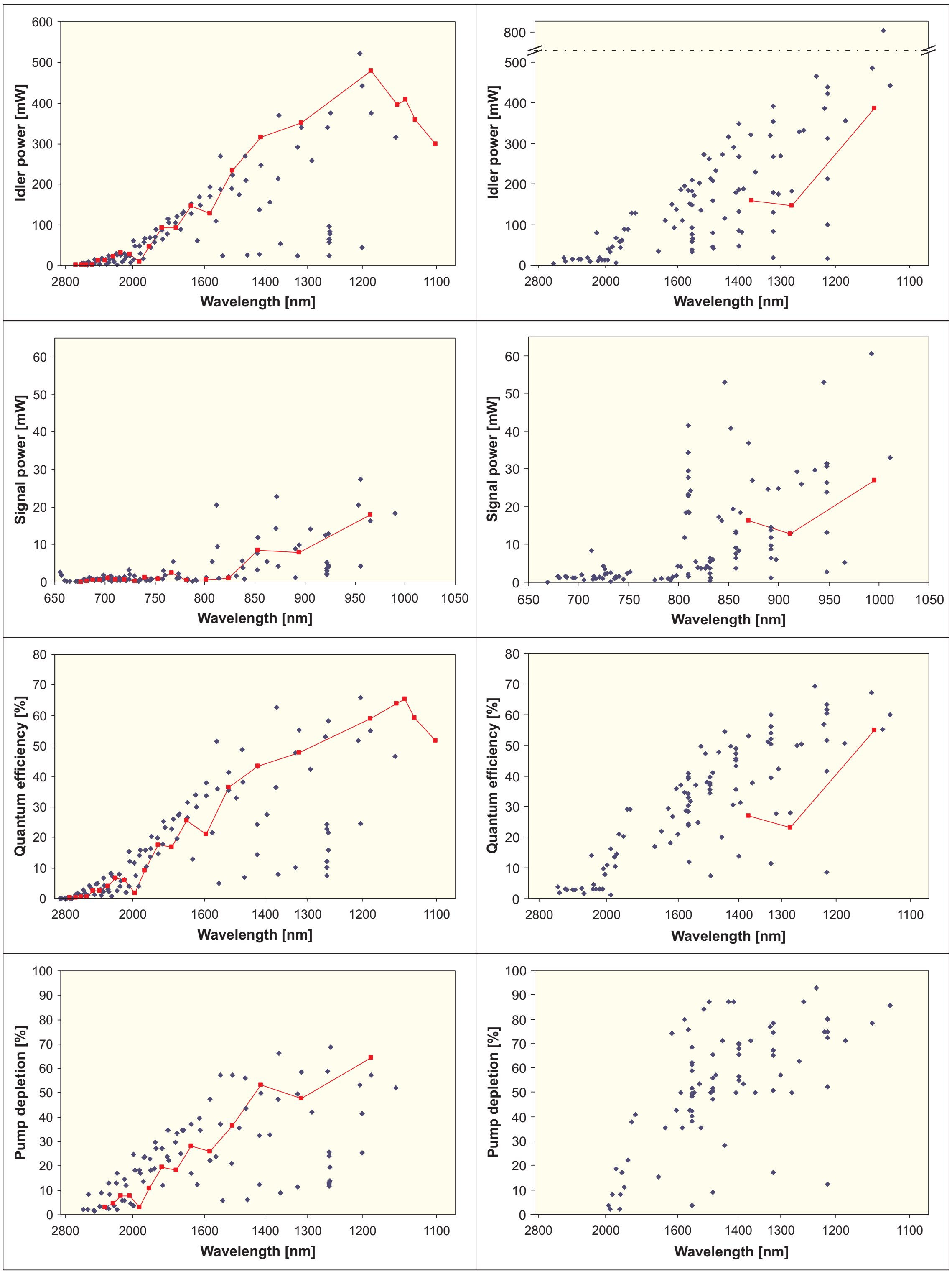

Figure 4.4: Measured idler and signal power, quantum efficiency, and pump depletion for PPLN (left) and PPKTP (right) for pump powers between 0.8 – 3.3 W. Dots: without etalon; connected dots: with 0.5 mm etalon.

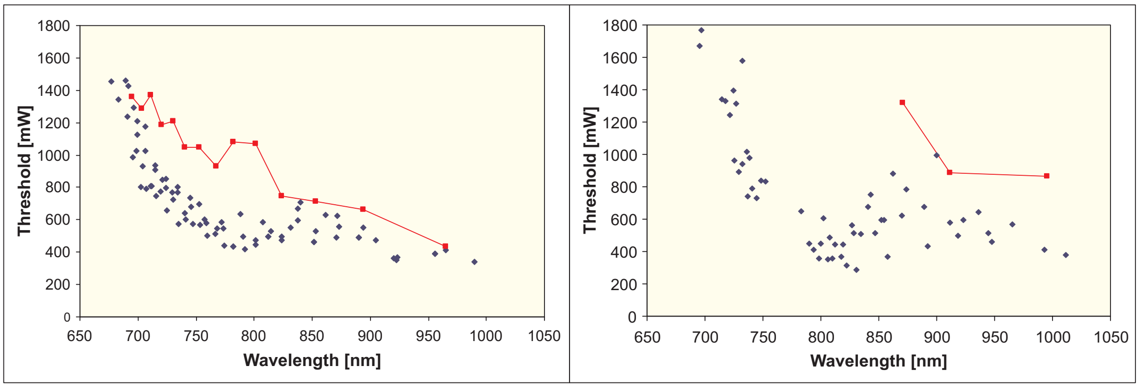

Figure 4.5: Oscillation threshold for PPLN (left) and PPKTP (right). Dots: without etalon; connected dots: with 0.5 mm etalon.

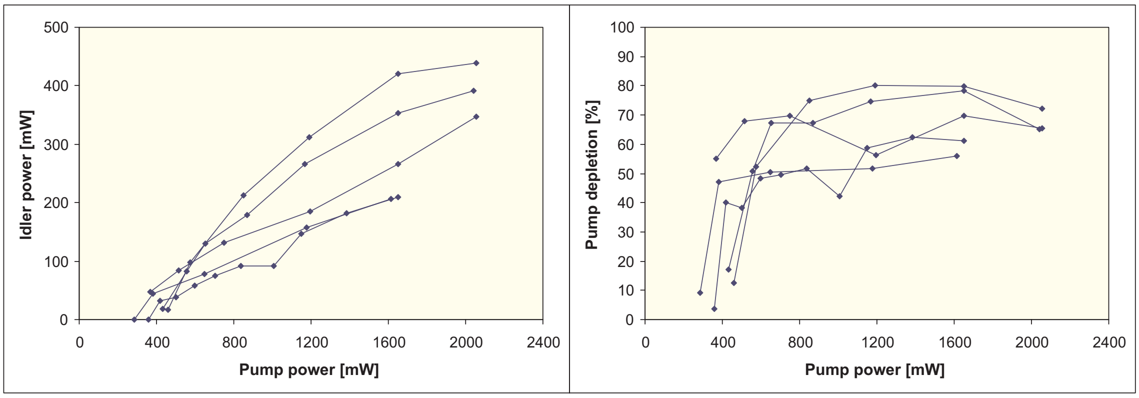

Figure 4.6: Idler power and pump depletion versus pump power measured without etalon for the PPKTP crystal at a wavelength of 1213.6, 1318.4, 1403.7, 1480.3, and 1553.2 nm.

However thermal lenses are expected to be weak at threshold because the resonating signal power is infinitesimal small. Finally it can not be determined what causes the observed deviation.

Photorefractive effects and gray tracking

Strong photorefractive effects occur in PPLN. Visible light creates electron hole pairs which become separated. This creates a space charge field which scatters the light and induces losses. While there exist experiments making use of photorefractive effects, they are to be avoided in an OPO. The electron hole pairs combine only slowly because of the low electric conductivity. The electric conductivity can be increased (and thus the photorefractive effects reduced) by increasing the crystal temperature or by doping with a few percent of MgO. Unfortunately $MgO{:}LiNbO_3$ is very difficult to pole. So the PPLN crystal has to be operated above 140 °C and it shows best efficiency above 200 °C.

The opposite is the case for PPKTP. It does not show any photorefractive effects due to its higher electric conductivity and therefore can be operated at room temperature. This is regarded as a main advantage over PPLN. The drawback of the higher electric conductivity is that it makes periodically poling much more difficult. We found that it operates below 150 °C only and best below 80 °C, which is in contradiction to the observations of other experiments [54]. It could not be determined whether this effect is due to the crystals or the coatings.

In the literature KTP has been reported to show gray tracking, a permanent or non permanent darkening of the crystal, if high power visible light above a threshold of 80 MW/cm^2 (for 10 ns pulses) is present in the crystal [54, 55]. We did not see any evidence of gray tracking in our experiments with one exception: the darkening that occurred to the crystal when it was emitting 800 mW idler (see above) can be interpreted as gray tracking.

4.3 Linewidth and beam profile

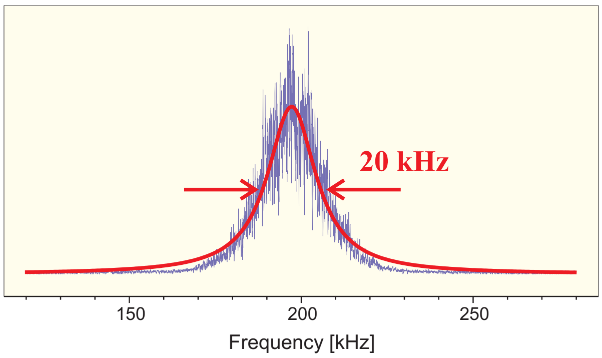

Figure 4.7: Spectrum of beat signal between the OPO signal wave and a 946 nm Nd:YAG laser. The OPO cavity is locked to the laser. 50 ms sampling time.

The linewidth was determined by a beat frequency measurement: The signal of the OPO was set to 946 nm and combined with the beam from a monolithic 946 nm Nd:YAG laser (InnoLight Mephisto QTL 50) at a beam splitter. The interference signal which contained the difference frequency between the OPO and the laser was detected with a fast (1 GHz) photodiode, downconverted with an RF-synthesizer, recorded with a sampling oscilloscope and fast-Fourier-analyzed in a computer.

The OPO signal was frequency locked with a control bandwidth of 4 kHz to the Nd:YAG laser using the fast piezo and the downconverted beat frequency as an error signal. It showed a linewidth of 20 kHz (fig. 4.7), which is one of the narrowest ever measured for an OPO, and which is only $5 \cdot 10^{-11}$ of the total emission range. We also demonstrated the possibility to lock the idler to a stable reference cavity which can be manufactured for any desired wavelength.

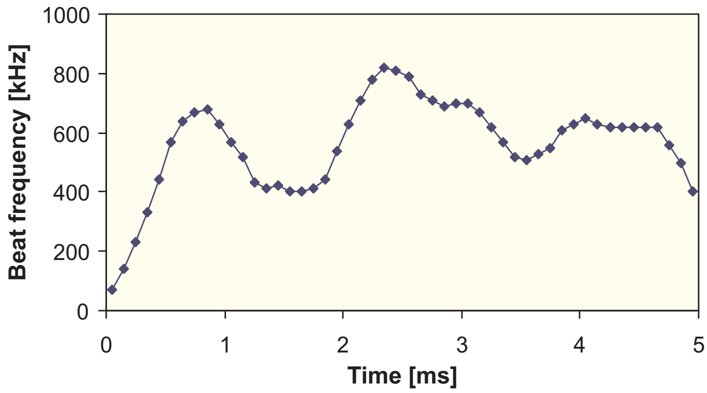

Figure 4.8: Jitter of the beat signal. The OPO is free running.

When the OPO is free running the short term linewidth is 20 kHz over 50 μs with 300 kHz jitter over 5 ms and 5 MHz over 1 s. Fig. 4.8 shows the beat frequency averaged over 100 μs windows during a time of 5 ms. A fast Fourier transform of fig. 4.8 contains mainly frequencies up to 800 Hz what can easily be compensated for using a feedback loop and the fast piezo of the OPO. The idler frequency, which is the difference between the pump and the signal frequencies, is expected to have a similar linewidth but the larger jitter of the pump laser.

Up to 87 % modematching of the idler into the frequency doubler cavity was obtained. That proves the near diffraction-limited mode quality of the idler.

4.4 Continuous tuning

For many applications e.g. spectroscopy it is necessary to tune the laser source continuously (without mode-hops). So far this has been achieved mainly by use of tunable pump lasers. Depending on the OPO configuration the laser tuning is transferred to the signal or idler or both of them [6, 8, 9, 56, 57].

We tune both signal and idler by changing the cavity length using a piezo and synchronously tilting the etalon, which is either controlled by a feedforward or a feedback loop. Note that pump frequency tuning is not necessary. The feedforward loop is simply an electronic attenuator which applies a voltage proportional to the piezo voltage to the galvo drive thereby tilting the etalon. The error signal for the feedback loop is obtained by dithering the etalon at 1.9 kHz with 0.34 mrad amplitude and using the emitted idler power as input for a lock-in amplifier.

A maximum tuning range of 38 GHz for the signal and idler (1.9 cm^{-1}) was achieved for PPKTP (fig. 4.9), limited by the walk-off losses induced by the etalon tilt angle as discussed in section 3.4. This tuning range is 54 times the free spectral range, $2 \cdot 10^6$ times the linewidth, and over twenty times larger than what has previously been achieved with a non-tunable pump [4]. Only Klein et al. [8] achieved a larger tuning range of 56 GHz.

PPLN shows photorefractive effects which cause ripples in the gain profile and memory effects. The output wavelength not only depends on the poling period, crystal temperature and etalon tilt angle but also on the history of the crystal. This distorts the error signal and limits the continuous tuning range to typical values of 5 – 16 GHz. Probably better error signals and further tuning can be obtained by creating sidebands at MHz frequencies using an EOM in the pump beam path, or by using a feed forward loop which tilts the etalon proportionally to the square root of the piezo displacement as discussed in section 3.4.

A much larger tuning range will require using an air-spaced etalon which can be tuned piezoelectrically thus avoiding walk-off losses. For more than 300 GHz tuning the gain profile of the OPO has to be moved synchronously with the transmission profile of the etalon by changing the crystal temperature. Additionally an even larger piezo has to be used.

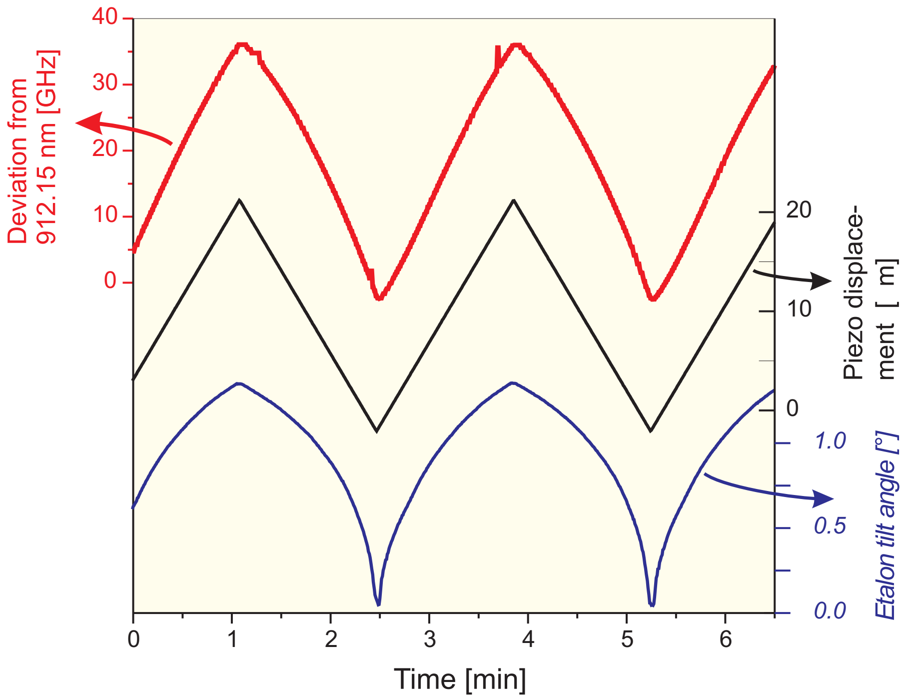

Figure 4.9: Continuous tuning of the PPKTP OPO, with closed loop control of etalon tilt. Pump wavelength is fixed. The spikes are probably due to wavemeter malfunction.

4.5 Frequency and power stability

A high long-term frequency stability can be achieved by locking the OPO cavity length to the pump laser as described in section 3.3.1. Due to the low pump frequency drift the signal and idler frequencies are then stable with a drift $< 50\,\mathrm{MHz/h}$ as shown in fig. 4.10. Similar results were obtained on many different wavelengths for up to 4 hours. When the OPO is free running, it shows a mode-hop of one free spectral range (680 MHz) typically every 10 minutes. By monitoring the interference signal imprinted on the pump beam that is reflected off mirror M1 it has been verified that this is purely due to thermal expansion of the mechanical setup.

The output power of the PPLN OPO decreases by about 10 %/h. After at most 4 hours of operation on the same frequency, the OPO turns off completely. It recovers after moving the crystal or turning the pump off for some hours. Photorefractive effects are assumed to be responsible for this effect.

The longest period of mode-hop free operation obtained for the PPKTP crystal was 20 minutes. At present it is not understood what is limiting this time.

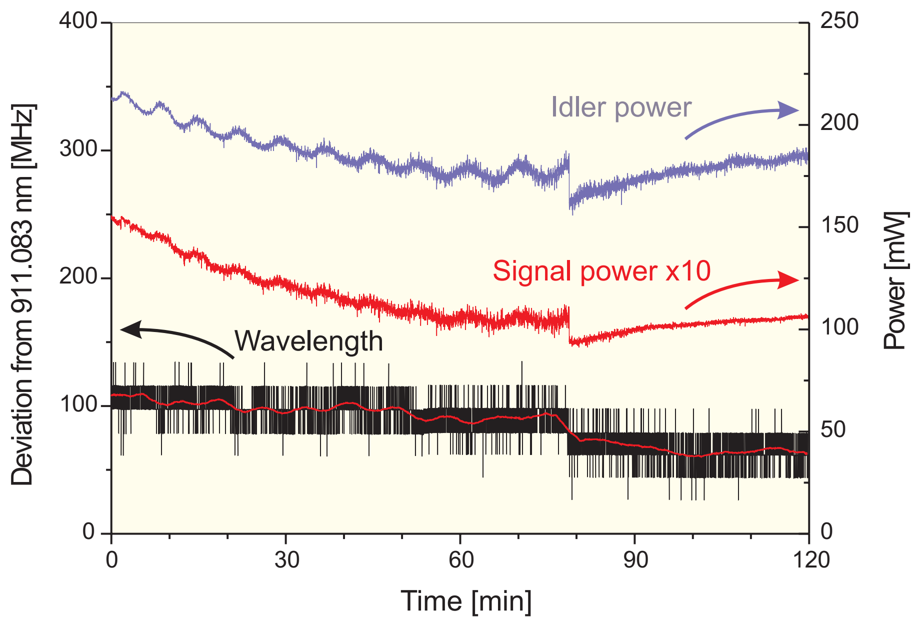

Figure 4.10: Frequency and power stability of the PPLN OPO over 2 hours.

4.6 Comparison of the nonlinear materials

The simultaneous use of PPLN and PPKTP allowed for a direct comparison of their performance. Let us summarize and contrast properties that have been discussed above:

- PPLN has higher gain and higher losses than PPKTP. Thus the emitted signal power is lowered by a factor of 2, while threshold, idler power, and signal power that could be extracted using an optimized output coupler are comparable. PPLN almost reaches the same emission range and output power with and without etalon. This is not the case for PPKTP.

- The thermal lenses are 5 times stronger in PPLN. So stable operation only is obtained with an etalon or far from degeneracy, while PPKTP always runs stably. The output power is limited by thermal lenses for PPLN and by the damage threshold of the crystals or the coatings for PPKTP.
- PPLN shows photorefractive effects. Thus it reaches best efficiency above 200 °C. Memory effects and ripples in the gain profile limit the continuous tuning range. PPKTP, which does not show photorefractive effects, reaches best efficiency below 80 °C and its smooth gain profile allows for a large continuous tuning range.
- Large area, high quality PPLN crystals are readily available from several different manufacturers in large quantities. In contrast, it is still difficult to manufacture large multigrating PPKTP crystals. There are only few scientific and commercial suppliers for PPKTP worldwide.
- All of the PPLN crystals we used are still intact. No decrease in efficiency for PPLN was observed for more than six months of operation. However, we encountered damage for two PPKTP crystals at high temperatures and high power. We do not have experience with long term operation for PPKTP.

The final question about which material to choose is difficult to answer. There are advantages and disadvantages for both of them. For the application in which we used the OPO as a light source only to set up the frequency doubler we choose PPLN because of the better frequency stability.

The reliability as well as possible future improvements will be discussed in sections 4.8 and 4.9.

4.7 Frequency Doubler

The frequency doubler converts part of the idler spectrum into visible light and thus covers a spectral region that was previously only obtained from dye lasers.

4.7.1 Bandwidth

The frequency doubler extends the spectral coverage of the OPO system into the red, orange, yellow and green spectral range from 550 – 770 nm. This overlaps with the signal emitted by the OPO directly, thus leaving no gaps in the optical spectrum. The total spectral spanning factor is 5.1 !

To our knowledge, this is the most broadband frequency doubler ever built. The bandwidth is limited by the mirror coatings on the red side and by the idler range of the OPO on the green side. The frequency doubler itself is designed to generate wavelengths down to 532 nm.

The Sellmeier equation by Jundt [42] predicts the phasematching temperatures correctly within 1 °C at a fundamental wavelength of 1100 nm and 14 °C lower than those measured (corresponding to 2.4 nm) at 1540 nm. The predictions of the equation by Edwards and Lawrence [43] show larger deviations.

4.7.2 Efficiency

The output power and doubling efficiency is shown in fig. 4.1 and 4.11. The power reaches up to 70 mW corresponding to a doubling efficiency of up to 23 %. The decrease in power and efficiency at longer wavelengths is due to the lower OPO power as well as the ω^3-dependence of the doubling efficiency. The reduced efficiency around 650 nm is due to excess resonator losses probably originating from the crystal

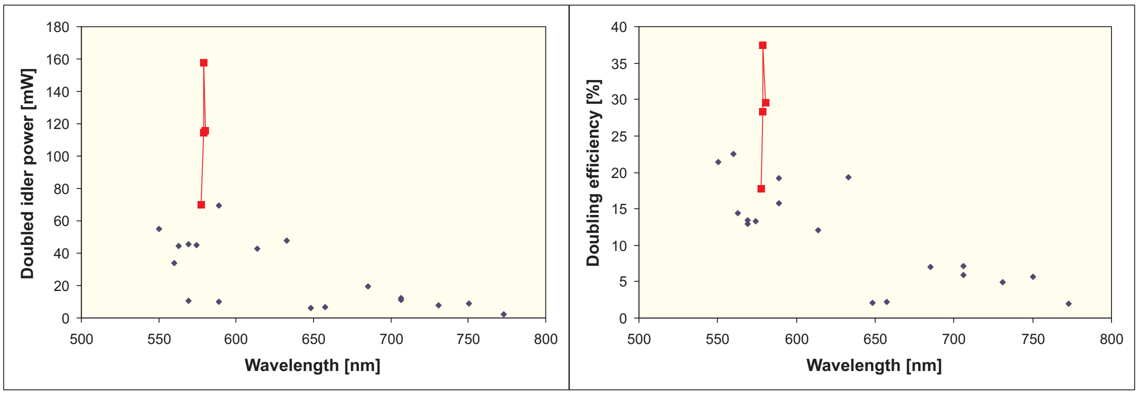

Figure 4.11: Output power and efficiency of the frequency doubler for idler powers between 62 – 422 mW. Dots: with 1.7 % input coupler; connected dots: with 5 – 36 % input coupler.

coatings. The overall efficiency is lower than expected because the input coupler (1.7 % transmission) was optimized for input powers of 30 mW only and the crystal losses are higher than expected. With another input coupler providing impedance matching 160 mW of yellow light at 580 nm were obtained.

The power stability is shown in figure 4.12. The slight decrease in output power is purely due to the decrease in idler power while the doubling efficiency remains constant.

The power circulating in the resonator and the round trip losses can be determined from the input coupler transmission, the modematching, and the incoupling of the idler into the SHG resonator. The linear losses were found to be 4 – 5 % per round trip. About 1 % can be attributed to mirror losses so that the crystal losses must be 3 – 4 %. This is much more than what has been reported in the literature [43]. Therefore the 1.7 % input coupler does not provide impedance matching and the incoupling is 25 – 70 % only.

With the idler power P_{circ} that is actually circulating in the resonator, the expected second harmonic power is

$$P_{2\omega} = \frac{2}{\pi} \frac{\mu_0}{c^2} \frac{\omega^3 d_{\mathrm{eff}}^2 L}{n_\omega n_{2\omega}} h_{\mathrm{BK}} \, P_{\mathrm{circ}}^2 \quad , \tag{4.1}$$

where $d_{\mathrm{eff}} = d_{33} \cdot 2/\pi = -17.2\,\mathrm{pm/V}$ and $L = 43\,\mathrm{mm}$ is the crystal length [20]. The experimentally obtained powers are between 40 – 95 % of this theoretical maximum.

Impedance matching was obtained by replacing the 1.7 % input coupler with a

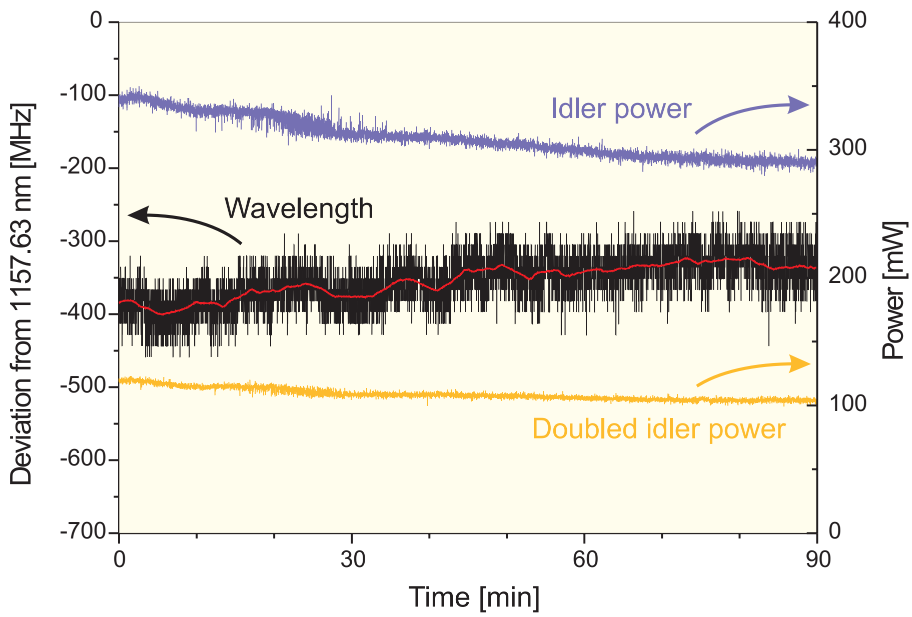

Figure 4.12: Frequency and power stability of the PPLN OPO and frequency doubler over 1.5 hours.

15 % input coupler which was only available at 1160 nm.[1] This increased the output power to 160 mW at 580 nm with an efficiency of 37 % (69 % incoupling). As shown as line in fig. 4.1 a similar increase in output power to a level above 100 mW over most of the emission range can be obtained for all wavelengths using a broadband 15 % input coupler. A further increase in efficiency can be obtained by using shorter crystals.

4.7.3 Practical operation

Operating the frequency doubler is absolutely straight forward once the OPO is running stably. The appropriate crystal position and phase matching temperature is set according to table A.3 and has to be fine-adjusted experimentally to optimize the conversion efficiency. For each wavelength some minor realignment is necessary to compensate for the dispersion of the modematching lenses. A modematching of up to 87 % has been achieved. The cavity length is locked to the idler wavelength simply by closing the feedback loop.

The phase matching bandwidth has been measured to be 0.9 °C (FWHM at 1180 nm), which is in reasonable agreement with theory. A bandwidth of 0.5 °C can be expected, neglecting the effects of impedance matching and pump depletion. No effect of thermal lenses or photorefractive effects has been observed when operating the frequency doubler.

[1] Actually, it was a high reflecting mirror for 1064 and 1083 nm and the OPO was tuned to a wavelength for which the mirror transmission provided impedance matching.

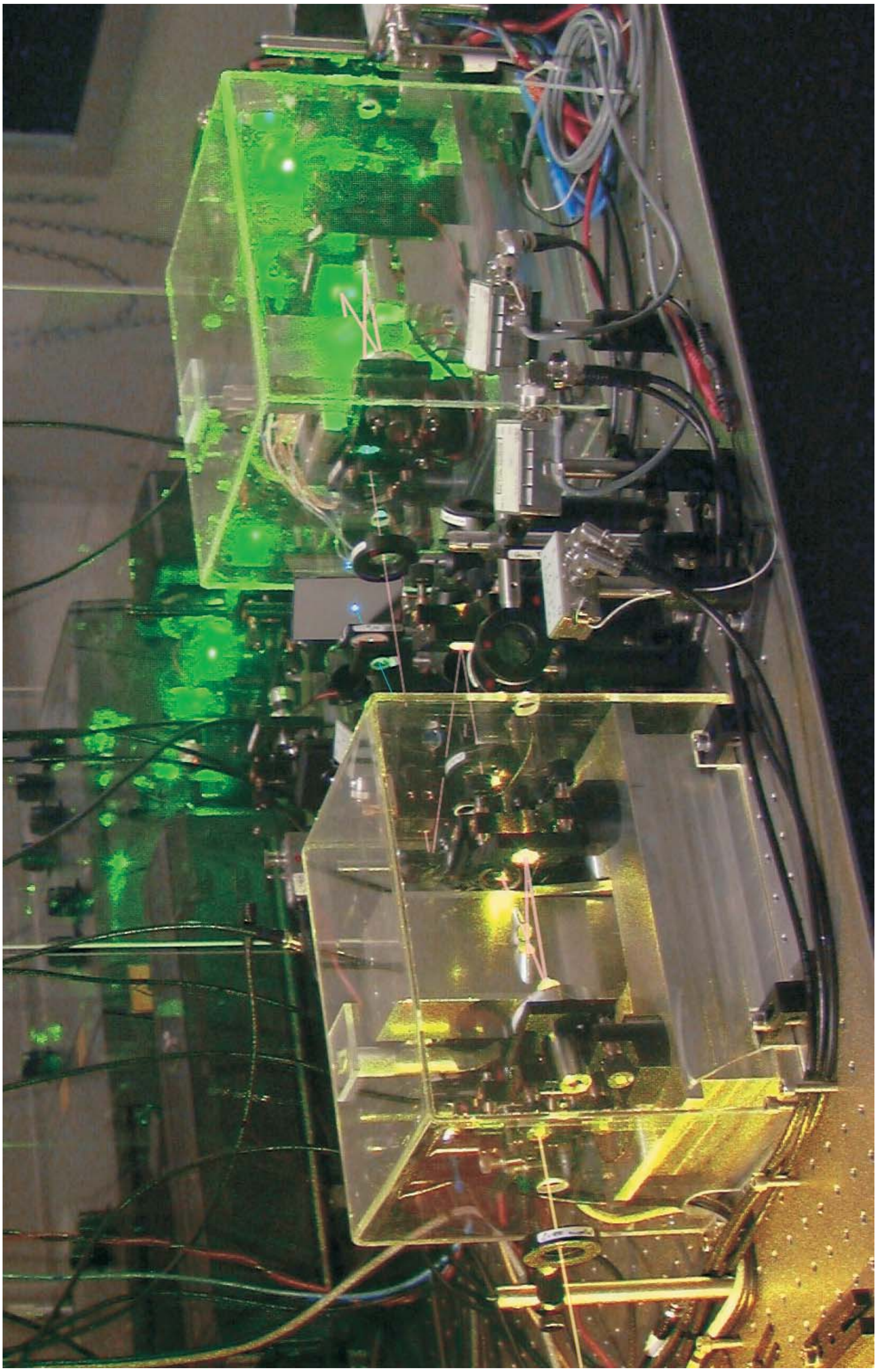

Figure 4.13: OPO (right) and frequency doubler (left) in operation. The blue spot in the middle is the second harmonic of the signal. The laser beams are retouched.

4.8 Reliability

With this system we have demonstrated all properties that are desirable for an ideal cw light source. It is the zeroth iteration of development and was designed as a scientific research project. But how does the system perform for applications where reliability and ease of use are crucial aspects?

Using the OPO system is comparatively easy. It is possible to turn it on and access any desired wavelength within ± 400 GHz in a few minutes and within less than 1 GHz in a few hours. Only minimal day-to-day realignment is necessary thanks to the high stability of the pump laser and the mechanical setup, even though the system is located in a room without air conditioning.

However, the system was neither intended to be nor is a turn-key device. A user will have to spend a certain fraction of the daily work time on the OPO especially if it is to be stabilized to a frequency reference or to be tuned continuously. Tuning will become easier with optimized control electronics.

We have been operating the OPO for several months and we were able to access any desired wavelength reliably with a reasonable output power and stability. We believe that the linewidth, which was measured at only one wavelength, will be constant over the entire emission range. In contrast, the achievable continuous tuning range does depend on wavelength.

The device has been running with the same PPLN crystal for more than six months without any damage or decrease in efficiency.

4.9 Future improvements

Although this OPO shows excellent performance, it could probably be improved by use of stoichiometric lithium tantalate (SLT) or gray-track-resistant KTP, two new nonlinear materials which are currently being developed and which will be available in the near future.

Stoichiometric lithium tantalate

Traditionally only congruent lithium niobate (CLN) was available, which is 48.5 % Li and 51.5 % NbO_3 and thus has many crystal defects. Stoichiometric lithium niobate and tantalate (SLN, SLT) are newly developed materials consisting of 50 % Li and 50 % NbO_3 or TaO_3 respectively. First measurements indicate that especially SLT shows much less photorefractive effects, hardly any GRIIRA, and is easier to pole than CLT or CLN due to its 10 times lower coercitive voltage [58, 59].

However up to now no short poling periods suitable for frequency conversion of visible light have been demonstrated, the Sellmeier equations are not known precisely, and the raw material is one order of magnitude more expensive than CLN. Nevertheless we expect samples of periodically poled SLT to be available to the scientific community in 2002.

If the material meets our expectations we are quite certain that it will improve the performance of the OPO in terms of long term stability, output power, and possibly even tunability.

Gray track resistant KTP

Efforts are underway to make KTP (more) resistant against gray tracking and thus make it suitable for even higher powers of visible light. At present it seems to be very difficult to pole this material. But once the crystal manufacturers have solved this problem gray track resistant KTP might improve the performance of the OPO, especially with respect to the output power.

Other improvements

Apart from the choice of material, there are some minor improvements that might be implemented in the next step of development:

Both signal and doubled idler power will increase to well above 100 mW with optimized out- and incoupling mirrors as discussed in section 4.2 and 4.7.2.

A pump depletion of up to 93 % indicates that the nonlinear crystals are longer than necessary. Shortening the crystals to a length of 10 to 15 mm will also reduce the thermal lenses and thus increase the output power by an estimated factor of 1 – 2.

The losses induced by tilting the etalon (see section 3.4) can be avoided by using an air-spaced etalon with a piezo. A thicker etalon and a smaller OPO resonator (larger free spectral range) will improve frequency stable operation and tunability.

The efficiency of the nonlinear crystals can be optimized by moving them vertically and horizontally through the beam path. To make use of that degree of freedom a horizontal translation stage should be added to the OPO.

The OPO is locked to the pump laser to compensate for thermal drifts in the cavity length. This is not necessary if the temperature of the baseplate of the mechanical setup is stabilized.

Tuning the OPO will become much easier by creating sidebands at MHz frequency using an EOM or by controlling the etalon using an optimized feed-forward loop as discussed in section 4.4.

3 – 4 W of pump laser power is sufficient to operate the OPO. We used a 10 W Verdi laser only because it was available.

We believe that the optical isolator can be removed because the OPO is set up with a ring cavity.

To avoid the need for realignment of the frequency doubler after changing the wavelength, achromatic lenses should be used to couple the light from the OPO into the doubler.

The efficiency of the frequency doubler can be increased substantially by employing an optimized input coupler and shorter crystals as discussed in section 4.7.2.

38 GHz of continuous tuning range have been demonstrated with the OPO. But the tuning range of the frequency doubler is limited to 15 GHz by the piezo stroke. This limitation can be overcome by adding a larger piezo. A tuning range of 200 GHz can be achieved without the need for changing the crystal temperature.

4.10 Application: Iodine Spectroscopy

To demonstrate the versatility and reliability of the light source it was used to perform a spectroscopy experiment. Doppler free spectroscopy of the hyperfine spectrum of molecular iodine (I_2) in the yellow spectral range was chosen because the iodine spectrum is well known and thus gives the chance to demonstrate the performance of the complete OPO system, including the frequency doubler. The results will be published in [77].

The experiment was set up as a frequency-modulation-spectroscopy in standard pump and probe technique. The beam was frequency modulated using the EOM in front of the frequency doubler and the same frequency (12.7 MHz) that also was used for locking the doubler. Additionally the Doppler-broadened background was suppressed by chopping the pump beam at a frequency of 46 kHz using an acousto-optic modulator and a lock-in amplifier. The OPO wavelength was varied by slowly scanning the piezo at a frequency of 50 – 100 mHz. The iodine was contained in a 10 cm long glass cell at room temperature with Brewster windows.

A spectrum measured at 579.6605 nm (17251.477 cm^{-1}) is shown in fig. 4.14. It shows a linewidth of $\approx$ 6 MHz, which is mainly determined by pressure broadening (11 MHz/mbar) and the jitter of the OPO ($\approx$ 5 MHz) which, for convenience, was not compensated for. The natural linewidth is 380 kHz [60].

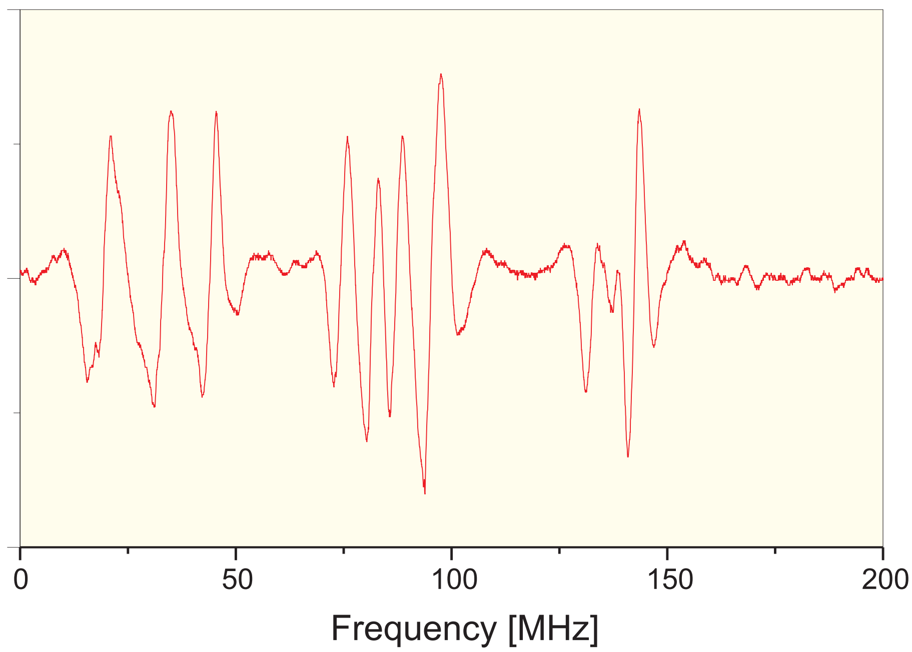

Figure 4.14: Hyperfine spectrum of molecular iodine at 579.6605 nm.

Chapter 5

Other OPO Projects

Summary

In this chapter we describe two OPOs developed earlier to the one presented in the last two chapters. Both are configured as singly resonant OPO with pump-wave enhancement (PR-SRO) in a linear standing wave cavity and pumped by a single-frequency 532 nm laser.

One of them uses periodically poled $LiTaO_3$ (PPLT) multigrating crystals. It shows an emission range from 0.77 to 1.73 μm which at the time was unprecedented. Up to 60 mW output power, mode-hop free operation for up to 50 minutes, and a low frequency drift (< 70 MHz/hour) have been obtained. Thus it was the first cw OPO pumped in the visible and emitting in the near-IR that was stable, widely tunable, and single-frequency. These are crucial aspects for many applications, including spectroscopy, metrology, and the characterization of optical components.

The second OPO was based on periodically poled $KTiOPO_4$ (PPKTP) which has emerged recently as a new nonlinear material. It shows a high nonlinearity and no photorefractive effects and thus is an interesting alternative to PPLN and PPLT. The OPO has an emission range from 865 to 1384 nm with a single 9 μm period grating, output powers up to 72 mW and up to 69 minutes of mode-hop free operation. The main goal of this project was to gain experience with PP-KTP and examine its usability for high power short wavelength cw frequency conversion.

As a pump source for future high power OPOs we set up a 10 W cw single-frequency narrow-linewidth Nd:YAG laser based on a commercial system developed for the LIGO gravitational wave interferometer. To obtain high power 532 nm radiation we implemented three different methods to frequency double the output of this laser and we characterized a commercial 532 nm Verdi laser.

5.1 Singly-resonant OPO using PPLT

The goal of this project was to set up a widely tunable cw single-frequency narrow-linewidth OPO pumped in the visible and emitting in the near infrared. Until 1999, when this project was carried out, such a device had not been demonstrated.

To achieve this goal we set up a semimonolithic pump-resonant singly-resonant OPO (PR-SRO) pumped at 532 nm. We use periodically poled $LiTaO_3$ (PPLT) which has emerged as a new nonlinear material for frequency conversion of both short wavelength and near-IR radiation. It is used here, to our knowledge for the first time in a visible-pumped OPO. This project is published in Optics Letter [61].

Setup

A schematic of the setup is shown in fig. 5.1. As a pump source we use a diode-pumped monolithic Nd:YAG ring laser with a single-frequency output power of 1.35 W at 1064.52 nm, a linewidth of approximately 1 kHz and a typical frequency drift of 100 MHz/hour. The output frequency can be slowly tuned over a range of 8 GHz by controlling the laser crystal temperature. A Faraday isolator is used to prevent back-reflection into the laser.

The laser is externally frequency-doubled in a semimonolithic bulk $MgO:LiNbO_3$ resonator. The resonator is locked to the laser using a Pound-Drever-Hall technique and a piezo mounted mirror. The error signal is generated by electro-optically modulating the doubler crystal at 6 MHz [62]. After passing through another Faraday isolator and focusing optics, 450 mW of green light at 532.26 nm is available for pumping the PR-SRO.

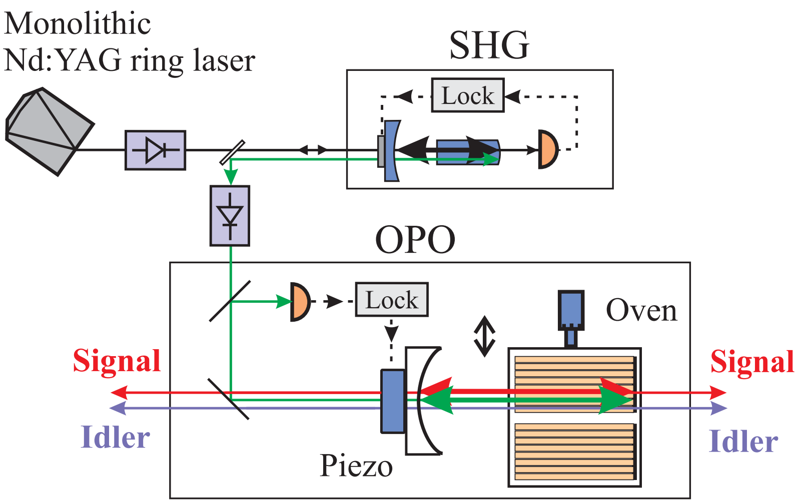

Figure 5.1: Experimental setup of the PPLT PR-SRO. One endface of the crystals is coated to act as resonator mirror. Signal and idler are emitted on both sides of the resonator.

The OPO is resonant for both signal and pump. It is configured as a semimonolithic linear standing-wave resonator, formed by one mirror coated directly onto one flat endface of the nonlinear crystals and an external mirror mounted onto a piezo translator. The broadband dielectric mirror coated onto the outer endface of the crystals provides a reflectivity of 99 % for the pump (532 nm), > 99.7 % for the signal (670 – 1030 nm) and < 20 % for the idler (1100 – 2600 nm). The inner endface is antireflection coated with residual reflectivities < 0.5 %, < 0.5 % and < 20 % for pump, signal and idler, respectively. The external mirror has a radius of curvature of 25 mm and provides reflectivities of 95.5 %, > 99.7 % and < 20 % for pump, signal and idler, respectively.

As nonlinear material we use two periodically poled $LiTaO_3$-multigrating crystals, produced by Jan-Peter Meyn in Kaiserslautern. Each is 25 x 25 x 0.5 mm in size, with altogether 35 different poling periods from 7.3 to 10.7 μm. To reduce photorefractive effects the crystals are heated in a copper oven to temperatures between 160 and 240°C with a temperature stability of 5 mK.

The OPO resonator is locked on resonance with the pump frequency via a Pound-Drever-Hall technique, where the phase modulation of the pump is obtained by

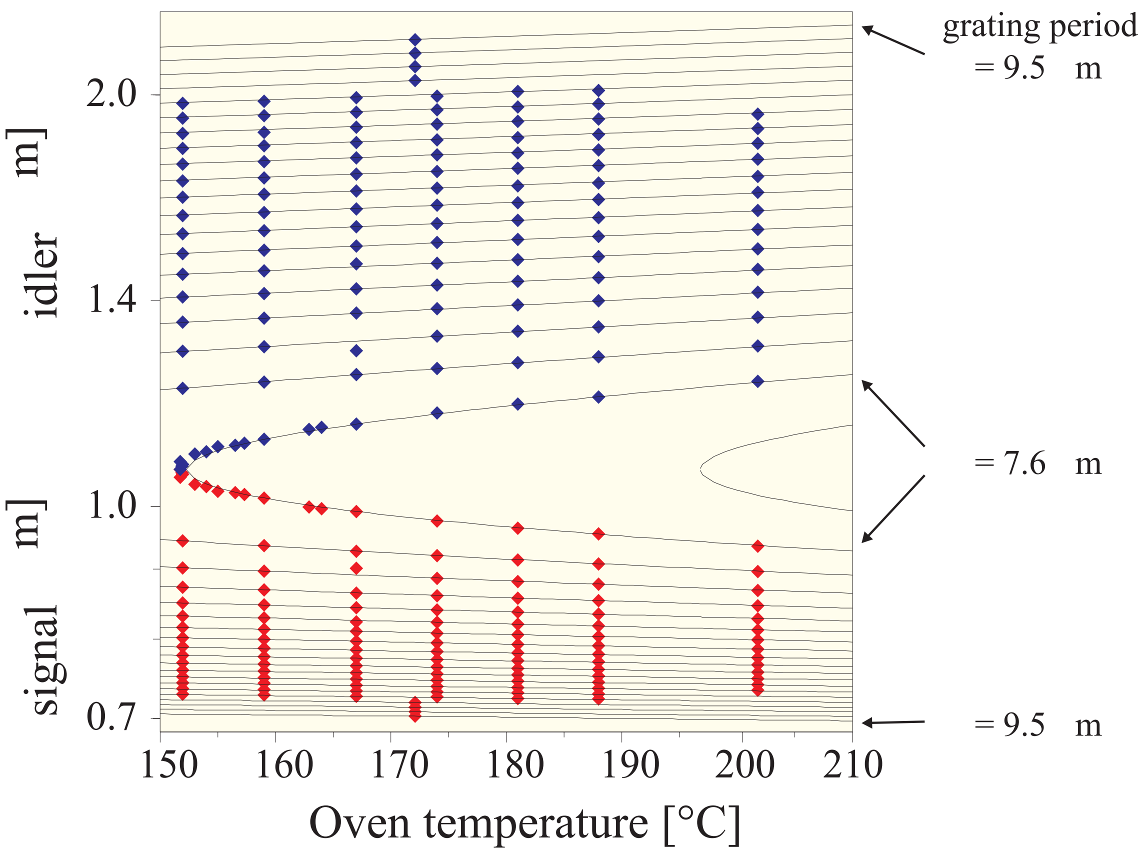

Figure 5.2: OPO output wavelengths as a function of poling period and of oven temperature: Squares: data, shifted by -8 K; lines: theory.

electro-optic modulation of the frequency doubler crystal at an additional frequency of 14.5 MHz. A round-trip pump absorption of $V_p \simeq 8\,\%$ in the OPO crystal causes the crystal temperature and therefore the cavity optical length to change by about one free spectral range within 1 ms when the cavity length is locked. Despite these thermal effects a stable cavity lock was achieved by increasing the servo loop control bandwidth to 12 kHz and by actively compensating for the change in optical path length with a feed-forward system.

The external threshold of a PR-SRO is

$$P_{th} = \left(\frac{T_p + V_p}{T_p}\right) \frac{(T_p + V_p)(T_s + V_s)}{8\,E_{sp}}\,, \tag{5.1}$$

where T_p is the pump input mirror transmission, T_s is the signal outcoupling mirror transmission, V_p and V_s are the pump and signal round-trip losses, and E_{sp} is the effective single-pass nonlinearity [22]. We have measured $T_p = 4.5\,\%$, $V_p \simeq 8\,\%$ and estimate $T_s + V_s \simeq 1.5\,\%$. With $d_{33} = -14\,\mathrm{pm/V}$ for $LiTaO_3$ [31] and a focal waist of 37 μm on the flat end face of the crystal, a nonlinearity E_{sp} varying between 1.1 %/W near degeneracy and 0.6 %/W at $\lambda_s = 0.7\,\mu$m is calculated, leading to an estimated external threshold between 59 and 111 mW.

Experimental results

Fig. 5.2 shows the emission range where oscillation was reached on different poling periods and temperatures while scanning the cavity length. The range extends from 0.70 to 2.20 μm. The output wavelengths coincide within 6 nm with the ones calculated from a published Sellmeier equation [31] if one allows for an -8 K offset

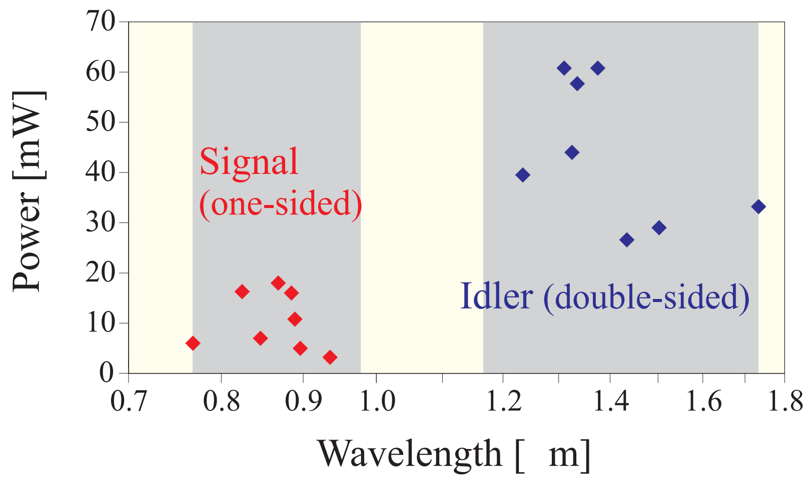

Figure 5.3: Emission range (shaded regions) and output power of the PR-OPO in stable operation. The signal power refers to the output on the crystal side, the idler power is emitted in equal parts on both sides of the cavity.

of the temperature measurement. Emission occurred also near degeneracy, where the cavity is resonant for both signal and idler. At 9 discrete wavelengths the OPO crystal provides quasi phase-matching in 2nd, 3rd, 4th or 5th order for SHG of the signal producing up to 14 mW peak power of blue light between 365 and 474 nm in scanned operation. At 12 wavelengths the SFG of signal and pump is quasi phase-matched in 5th to 9th order producing UV light between 310 and 341 nm. The phase-matching temperatures for these processes coincide with the expected ones within 3 K, confirming the published Sellmeier equation.

On 9 gratings with poling periods from 7.6 to 8.4 μm a stable OPO cavity lock was obtained. In cw operation the threshold was found to increase relative to scanned operation, resulting in a reduced emission range from 768 – 978 nm for the signal and from 1167 – 1733 nm for the idler. The external oscillation threshold P_{th} varies between about 100 mW near degeneracy and 350 mW at the edges of the emission range. Fig. 5.3 shows the output power at a pump power of 450 mW. The maximum idler output power corresponds to an internal photon conversion efficiency of 70 % with respect to the actual incoupled power (50 % of incident power). The maximum total power conversion efficiency of pump to signal plus idler is 22 %. Threshold and efficiencies agree within a factor of 2 with the estimated values when the 85 % modematching of the pump is taken into account. Over the whole emission range, blue light from 384 – 489 nm at a level of μW was generated by non-phase-matched SHG of the signal.

The OPO runs stably for extended periods of time as shown in fig. 5.4. The longest

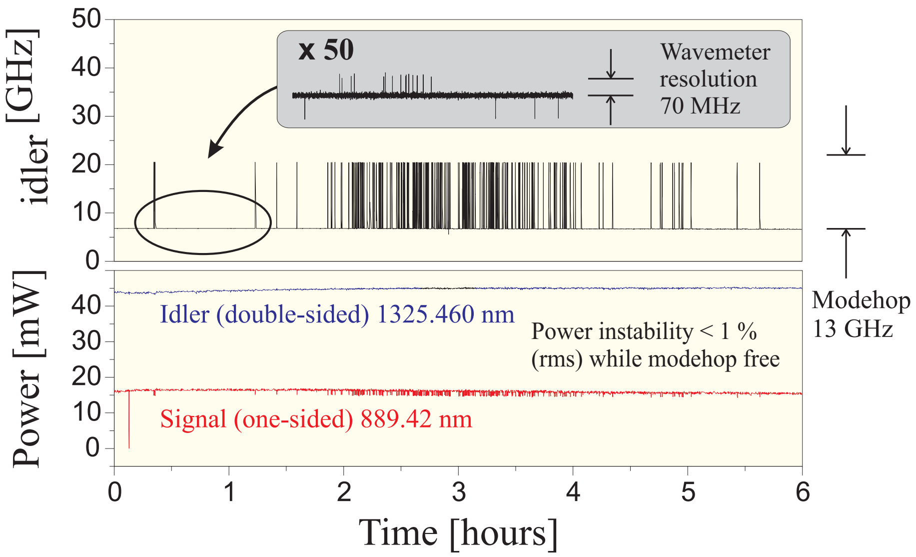

Figure 5.4: Long-term measurement of idler frequency, measured with a high-resolution wavemeter (Burleigh WA 1500) and output powers. A slow drift in pump wavelength or crystal temperature causes the signal frequency to jump between two cavity modes spaced 6 free spectral ranges apart, with corresponding idler frequency change.

time without mode-hops was 52 minutes. As long as there are no mode-hops the frequency drift is less than 70 MHz/hour (see inset in fig. 5.4), which is an upper limit set by the finite resolution of the wavemeter employed. The rms fluctuations of the signal and idler power are below 1 %. The figure shows that upon a mode-hop, the idler frequency changes by 13 GHz, corresponding to 6 free spectral ranges of the OPO, with opposite change of the signal frequency. This large jump is probably due to a parasitic etalon between the AR-coated crystal endface and the external mirror.

Signal and idler frequency can be tuned continuously by tuning the pump frequency. The tuning coefficients are $d\nu_{s/i} \,/\, d\nu_p \approx \nu_{s/i} \,/\, \nu_p$. The largest continuous tuning range measured was 400 MHz for the idler, corresponding to 700 MHz for the signal (see fig. 5.5).

After four days of operation the glue that mounts the external mirror to the piezo failed and the OPO could not be locked any more. To increase the reliability the electronic control bandwidth should be increased further by using a fast piezo with a high slew rate, an EOM, or by locking the pump laser to the OPO for high control frequencies and vice versa for low frequencies.

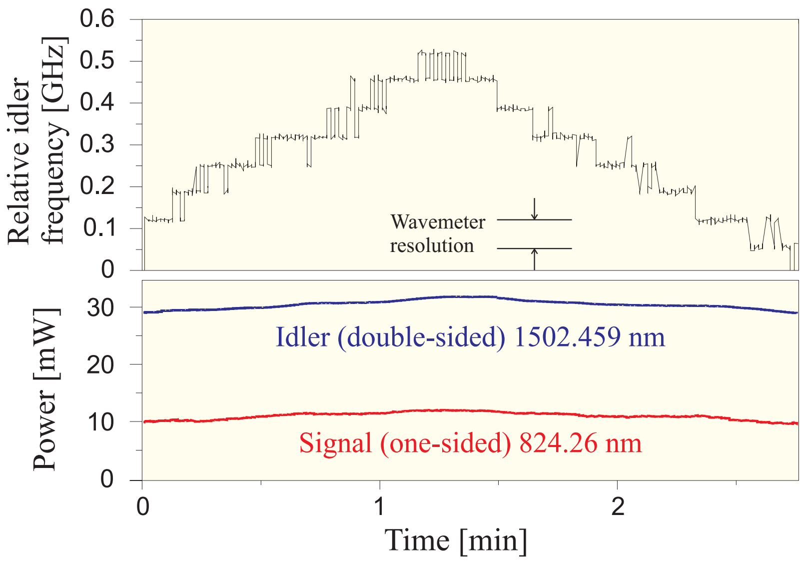

Figure 5.5: Idler frequency tuning via tuning the pump frequency by 1.1 GHz, and output powers.

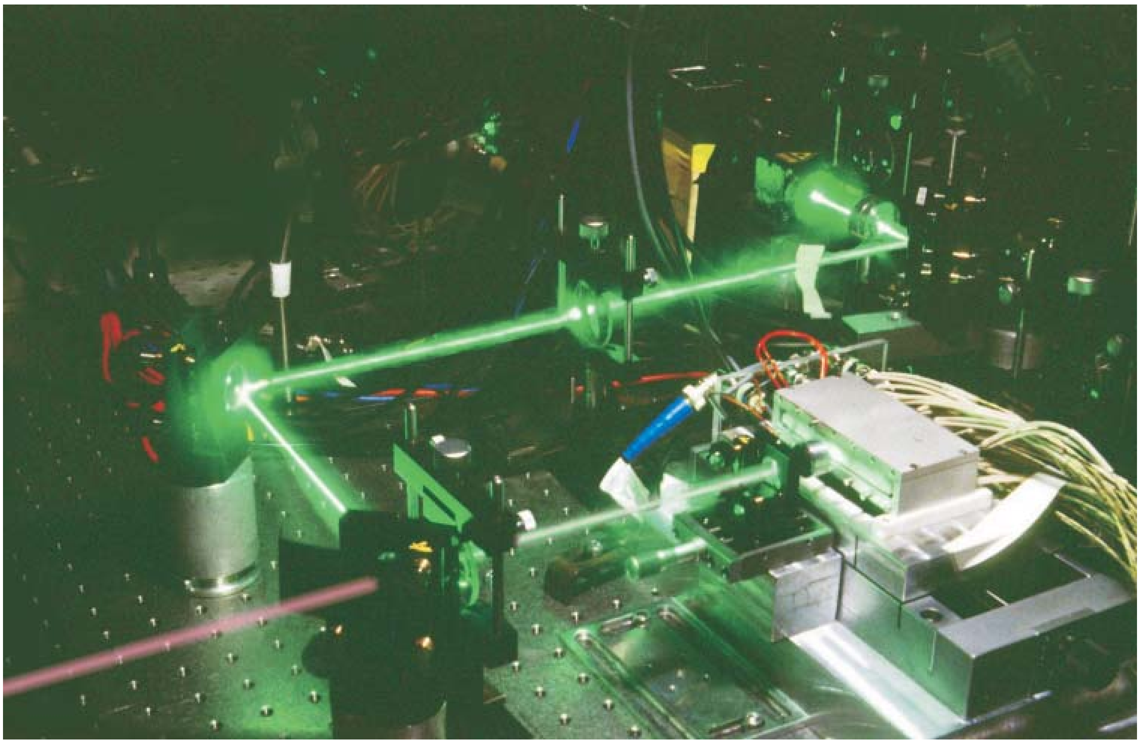

Figure 5.6: Photo of the PPLT OPO. The OPO resonator is at the right in the front. Photo: H. Schnitzler, retouch: H. Hansen

5.2 Singly-resonant OPO using PPKTP

We built another pump-resonant singly-resonant cw OPO using a PPKTP crystal which we had obtained via a collaboration from Tel Aviv University. The main goal here was to examine the usability of this relatively new material for high power cw frequency conversion with short wavelengths over a large temperature range. Progress in the electric field poling of flux-grown KTP had made PPKTP a very promising candidate [35, 63]. With its high nonlinearity of $|d_{\mathrm{eff}}| \approx 9.5\,\mathrm{pm/V}$, PPKTP is an interesting alternative to PPLN and PPLT. We took advantage of the fact that PPKTP does not show photorefractive effects and therefore can be operated near room temperature. This project has been published in Optics Communications [64].

Setup

The flux-grown crystal used in this device was obtained from North Crystal Materials Corp. (Beijing, China) and structured at Tel Aviv University by low temperature electric field poling [35]. It has a length of 10 mm and a poling period of $9\,\mu$m, which gives phasematching for second harmonic generation of 1064 nm light near room temperature [65].

Fig. 5.7 shows a schematic of the experimental setup. The SRO is pumped by the frequency-doubled Nd:YAG laser system described in section 5.3.1 and 5.3.2. A Faraday isolator integrated in the laser system prevents back-reflections from the SRO into the laser.

The OPO resonator consists of two concave mirrors with a radius of curvature of $R = -25\,\mathrm{mm}$. They form a 5 cm long standing-wave cavity with a TEM_{00} waist

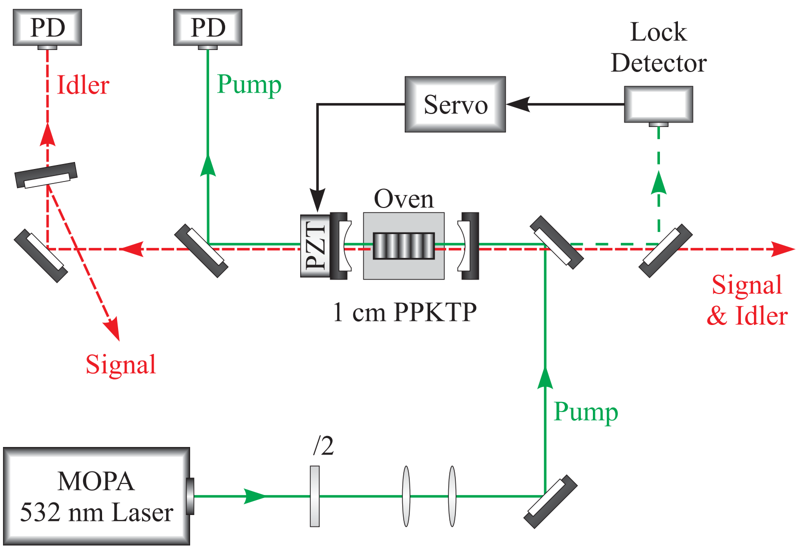

Figure 5.7: Experimental setup of the PPKTP PR-SRO. PD = Photodiode.

of $w_0 = 35.2\,\mu$m for the 532 nm pump. One of the cavity mirrors is mounted on a piezoelectric transducer that allows fine adjustment of the cavity length. The PPKTP crystal with an aperture of 0.5×2 mm is located in the center of the resonator. Its two flat endfaces carry dichroic AR coatings for 1064 nm and 532 nm. Both cavity mirrors are transmitting for the idler ($R < 20\,\%$) and highly reflecting for the signal ($R > 99.7\,\%$).

To keep the external threshold low, the pump wave is also resonated. The reflectivity of the input coupler was measured to be 94.8 % at 532 nm, while the other cavity mirror has a reflectivity of 97.1 % at this wavelength. Together with the observed finesse of $\mathcal{F} = 36$, these values indicate a relatively high absorption loss of 4 % per cm at 532 nm in the PPKTP crystal.

At the output of the SRO, signal and idler waves were separated from the pump by a dichroic mirror. Another dichroic mirror was used to remove any residual signal radiation from the idler wave.

Experimental results

Tuning of the signal and idler wavelengths was achieved by varying the temperature of the PPKTP crystal in an oven that featured an absolute temperature stability of ±0.01 K. For temperatures between 37.5 °C and 225 °C, the idler wavelength was

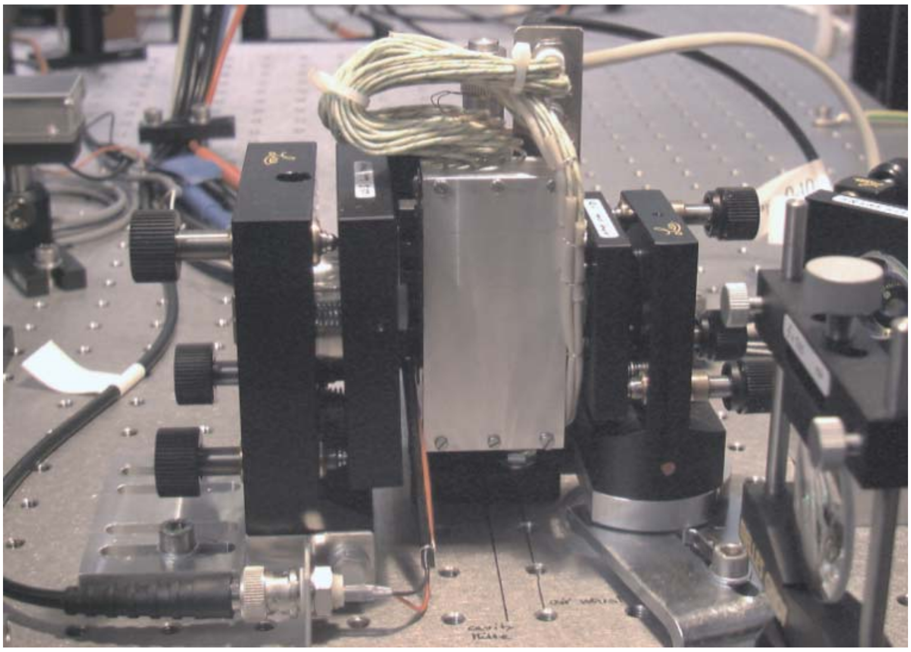

Figure 5.8: Photo of the PPPKTP OPO. The resonator mirrors are in the left and right, the crystal oven in the middle. The OPO is pumped from the right. The signal and idler are emitted in both directions. Photo: D. Weise.

measured with an optical spectrum analyzer (Anritsu MS9701B) while scanning the cavity length using the piezo. As shown in fig. 5.9, idler emission from 1100 nm to 1384 nm was achieved. This corresponds to signal wavelengths between 865 nm and 1032 nm. On the high temperature side, the tuning range was only limited by the heating power of the oven. Oscillation near degeneracy was prevented by the decreasing reflectivity of the cavity mirrors for the signal.

The emission range obtained here exceeds the emission range of all single-grating $LiNbO_3$-SROs demonstrated so far [19]. This is mainly due to the absence of photorefractive effects in PPKTP, so that in contrast to PPLN and PPLT the crystal can be operated near room temperature. The total temperature interval accessible for wavelength tuning is therefore much larger.

Fig. 5.9 also shows theoretical tuning curves calculated from published Sellmeier equations [72, 44, 48]. Since Arie et al. [65] observed phasematching for second harmonic generation of 1064 nm at 35 °C in a PPKTP-crystal with the same grating period, the degeneracy point of each curve was shifted to this temperature. While the prediction according to Fan et al. and Wiechmann et al. [72, 44] is better than the one by Kato [48], the deviations at crystal temperatures above 120 °C indicate that the Sellmeier equations for KTP are still not accurately known.

Typical output powers of the SRO are shown in fig. 5.10 for an idler wavelength of 1215.2 nm. All values were measured in scanned operation with a calibrated InGaAs photodiode and refer to the total power from both sides of the cavity. 67 mW of idler power were obtained from 1.18 W of pump power at 532 nm modematched into the cavity. The relatively low quantum efficiency of 13 % can be explained by the high absorption loss of the pump wave in the PPKTP crystal and non-optimized

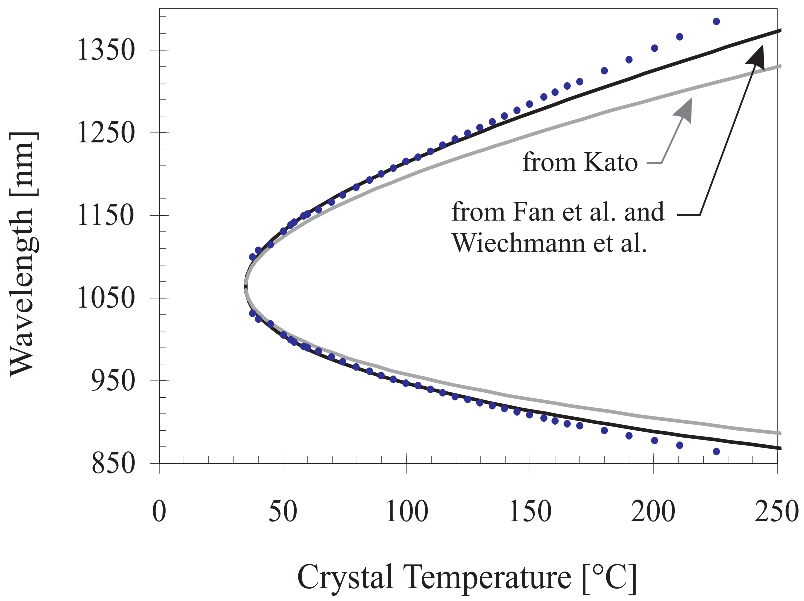

Figure 5.9: Measured emission wavelengths (dots) obtained with a 9 μm grating period compared to theory (solid lines).

reflectivities of the cavity mirrors. For example, if the pump input coupler and backreflector had reflectivities of 91 % and 100 %, respectively, a maximum idler quantum efficiency of 55 % would be expected at a pump power of 675 mW.

Solid curves represent a theoretical fit [22] with an oscillation threshold of 263 mW, corresponding to an internal pump power of 960 mW. The values imply a round trip loss of 2.2 % for the signal wave at 947 nm. Approximately 1.2 % can be attributed to reflections at the crystal faces, so that a crystal absorption loss of 0.5 % per cm at 947 nm can be deduced. This value is consistent with the result of Garashi et al. [67], who did not see any indication of induced infrared absorption in PPKTP with 80 mW at 532 nm present in the crystal. Since no increased absorption was observed in the present experiment, green induced infrared absorption in PPKTP should be negligible for 532 nm powers up to 2 W, corresponding to intensities of 51 kW/cm^2.

Oscillation threshold and output powers varied significantly when translating the PPKTP crystal without changing its temperature, indicating that absorption loss or poling quality were rather inhomogeneous throughout the material. This can be attributed to the fact that periodic poling of KTP is still a delicate task and strongly depends on the quality of the starting material. By carefully selecting the crystal position a minimum oscillation threshold of 165 mW at a crystal temperature of 100 °C was obtained. Given the measured value of the absorption loss at the pump wavelength, this value indicates a nonlinearity close to the optimum of 9.5 pm/V. At the corresponding idler wavelength of 1215 nm, output powers of 28 mW for the signal and 72 mW for the idler were observed.

Frequency-stable operation of the SRO was achieved by actively locking the cavity length to the pump frequency using a Pound-Drever-Hall technique [46]. For that

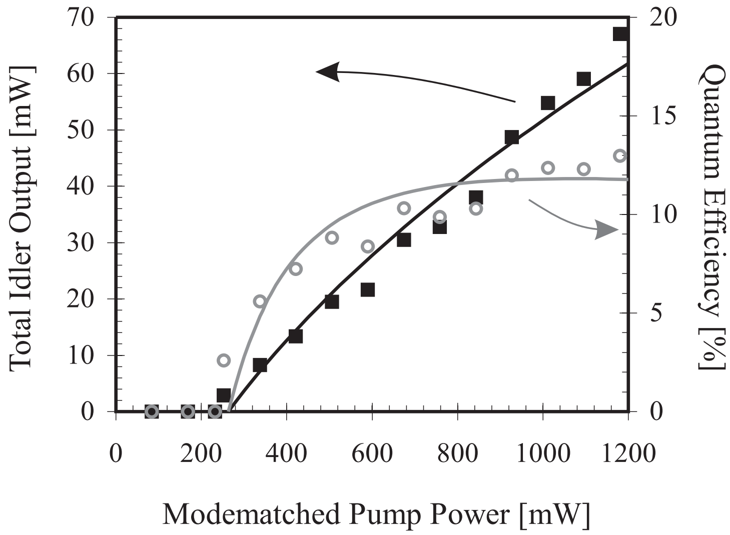

Figure 5.10: Idler output power and quantum efficiency as a function of pump power.

purpose, the pump light reflected from the cavity was detected as leakage through a 45° mirror. The idler wavelength at 1172 nm was measured using a Wavemeter (Burleigh WA-1500). As shown in fig. 5.11, up to 69 minutes of modehop-free oscillation were achieved at a pump power of approximately 1.2 W. Hops between different longitudinal signal modes, which would also change the idler frequency by at least one free spectral range (2.54 GHz), did not occur during that time. While the intensity noise is only 0.8 % rms over 50 ms, the idler power was unstable over longer time scales during the measurement due to unavoidable temperature fluctuations and other external influences affecting alignment. Improved long term power and frequency stability should be feasible with an optimized servo loop and passive damping of the SRO setup.

Local heating of the PPKTP-crystal through the strong absorption of the pump wave led to substantial thermal effects. In comparison to PPLN or PPLT, however, these effects seem to have less influence on the frequency-stabilization of the SRO. They should thus become much less important if the loss in PPKTP can be lowered to a level below 1.5 % per cm as observed in some unpoled KTP crystals.

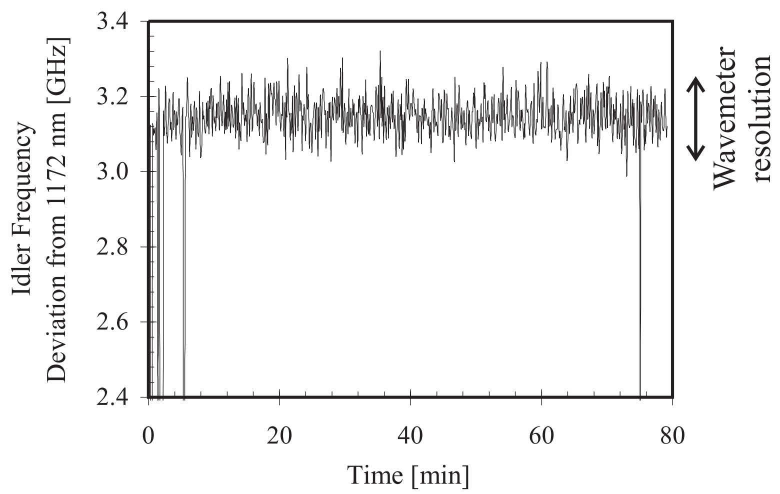

Figure 5.11: Modehop-free operation over a period of 69 min. During that time, deviations of the idler frequency remain within the resolution of the wavemeter (220 MHz).

5.3 Single frequency pump sources

One requirement for a narrow linewidth cw OPO is a cw, high power, narrow linewidth, and frequency stable pump laser as discussed in chapter 2. Additionally the laser has to be tunable in order to be able to tune the OPO via pump tuning. We realized such a pump source at 1064 nm as well as at 532 nm by different methods.

5.3.1 10 W single frequency Nd:YAG laser system

We set up a powerful Nd:YAG laser as a versatile OPO pump source and as a basis for a high power 532 nm laser. It is described in detail in [74].

The laser is configured as a master oscillator power amplifier system (MOPA) as shown in fig. 5.12 and fig. 5.13. As master laser we use a commercial monolithic non planar ring oscillator (NPRO) Nd:YAG laser (Lightwave Electronics 122) with an output power of up to 520 mW, a narrow linewidth of less than 5 kHz and a high frequency stability with a drift of less than 50 MHz/h. The output wavelength can be varied by $\pm$ 30 MHz with a bandwidth of 100 kHz using a built in piezo and slowly by $\pm$ 40 GHz by changing the crystal temperature using a built in peltier element.

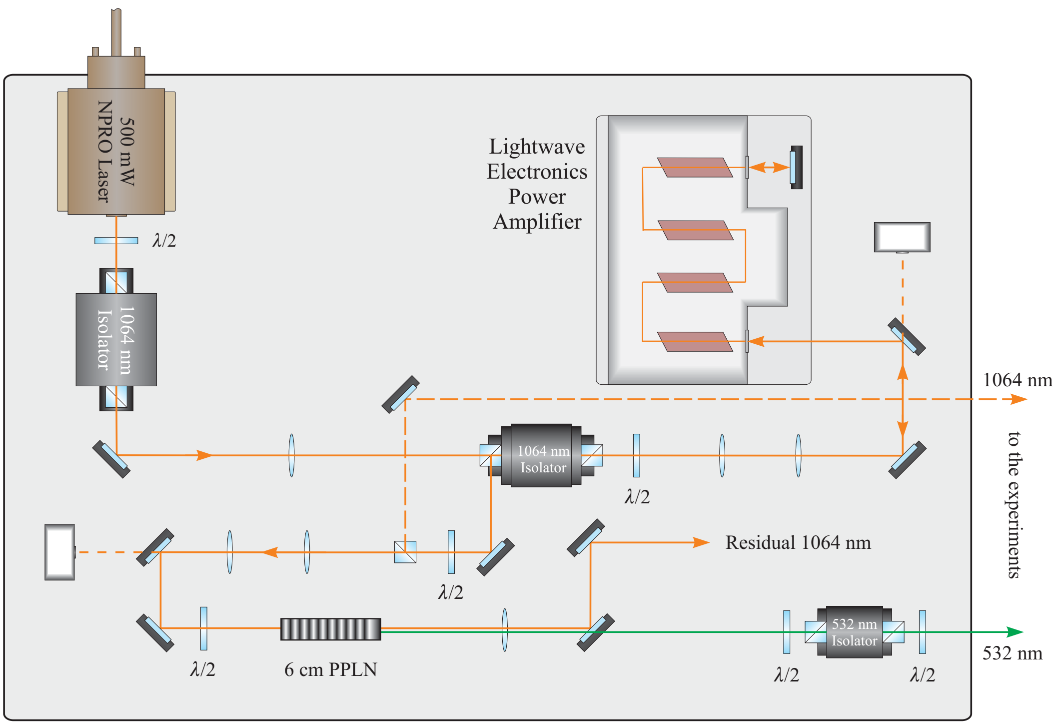

Figure 5.12: Setup of the MOPA laser system and single pass PPLN frequency doubler.

The laser power is coupled via two optical isolators into a power amplifier (Lightwave Electronics 126) which was developed for the LIGO gravitational wave interferometer [73]. It consists of four Brewster cut Nd:YAG rods, sidepumped by two 20 W diode arrays each. It is water chilled. It amplifies the light in a double pass to a power of 10 W. The amplified light is separated from the incoming light at the second isolator and either can be used directly or is frequency doubled in the single pass PPLN frequency doubler described in section 5.3.2.

In the amplification process the frequency, linewidth, and tunability of the master laser are transferred to the output. Since the amplifier is operating in the saturation regime there is no additional noise. In principle the output even can be shot noise limited.

The MOPA system shows an output power of up to 10.4 W with near diffraction limited beam quality $M^2_{x,y} < 1.1$ and 0.3 % rms amplitude noise. An output of 8.6 W was reproducible.

The whole system, including a frequency doubler described in section 5.3.2 and a subsequent optical isolator, is set up rigidly and mounted on a $600 \times 900\,\mathrm{mm}^2$ optical breadboard (weight: 70 kg). Thus it is mobile.

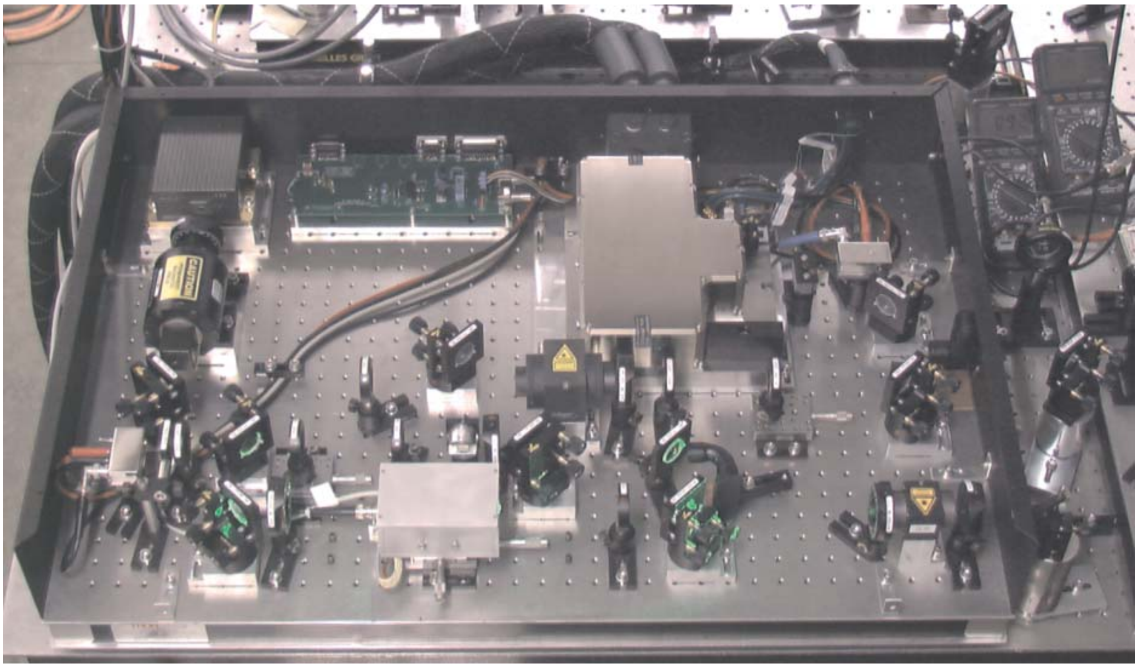

Figure 5.13: Photo of the MOPA system and single pass PPLN frequency doubler. Photo: D. Weise.

5.3.2 Single pass SHG in PPLN

To obtain high power green light, the 10 W MOPA laser is frequency doubled in a single pass frequency doubler which is described in [74]. In principle this should be an easy way to obtain 532 nm radiation because the light simply has to be focused into a nonlinear crystal and no resonator alignment or control electronics except for a temperature controller are required.

Setup

As nonlinear media we employ several PPLN crystals manufactured by Jan-Peter Meyn in Kaiserslautern with poling periods between 6.35 and 6.65 μm. With a size of 60 x 8 x 0.5 mm they are among the longest bulk crystals ever used in second harmonic generation. The crystal end-faces are polished at an angle of 0.25 ° and antireflection coated for 1064 and 532 nm. The crystals are heated in a gold coated copper oven to the phasematching temperature between 120 and 300 °C. The absorption of the second harmonic power (which is higher at the crystal end) causes a temperature gradient between the crystal input and exit face along the beam path in the order of 1 °C. To compensate for this an inverse temperature gradient is created in the oven by heating the front and back half differently.

The output of the MOPA laser is focused to a waist of 40 μm (near confocal focusing) in the center of the crystal. A dichroic mirror separates the fundamental and second harmonic wave.

Taking pump depletion into account, an output power of 7.0 W is expected from

$$\frac{P_{2\omega}}{P_\omega} = \tanh^2\left(\sqrt{\frac{\mu_0}{c}}\,\frac{\omega d_{\mathrm{eff}} L}{n_\omega\sqrt{n_{2\omega}}}\,\sqrt{2P_\omega\frac{\omega n_\omega h_{\mathrm{BK}}}{\pi c L}}\right) \tag{5.2}$$

if absorption losses in the crystal, photorefractive effects, and thermal lenses are neglected.

Results

An output power up to 3.2 W with a doubling efficiency of 42 % was obtained. This is, to the best of our knowledge, the highest output power ever obtained in a cw single-pass second harmonic generation and the efficiency is the same as the highest reported so far by Miller et al. [76].

Due to energy conservation the second harmonic wave must have the same linewidth, tunability, and (if present) modulation as the fundamental light. At a power level above 2 W a high long-term stability with an rms noise of 1.5 % over 21 h was demonstrated. The beam profile was measured to be near diffraction-limited ($M^2 \approx 1$).

But in contrast to our expectations, the frequency doubler requires daily realignment. Neither the output power nor the beam shape nor the beam direction are reproducible from day to day. Especially at high output powers the beam is not always diffraction limited. No dependence of these effects on the crystal temperature was found. The behavior improves if the input power is reduced to a level of 7 – 8 W.

These effects and the deviation from the theoretical maximum of 7.0 W can be explained by photorefractive effects, absorption, green-induced infrared absorption (GRIIRA, see section 4.2), and thermal lenses which become very strong at the power levels present. This is in good agreement with the observations of Myers [28]. They performed similar experiments with different nonlinear materials and obtained very promising results for several hours but did not obtain long-term stability and reproducibility.

Double-pass SHG

To test the crystal in double-pass configuration a concave mirror with 50 mm radius of curvature, reflecting both 532 and 1064 nm, was placed behind the crystal. The relative phase between the two back-reflected waves is important. This phase is determined by the position of the crystal end face relative to the poling domains and is arbitrary in a usual fabrication process. The phase was adjusted by translating the (angle polished) crystal horizontally.

As expected the doubling efficiency increased by a factor of 4 at low input powers of 50 mW.

But at high powers the thermal effects became even worse, totally distorting the beam profile and limiting the output power to values up to 2.2 W. This agrees well with the expectations from a computer simulation.

5.3.3 Single pass SHG in PPKTP

To circumvent the problems arising from thermal and photorefractive effects in PPLN we used PPKTP, which is known to show no photorefractive effects and to be be less sensitive to thermal lenses.

The $20 \times 2 \times 0.5$ mm antireflection-coated crystal with a poling period of 9 μm was provided from Raicol Crystals Ltd. The infrared laser beam was focused to a waist radius of 38 mm, corresponding to a Rayleigh range of 7.8 mm. In theory this gives approximately 15 % less efficiency than an optimallyfocused beam with a Rayleigh range of 3.52 mm.

In single-pass configuration, assuming an effective nonlinear coefficient of 9.5 pm/V, we expect a SHG efficiency of 1.21 %/W cm for our focusing. Experimentally we obtained 990 mW of green light at 532 nm from 8.3 W of infrared light, corresponding to an efficiency of 0.72 %/W cm, which is 60 % of the expected value. 930 mW of stable green light was obtained reproducibly for hours. The beam cross section was round as seen by the naked eye. The efficiency varied by about 20 % across the crystal aperture.

The phase-matching temperature was found to be 34.08 °C at full laser power and 1 °C higher at an IR power of 1 W. This difference is believed be due to absorption of the laser power in the crystal which creates a temperature gradient between the crystal and the oven. At both powers the phase-matching bandwidth is broadened relative to a sinc^2 fit with a width of 2.9 °C (the fitted width was chosen to match the position of the side maximums), as shown in fig. 5.14. As expected, the green power scales quadratically with the IR power.

To test the crystal in double-pass configuration, a concave mirror reflecting both 532 and 1064 nm was placed behind the crystal. The relative phase between the

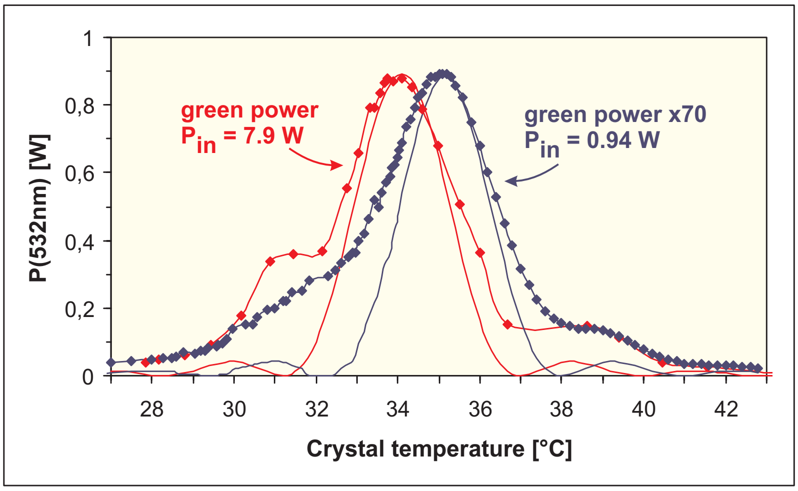

Figure 5.14: Phase-matching bandwidth of a single pass SHG in PPKTP. Dots: measurement; lines: sinc^2 *fit.*

two back-reflected waves could be adjusted in a limited range by translating the crystal horizontally because the crystal endface was not exactly parallel to the poling domains. The effect of a mismatch of this phase can be reduced by changing the temperature.

With an input power of 7.4 W we achieved a maximum output power of 1.54 W at a temperature of 34.08 °C. However the output was neither stable, nor reproducible, nor did it show a round beam shape. We assume thermal lenses originating from absorption of the green light to be responsible for this effect.

To get rid of the thermal lenses we chopped the laser beam with a frequency of 25 – 50 Hz and 4.2 % duty cycle. We obtained a double-pass peak power of 1.74 W of green light for 7.3 W of infrared light, but we still did not obtain four times the single pass power as expected from theory. The beam was stable, reproducible and round as seen with the naked eye. This shows that thermal effects are limiting the performance of high power SHG in PPKTP.

5.3.4 Resonant SHG in $MgO{:}LiNbO_3$

In a third approach to obtain high power green light from the MOPA laser, we set up a semimonolithic resonant frequency doubler similar to the one developed by Schneider et al. [62].

The use of a resonator causes the device to suppress the effect of thermal lenses to a certain extent. Photorefractive effects are reduced by using a bulk $MgO{:}LiNbO_3$ crystal and non-critical birefringent phasematching. The nonlinearity is lower than in PPLN, but this is not really a disadvantage because the conversion efficiency reaches values above 80 % anyway.

The setup is shown in fig. 5.15. The resonator consists of a 7.5 mm long MgO: $LiNbO_3$ crystal (heated in an oven to the phasematching temperature of about 111 °C) and an external mirror separated by 24 mm. One end face of the crystal is polished with a 10 mm radius of curvature whereas the other end face is flat. The crystal carries a high reflection coating for 1064 and 532 nm on the spherical face and an anti-reflection coating for both wavelengths on the flat face. A 25 mm radius of curvature mirror with a reflectivity of 88 % at 1064 nm and < 5 % at 532 nm serves as the input coupler for the fundamental and as the output coupler for the second-harmonic wave. The resonator mode has an $1/e^2$ waist radius of 18.5 μm. 90 % of the laser power are modematched to the fundamental resonator mode. The mirror is mounted on a piezo to lock the cavity length on resonance with the laser using a modified Pound Drever Hall technique [46] with a servo bandwidth of 5.5 kHz. This makes the lock quite robust against mechanical perturbations.

With an input power of 2.08 W we obtained a stable output of 1.47 W with a round beam shape as seen by the naked eye. This corresponds to a conversion efficiency of 71 % (81 % of the modematched power if the green light reflected off the dichroic mirror is included). The total conversion efficiency is only 2 % lower than the efficiency obtained by [62].

At higher powers thermal lenses increasingly deteriorate the mode profile and induce bistability. At an input power of 2.44 W we obtained an output of 1.68 W (69 %) in a spherically symmetric but non-Gaussian mode. At 3.02 W we obtained

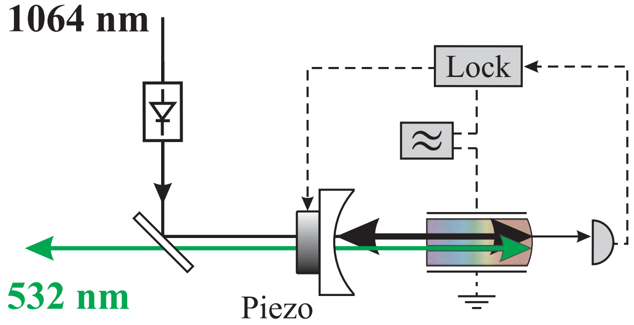

Figure 5.15: Setup of the resonant frequency doubler.

1.9 W (63 %) in a cloverleaf like mode. At 6.8 W only 1.4 W of output were obtained.

The infrared laser was modematched to the TEM_{20} mode of the resonator which has a larger volume than the TEM_{00} mode and thus is less sensitive against thermal lenses. With an input power of 6.56 W a stable output of 1.65 W in the TEM_{20} mode was obtained, which is 62 % of the modematched power (40 % modematching). This is an interesting result even if it is useless for most practical applications.

To obtain higher power it should be feasible to split the laser into four beams of 2 W each, frequency double them in four separate resonators and then combine the green beams at three beam splitters with the phases controlled to ensure constructive interference. Assuming the green beams are combined with a modematching of 80 % this will provide 4.5 W of output power at 532 nm. A disadvantage is that the modematching at four resonators and three beam splitters has to be aligned and seven feedback loops are required (one for each resonator and one for each beam splitter).

Another way of increasing the power is to use a crystal of about 2 mm length and tighten the focusing. This reduces the sensitivity to thermal lenses but simultaneously increases the circulating power density. About 50 % increase in output power can be expected from this setup.

Alternatively LBO or KTP could be used, two nonlinear materials that are known to be less sensitive against thermal problems in high power applications (especially LBO) but having a lower nonlinearity.

5.3.5 Characterization of a 5 W-Verdi laser

The Coherent Verdi laser (see section 3.1) fulfills all conditions required for an ideal pump source except tunability. Therefore we examined the spectral properties of a 5 W Verdi laser by a beat frequency measurement against a monolithic, externally frequency-doubled Nd:YAG laser from the Laser Zentrum Hannover.

The beams of both lasers were combined at a beam splitter. The interference signal which contains the difference frequency between the OPO and the laser was detected with a fast (1 GHz) photodiode, downconverted with an RF-synthesizer, recorded with a sampling oscilloscope and fast Fourier analyzed in a computer.

The beat signal has a 20 kHz short-term linewidth over 50 μs and a 500 kHz jitter over 1 ms. As the beat measurement determines the linewidth and jitter of the difference frequency between the two lasers it can not be determined which laser causes the observed effects. The measured jitter and linewidth are thus an upper limit for both lasers.

The frequency drift was measured absolutely with a high resolution wavemeter (Burleigh WA 1500, 50 MHz resolution) over 10 hours. It was measured to be less than 50 MHz/h.

Chapter 6

Summary and Outlook

We have developed a single-frequency continuous-wave laser source with an emission range from green to mid infrared (550 – 2830 nm, almost 2.5 octaves in the optical spectrum). This is to our knowledge by far the broadest tuning range of any single frequency source.

It employs a singly resonant optical parametric oscillator and a subsequent broad-band frequency doubler. This source exhibits high output powers of typically 30 – 500 mW over most of the emission range, has near diffraction limited beam quality, and excellent spectral properties. It shows mode-hop-free oscillation for several hours and a high absolute frequency stability with a drift of less than 50 MHz per hour. The linewidth has been measured to be 20 kHz, one of the narrowest ever reported for an OPO. A novel feature is a large continuous frequency tuning range up to 38 GHz ($> 1\,\mathrm{cm}^{-1}$) without pump tuning.

This makes this OPO a versatile light source for a wide variety of applications such as high resolution spectroscopy, precision metrology, laser trapping and cooling, characterization of optical components, and many others. To demonstrate its performance, flexibility, and reliability it was used to measure a Doppler free hyper-fine spectrum of molecular iodine in the yellow spectral region.

We built two additional single frequency OPOs, which represented a significant step in scientific research at the time they were developed, and several high power single frequency pump sources in the green and infrared.

The performance of these OPOs can be improved further by using stoichiometric lithium tantalate or gray track resistant KTP, two new nonlinear materials which are currently being developed and will be available in the near future. With these materials and some engineering effort there is a good chance to convert this scientific research project into a commercial laser source with the performance presented above and a usability, reliability, and price comparable to that of a single frequency Ti:sapphire laser. If this can be achieved this device will enable scientists and engineers to perform new experiments and bring advances to many research areas. And there will be a commercial market.

Appendix

A.1 Wavelength tables

Table A.1: Poling periods and output wavelengths of the **PPKTP OPO** *calculated according to Sellmeier equation of Ref. [47, 44]. Period #10 and #11 are almost equal.*

Crystal-Map

Signal wavelength — Degeneracy: 61.4°C

Transl. stage [mm]	Nr.	Poling period [µm]	20°C	40°C	60°C	80°C	100°C	120°C	140°C	160°C	180°C	200°C
38.65	1	8.96				0.999	0.974	0.956	0.940	0.928	0.916	0.906
37.00	2	9.12	0.934	0.922	0.911	0.902	0.893	0.885	0.877	0.870	0.863	0.857
35.35	3	9.28	0.884	0.877	0.869	0.863	0.856	0.850	0.845	0.839	0.834	0.829
33.70	4	9.44	0.851	0.845	0.840	0.834	0.829	0.824	0.820	0.815	0.811	0.807
32.05	5	9.60	0.826	0.821	0.816	0.812	0.808	0.804	0.800	0.796	0.792	0.788
30.40	6	9.76	0.805	0.801	0.797	0.793	0.790	0.786	0.783	0.779	0.776	0.773
28.75	7	9.92	0.788	0.784	0.781	0.778	0.774	0.771	0.768	0.765	0.762	0.759
27.10	8	10.08	0.773	0.770	0.767	0.764	0.761	0.758	0.755	0.752	0.749	0.747
25.45	9	10.24	0.760	0.757	0.754	0.752	0.749	0.746	0.743	0.741	0.738	0.736
23.80	10	10.40	0.748	0.746	0.743	0.741	0.738	0.736	0.733	0.731	0.728	0.726
37.50	11	10.385	0.750	0.747	0.744	0.741	0.739	0.736	0.734	0.732	0.729	0.727
35.85	12	10.586	0.736	0.734	0.731	0.729	0.727	0.724	0.722	0.720	0.718	0.716
34.20	13	10.787	0.725	0.722	0.720	0.718	0.716	0.714	0.712	0.710	0.708	0.706
32.55	14	10.988	0.714	0.712	0.710	0.708	0.706	0.704	0.702	0.700	0.698	0.696
30.90	15	11.189	0.705	0.703	0.701	0.699	0.697	0.695	0.693	0.692	0.690	0.688
29.25	16	11.390	0.696	0.694	0.692	0.691	0.689	0.687	0.685	0.684	0.682	0.680
27.60	17	11.591	0.688	0.686	0.685	0.683	0.681	0.680	0.678	0.676	0.675	0.673
25.95	18	11.792	0.681	0.679	0.677	0.676	0.674	0.673	0.671	0.670	0.668	0.666
24.30	19	11.993	0.674	0.672	0.671	0.669	0.668	0.666	0.665	0.663	0.662	0.660
22.65	20	12.194	0.667	0.666	0.664	0.663	0.661	0.660	0.658	0.657	0.656	0.654

Idler wavelength — Degeneracy: 61.4°C

Transl. stage [mm]	Nr.	Poling period [µm]	20°C	40°C	60°C	80°C	100°C	120°C	140°C	160°C	180°C	200°C
38.65	1	8.96				1.139	1.173	1.201	1.226	1.249	1.270	1.290
37.00	2	9.12	1.206	1.231	1.253	1.274	1.294	1.313	1.331	1.349	1.367	1.384
35.35	3	9.28	1.313	1.332	1.350	1.367	1.385	1.402	1.418	1.435	1.451	1.467
33.70	4	9.44	1.399	1.416	1.432	1.449	1.465	1.481	1.497	1.513	1.529	1.544
32.05	5	9.60	1.476	1.493	1.508	1.524	1.540	1.556	1.572	1.587	1.603	1.619
30.40	6	9.76	1.549	1.565	1.581	1.597	1.613	1.628	1.644	1.660	1.675	1.691
28.75	7	9.92	1.620	1.635	1.651	1.667	1.682	1.698	1.714	1.730	1.746	1.762
27.10	8	10.08	1.688	1.703	1.719	1.735	1.751	1.767	1.783	1.800	1.816	1.832
25.45	9	10.24	1.755	1.771	1.787	1.803	1.819	1.836	1.852	1.869	1.886	1.902
23.80	10	10.40	1.821	1.838	1.854	1.871	1.888	1.904	1.921	1.938	1.955	1.972
37.50	11	10.385	1.815	1.831	1.848	1.865	1.881	1.898	1.915	1.931	1.948	1.965
35.85	12	10.586	1.898	1.915	1.932	1.949	1.966	1.984	2.001	2.018	2.036	2.053
34.20	13	10.787	1.981	1.999	2.016	2.034	2.052	2.070	2.088	2.106	2.124	2.142
32.55	14	10.988	2.065	2.083	2.102	2.120	2.138	2.157	2.176	2.195	2.213	2.232
30.90	15	11.189	2.150	2.169	2.188	2.207	2.226	2.246	2.265	2.284	2.304	2.324
29.25	16	11.390	2.236	2.255	2.275	2.295	2.315	2.335	2.356	2.376	2.397	2.418
27.60	17	11.591	2.323	2.344	2.364	2.385	2.406	2.427	2.449	2.470	2.492	2.514
25.95	18	11.792	2.413	2.434	2.456	2.478	2.500	2.522	2.544	2.567	2.589	2.612
24.30	19	11.993	2.504	2.527	2.550	2.572	2.595	2.619	2.643	2.666	2.690	2.715
22.65	20	12.194	2.599	2.622	2.646	2.671	2.695	2.720	2.745	2.770	2.795	2.821

Table A.2: Poling periods and output wavelengths of the **PPLN OPO** *calculated according to Sellmeier equation of Ref. [42].*

Crystal-Map

Signal wavelength — Degeneracy: 184.5°C

Transl. stage [mm]	Nr.	Poling period [µm]	140°C	150°C	160°C	170°C	180°C	190°C	200°C	210°C	220°C	230°C	240°C	250°C
35.4	1	6.51						1.016	0.986	0.966	0.95	0.936	0.924	0.913
34.0	2	6.65	0.974	0.958	0.944	0.932	0.922	0.912	0.903	0.895	0.887	0.880	0.873	0.866
32.6	3	6.79	0.899	0.892	0.885	0.878	0.872	0.866	0.860	0.855	0.849	0.844	0.839	0.834
31.2	4	6.93	0.858	0.853	0.848	0.843	0.839	0.834	0.830	0.825	0.821	0.817	0.813	0.809
29.8	5	7.07	0.828	0.825	0.821	0.817	0.813	0.810	0.806	0.803	0.799	0.796	0.792	0.789
28.4	6	7.21	0.805	0.802	0.799	0.796	0.793	0.790	0.787	0.784	0.781	0.778	0.775	0.772
27.0	7	7.35	0.786	0.784	0.781	0.778	0.776	0.773	0.770	0.768	0.765	0.763	0.760	0.758
25.6	8	7.49	0.770	0.768	0.765	0.763	0.761	0.758	0.756	0.754	0.752	0.749	0.747	0.745
24.2	9	7.63	0.756	0.754	0.752	0.750	0.748	0.746	0.744	0.742	0.740	0.738	0.736	0.734
22.8	10	7.77	0.744	0.742	0.740	0.738	0.736	0.735	0.733	0.731	0.729	0.727	0.725	0.723
21.4	11	7.91	0.733	0.731	0.730	0.728	0.726	0.724	0.723	0.721	0.719	0.718	0.716	0.714
20.0	12	8.05	0.723	0.722	0.720	0.718	0.717	0.715	0.714	0.712	0.711	0.709	0.708	0.706
18.6	13	8.19	0.714	0.713	0.711	0.710	0.708	0.707	0.706	0.704	0.703	0.701	0.700	0.698
17.2	14	8.33	0.706	0.705	0.703	0.702	0.701	0.699	0.698	0.697	0.695	0.694	0.693	0.691
15.8	15	8.47	0.698	0.697	0.696	0.695	0.693	0.692	0.691	0.690	0.688	0.687	0.686	0.685
14.4	16	8.61	0.691	0.690	0.689	0.688	0.687	0.686	0.684	0.683	0.682	0.681	0.680	0.679
13.0	17	8.75	0.685	0.684	0.683	0.682	0.681	0.680	0.678	0.677	0.676	0.675	0.674	0.673
11.6	18	8.89	0.679	0.678	0.677	0.676	0.675	0.674	0.673	0.672	0.671	0.670	0.668	0.667
10.2	19	9.03	0.673	0.672	0.671	0.670	0.669	0.668	0.667	0.666	0.665	0.664	0.663	0.662
8.8	20	9.17	0.668	0.667	0.666	0.665	0.664	0.663	0.662	0.661	0.660	0.660	0.659	0.658
7.4	21	9.31	0.663	0.662	0.661	0.660	0.659	0.659	0.658	0.657	0.656	0.655	0.654	0.653
6.0	22	9.45	0.658	0.657	0.657	0.656	0.655	0.654	0.653	0.652	0.651	0.650	0.650	0.649
4.6	23	9.59	0.654	0.653	0.652	0.651	0.650	0.650	0.649	0.648	0.647	0.646	0.645	0.645

Idler wavelength — Degeneracy: 184.5°C

Transl. stage [mm]	Nr.	Poling period [µm]	140°C	150°C	160°C	170°C	180°C	190°C	200°C	210°C	220°C	230°C	240°C	250°C
35.4	1	6.51						1.117	1.156	1.186	1.211	1.234	1.255	1.275
34.0	2	6.65	1.174	1.198	1.220	1.240	1.260	1.278	1.296	1.313	1.331	1.347	1.364	1.381
32.6	3	6.79	1.304	1.320	1.336	1.351	1.366	1.381	1.396	1.411	1.426	1.441	1.456	1.471
31.2	4	6.93	1.402	1.416	1.429	1.443	1.457	1.471	1.485	1.499	1.513	1.527	1.541	1.555
29.8	5	7.07	1.489	1.502	1.514	1.527	1.540	1.554	1.567	1.580	1.594	1.608	1.622	1.635
28.4	6	7.21	1.570	1.582	1.595	1.607	1.620	1.633	1.646	1.659	1.672	1.686	1.699	1.713
27.0	7	7.35	1.648	1.660	1.672	1.684	1.697	1.709	1.722	1.735	1.749	1.762	1.776	1.789
25.6	8	7.49	1.723	1.735	1.747	1.759	1.772	1.785	1.797	1.810	1.824	1.837	1.851	1.864
24.2	9	7.63	1.797	1.809	1.821	1.834	1.846	1.859	1.872	1.885	1.898	1.912	1.925	1.939
22.8	10	7.77	1.871	1.883	1.895	1.907	1.920	1.933	1.946	1.959	1.972	1.986	2.000	2.014
21.4	11	7.91	1.944	1.956	1.968	1.981	1.993	2.006	2.019	2.033	2.046	2.060	2.074	2.088
20.0	12	8.05	2.017	2.029	2.041	2.054	2.067	2.080	2.093	2.107	2.121	2.135	2.149	2.163
18.6	13	8.19	2.090	2.102	2.115	2.128	2.141	2.154	2.167	2.181	2.195	2.209	2.224	2.238
17.2	14	8.33	2.163	2.176	2.189	2.202	2.215	2.228	2.242	2.256	2.270	2.285	2.300	2.314
15.8	15	8.47	2.237	2.250	2.263	2.276	2.290	2.303	2.317	2.332	2.346	2.361	2.376	2.391
14.4	16	8.61	2.312	2.325	2.338	2.351	2.365	2.379	2.394	2.408	2.423	2.438	2.453	2.469
13.0	17	8.75	2.387	2.400	2.414	2.428	2.442	2.456	2.471	2.486	2.501	2.516	2.532	2.548
11.6	18	8.89	2.463	2.477	2.491	2.505	2.519	2.534	2.549	2.564	2.580	2.596	2.612	2.628
10.2	19	9.03	2.541	2.555	2.569	2.583	2.598	2.613	2.629	2.644	2.660	2.676	2.693	2.710
8.8	20	9.17	2.620	2.634	2.649	2.663	2.678	2.694	2.710	2.726	2.742	2.759	2.776	2.793
7.4	21	9.31	2.700	2.715	2.729	2.745	2.760	2.776	2.792	2.809	2.826	2.843	2.860	2.878
6.0	22	9.45	2.782	2.797	2.812	2.828	2.844	2.860	2.877	2.894	2.911	2.929	2.946	2.965
4.6	23	9.59	2.865	2.881	2.897	2.913	2.929	2.946	2.963	2.981	2.998	3.017	3.035	3.054

Table A.3: Poling periods and phasematching wavelengths of the **SHG** *crystals calculated according to Sellmeier equation of Ref. [42]. Period # 31 and # 32 are repeated on both crystals.*

Transl. stage [mm]	Nr.	Poling period [µm]	130°C	140°C	150°C	160°C	170°C	180°C	190°C	200°C	210°C	220°C
			Idler wavelength									
Horizontal translation stage: 19.7 mm												
42.2	1	6.51	1.058	1.059	1.060	1.061	1.062	1.063	1.064	1.065	1.066	1.067
40.8	2	6.65	1.066	1.066	1.067	1.068	1.069	1.070	1.071	1.072	1.073	1.074
39.4	3	6.79	1.073	1.074	1.074	1.075	1.076	1.077	1.078	1.079	1.080	1.082
38.0	4	6.93	1.080	1.081	1.082	1.083	1.083	1.084	1.085	1.087	1.088	1.089
36.6	5	7.07	1.087	1.088	1.089	1.090	1.090	1.092	1.093	1.094	1.095	1.096
35.2	6	7.21	1.094	1.095	1.095	1.096	1.097	1.098	1.099	1.101	1.102	1.103
33.8	7	7.35	1.100	1.101	1.102	1.103	1.104	1.105	1.106	1.107	1.109	1.110
32.4	8	7.49	1.107	1.108	1.109	1.110	1.111	1.112	1.113	1.114	1.115	1.117
31.0	9	7.63	1.114	1.115	1.116	1.117	1.118	1.119	1.120	1.121	1.122	1.123
29.6	10	7.77	1.121	1.122	1.123	1.124	1.125	1.126	1.127	1.128	1.129	1.130
28.2	11	7.91	1.127	1.128	1.129	1.130	1.131	1.132	1.133	1.134	1.136	1.137
26.8	12	8.05	1.134	1.135	1.136	1.137	1.138	1.139	1.140	1.141	1.142	1.143
25.4	13	8.19	1.140	1.141	1.142	1.143	1.144	1.145	1.147	1.148	1.149	1.150
24.0	14	8.33	1.147	1.148	1.149	1.150	1.151	1.152	1.153	1.154	1.155	1.157
22.6	15	8.47	1.153	1.154	1.155	1.156	1.157	1.158	1.160	1.161	1.162	1.163
21.2	16	8.61	1.159	1.160	1.162	1.163	1.164	1.165	1.166	1.167	1.168	1.169
19.8	17	8.75	1.166	1.167	1.168	1.169	1.170	1.171	1.172	1.173	1.175	1.176
18.4	18	8.89	1.172	1.173	1.174	1.175	1.176	1.177	1.179	1.180	1.181	1.182
17.0	19	9.03	1.178	1.179	1.180	1.181	1.183	1.184	1.185	1.186	1.187	1.188
15.6	20	9.17	1.184	1.185	1.187	1.188	1.189	1.190	1.191	1.192	1.193	1.195
14.2	21	9.31	1.191	1.192	1.193	1.194	1.195	1.196	1.197	1.198	1.200	1.201
12.8	22	9.45	1.197	1.198	1.199	1.200	1.201	1.202	1.203	1.205	1.206	1.207
11.4	23	9.59	1.203	1.204	1.205	1.206	1.207	1.208	1.210	1.211	1.212	1.213
10.0	24	9.73	1.209	1.210	1.211	1.212	1.213	1.214	1.216	1.217	1.218	1.219
8.6	25	9.94	1.218	1.219	1.220	1.221	1.222	1.223	1.225	1.226	1.227	1.228
7.2	26	10.15	1.227	1.228	1.229	1.230	1.231	1.232	1.234	1.235	1.236	1.237
5.8	27	10.36	1.235	1.237	1.238	1.239	1.240	1.241	1.243	1.244	1.245	1.246
4.4	28	10.57	1.244	1.245	1.246	1.248	1.249	1.250	1.251	1.253	1.254	1.255
3.0	29	10.78	1.253	1.254	1.255	1.256	1.258	1.259	1.260	1.261	1.263	1.264
1.6	30	10.99	1.261	1.263	1.264	1.265	1.266	1.268	1.269	1.270	1.271	1.273
0.2	31	11.20	1.270	1.271	1.272	1.274	1.275	1.276	1.277	1.279	1.280	1.282
-1.2	32	11.41	1.279	1.280	1.281	1.282	1.283	1.285	1.286	1.287	1.289	1.290

Horizontal translation stage: 16.2 mm												
41.0	31	11.20	1.270	1.271	1.272	1.274	1.275	1.276	1.277	1.279	1.280	1.282
39.6	32	11.41	1.279	1.280	1.281	1.282	1.283	1.285	1.286	1.287	1.289	1.290
38.2	33	11.62	1.287	1.288	1.289	1.291	1.292	1.293	1.295	1.296	1.297	1.299
36.8	34	11.83	1.295	1.297	1.298	1.299	1.300	1.302	1.303	1.304	1.306	1.307
35.4	35	12.11	1.307	1.308	1.309	1.310	1.312	1.313	1.314	1.316	1.317	1.319
34.0	36	12.39	1.318	1.319	1.320	1.321	1.323	1.324	1.325	1.327	1.328	1.330
32.6	37	12.67	1.329	1.330	1.331	1.332	1.334	1.335	1.337	1.338	1.339	1.341
31.2	38	12.95	1.339	1.341	1.342	1.343	1.345	1.346	1.348	1.349	1.350	1.352
29.8	39	13.23	1.350	1.352	1.353	1.354	1.356	1.357	1.358	1.360	1.361	1.363
28.4	40	13.51	1.361	1.362	1.364	1.365	1.366	1.368	1.369	1.371	1.372	1.374
27.0	41	13.79	1.372	1.373	1.374	1.376	1.377	1.379	1.380	1.382	1.383	1.385
25.6	42	14.07	1.382	1.384	1.385	1.387	1.388	1.389	1.391	1.392	1.394	1.396
24.2	43	14.35	1.393	1.394	1.396	1.397	1.399	1.400	1.402	1.403	1.405	1.406
22.8	44	14.63	1.404	1.405	1.406	1.408	1.409	1.411	1.412	1.414	1.415	1.417
21.4	45	14.91	1.414	1.416	1.417	1.418	1.420	1.421	1.423	1.425	1.426	1.428
20.0	46	15.19	1.425	1.426	1.428	1.429	1.431	1.432	1.434	1.435	1.437	1.438
18.6	47	15.47	1.435	1.437	1.438	1.440	1.441	1.443	1.444	1.446	1.447	1.449
17.2	48	15.82	1.448	1.450	1.451	1.453	1.454	1.456	1.457	1.459	1.461	1.462
15.8	49	16.17	1.461	1.463	1.464	1.466	1.467	1.469	1.471	1.472	1.474	1.476
14.4	50	16.52	1.474	1.476	1.477	1.479	1.480	1.482	1.484	1.485	1.487	1.489
13.0	51	16.87	1.487	1.489	1.490	1.492	1.494	1.495	1.497	1.499	1.500	1.502
11.6	52	17.22	1.500	1.502	1.503	1.505	1.507	1.508	1.510	1.512	1.513	1.515
10.2	53	17.57	1.513	1.515	1.516	1.518	1.520	1.521	1.523	1.525	1.527	1.528
8.8	54	17.92	1.526	1.528	1.529	1.531	1.533	1.534	1.536	1.538	1.540	1.542
7.4	55	18.27	1.539	1.541	1.542	1.544	1.546	1.548	1.549	1.551	1.553	1.555
6.0	56	18.62	1.552	1.554	1.555	1.557	1.559	1.561	1.562	1.564	1.566	1.568
4.6	57	18.97	1.565	1.567	1.569	1.570	1.572	1.574	1.576	1.578	1.579	1.581
3.2	58	19.32	1.578	1.580	1.582	1.583	1.585	1.587	1.589	1.591	1.593	1.595
1.8	59	19.67	1.591	1.593	1.595	1.597	1.598	1.600	1.602	1.604	1.606	1.608
0.4	60	20.09	1.607	1.609	1.611	1.612	1.614	1.616	1.618	1.620	1.622	1.624
-1.0	61	20.51	1.623	1.625	1.626	1.628	1.630	1.632	1.634	1.636	1.638	1.640
-2.4	62	20.93	1.639	1.641	1.643	1.644	1.646	1.648	1.650	1.652	1.654	1.657

A.2 Publications

[1] U. Strößner, A. Peters, J. Mlynek, S. Schiller, J.-P. Meyn, R. Wallenstein, *Single-frequency continuous-wave radiation from 0.77 to 1.73 μm generated by a green-pumped optical parametric oscillator with periodically poled LiTaO*$_3$, Optics Letters **24**, 1602 (1999)

[2] D.R. Weise, U. Strößner, A. Peters, J. Mlynek, S. Schiller, A. Arie, A. Skliar, G. Rosenman,
Continuous-wave 532-nm-pumped singly resonant optical parametric oscillator with periodically poled KTiOPO$_4$,
Optics Communications **184**, 329 (2000)

[3] U. Strößner, J.-P. Meyn, R. Wallenstein, A. Arie, P. Urenski, G, Rosenman, J. *Mlynek, S. Schiller, A. Peters,*
Single-frequency cw OPO with an ultra-wide tuning range from 550 to 2830 nm,
in preparation for Journal of the Optical Society of America B

[4] A. Hecker, C. Braxmaier, U. Strößner, M. Havenith, S. Schiller, A. Peters,
High resolution Doppler-free spectroscopy of molecular iodine using a continuous wave optical parametric oscillator,
in preparation for Physical Review A

Acknowledgements

As usual the last page belongs to all who contributed to the success of this thesis. I would like to to thank:

... my advisor Prof. Dr. J. Mlynek who did a lot of organization in the background to enable us spend his money. He created an atmosphere of creativity inside our department and opened up our minds to things happening outside the University. I wish him a lot of success in his new job as the president of the Humboldt Universität zu Berlin.

... Achim Peters who was my direct supervisor. With his unbelievable experience and numerous discussions about the basic concepts as well as the technical details he fully shares the honor for the success of the project.

... Prof. Dr. S. Schiller who brought me to Konstanz and into the OPO business. He was my supervisor in the beginning of my thesis and pushed the project forward thanks to his knowledge, especially regarding theory.

... Oliver Benson, who generously lent me his Verdi laser and his lab.

My predecessor Klaus Schneider died in a tragic mountaineering accident three days before the beginning of my thesis. Although I hardly knew him I have more in common with him than just physics. As he was not there any more Alexander Beirer was the one to introduce me into the project and create the first setup.

My diploma student Dennis Weise did a great job setting up the MOPA laser, frequency doubler and the single grating PPKTP OPO. I profited a lot from his experience even after he finished his degree.

We have a great collaboration with Jan-Peter Meyn who is fabricating numerous PPLN and PPLT crystals for us. His experience and kindness make it a pleasure to work with him.

We also collaborate with the Tel Aviv group: Prof. Ady Arie, Prof. Gil Rosenman, Alex Skliar, Pavel Urenski, and Alexander Fisher. They did a great job manufacturing the PPKTP crystals for us.

Claus Braxmeier, and Evgeny Kowalchuk helped me with the linewidth measurement, and Andreas Hecker carried out the iodine spectroscopy.

I thank Thomas Aichele, Raid Al'Tahtamouni, Jo Bellanca, Kamel Bencheikh, Tobias Boley, Gerd Breitenbach, Richard Conroy, Daniel Dekorsy, Ulf Fröhlich, Luca Haiberger, Hauke Hansen, Robert Hauschild, Waltraud Heinzen, Ute Hentzen, Sven Herrmann, Patrick Kramper, Peter Lodahl, Alexander Lvovsky, Holger Müller, Sergei Orlov, Thorsten Petelski, Oliver Pradl, Pinno Ruosso, Anabel Schmidt, Harald Schnitzler, Jürgen Schoser, Rafael Storz, Surya P. Tewari, Daniel Ursescu and all mentioned above for making life more fun on P8.

I thank Stefan Eggert, our electronics engineer, Stefan Hahn, our mechanics technician and the people from the mechanical workshop, especially Mr. Beschle. Without their support I could not have built my OPOs.

I thank all companies that manufactured the equipment I used especially PMS GmbH who polished the crystals and Layertec GmbH and Tafelmeier GmbH who did the broadband mirror and crystal coatings, often at the limit of feasibility.

This work was financially supported by the German Ministry of Science and Research (BMBF), the German Israeli Foundation (GIF), and the Optikzentrum Konstanz (OZK).

Last but not least I want to thank my mother Inge Strößner who always supported me in my way through life whatever I was doing. Without her help and understanding I would very likely be a different person today.

About different colors

How many colors do you need to call something multicolored? Our OPO produces red, orange, yellow, and green. Some people ask for blue and purple but do not really recognize the near and mid infrared because they cannot see it. If you divide the 440 THz tuning range of the OPO by the 20 kHz linewidth you end up with 20 billion different colors, about as many as your computer hard disk has bytes. To look at each of them for 0.1 seconds takes more than 60 years. To transmit each of them through an optical fiber at the speed of a modern high speed optical telecommunication line takes half a second. So if a TV set, which has three discrete colors is multicolored, than our OPO definitely is.

Bibliography

[1] K. Schneider, P. Kramper, S. Schiller, J. Mlynek, Toward an optical synthesizer: a single-frequency parametric oscillator using periodically poled LiNbO3, Opt. Lett. **22**, 1293 (1997)

[2] F.G. Colville, M.H. Dunn, M. Ebrahimzadeh, Continuous-wave, singly resonant, intracavity parametric oscillator, Opt. Lett. **22**, 75 (1997)

[3] D. Chen, D. Hinkley, J. Pyo, J. Swenson, R. Fields, Single-frequency low-threshold continuous-wave 3-μm periodically poled lithium niobate optical parametric oscillator, J. Opt. Soc. Am. B **15**, 1693 (1998).

[4] P.E. Powers, T.J. Kulp, and S.E. Bisson, Continuous tuning of a continuous-wave periodically poled lithium niobate optical parametric oscillator by use of a fan-out grating design, Opt. Lett. **23**, 159 (1998)

[5] M. E. Klein, D.-H. Lee, J.-P. Meyn, K.-J. Boller, R. Wallenstein, Singly resonant continuous-wave optical parametric oscillator pumped by a diode laser, Opt. Lett. **24**, 1142 (1999)

[6] K. Schneider, P. Kramper, O. Mor, S. Schiller, and J. Mlynek, Continuous-wave, single-frequency parametric oscillator for the 1.45-4 μm spectral range using PPLN, in *Advanced Solid State Lasers*, W.R. Bosenberg, and M.M. Fejer, eds. OSA Trends in Optics and Photonics Series, Vol. **19**, 256 (1998)

[7] F. Kühnemann, K. Schneider, A. Hecker, A. A. E. Martis, W. Urban, S. Schiller, J. Mlynek, Photoacoustic trace gas detection with a single-frequency continuous-wave optical parametric oscillator, Appl. Phys. B **66**, 741 (1998)

[8] M.E. Klein, C.K. Laue, D.-H. Lee, K.-J. Boller, R. Wallenstein, Diode-pumped singly resonant continuous-wave optical parametric oscillator with wide continuous tuning of the near-infrared idler wave, Opt. Lett. **25**, 490 (2000)

[9] E. V. Kovalchuk, D. Dekorsy, A. I. Lvovsky, C. Braxmaier, A. Peters, J. Mlynek, S. Schiller, High-resolution Doppler-free molecular spectroscopy using a continuous-wave optical parametric oscillator, submitted to Opt. Lett.

[10] F.G. Colville, A.J. Henderson, M.J. Padgett, J. Zhang, M.H. Dunn, Continuous-wave parametric oscillation in Lithium triborate, Opt. Lett. **18**, 205 (1993)

[11] K. Schneider, S. Schiller, Narrow-linewidth, pump-enhanced singly-resonant parametric oscillator pumped at 532 nm, Appl. Phys. B **65**, 775 (1997)

[12] M. Tsunekane, S. Kimura, N. Taguchi, H. Inaba, Broadband tuning of a continuous-wave doubly resonant, lithium triborate optical parametric oscillator from 791 to 1620 nm, Appl. Opt. **37**, 6459 (1998)

[13] T. Petelski, R. Conroy, K. Bencheikh, J. Mlynek, S. Schiller, All-solid-state, tunable, single-frequency source of yellow light for high-resolution spectroscopy, Opt. Lett., **26**, 1013 (2001)

[14] W.J. Kozlovsky, C.D. Nabors, R.C. Eckardt, R.L. Byer, Monolithic MgO:$LiNbO_3$ doubly resonant optical parametric oscillator pumped by a frequency-doubled diode-laser-pumped Nd:YAG laser Opt. Lett. **14**, 66 (1989)

[15] D.C. Gerstenberger, R.C. Wallace, Continuous-wave operation of a doubly resonant lithium niobate optical parametric oscillator system tunable from 966 to 1185 nm, J. Opt. Soc. Am. B **10**, 1681 (1993)

[16] S.T. Yang, R.C. Eckardt, R.L. Byer, 1.9-W cw ring-cavity KTP singly resonant optical parametric oscillator, Opt. Lett. **19**, 475 (1994)

[17] G. Robertson, M.J. Padgett, M.H. Dunn, Continuous-wave singly resonant pump-enhanced type II LiB_3O_5 optical parametric oscillator, Opt. Lett. **19**, 1735 (1994)

[18] M. Scheidt, B. Beier, R. Knappe, K.J. Boller, R. Wallenstein, Diode-laser-pumped continuous-wave KTP optical parametric oscillator, J. Opt. Soc. Am. B **12**, 2087 (1995)

[19] R.G. Batchko, D.R. Weise, T. Plettner, G.D. Miller, M.M. Fejer, R.L. Byer, Continuous-wave 532-nm-pumped singly resonant optical parametric oscillator based on periodically poled lithium niobate, Opt. Lett. **23**, 168 (1998)

[20] A. Yariv, P. Yeh, *Optical Waves in Crystals*, Wiley, New York, 1984, pp. 504 – 548

[21] M.M. Fejer, G.A. Magel, D.H. Jundt, R.L. Byer, Quasi-Phase-Matched Second Harmonic Generation: Tuning and Tolerances, IEEE J. Quantum. Electron. **28**, 2631 (1992)

[22] S. Schiller, K. Schneider, J. Mlynek, Theory of an optical parametric oscillator with resonant pump and signal, J. Opt. Soc. Am. B, **16**, 1512 (1999)

[23] J.A. Armstrong, N. Bloembergen, J. Ducuing, P.S. Pershan, Interactions between light waves in a nonlinear dielectric, Phys. Rev., **127**, 1918 (1962)

[24] P.A. Franken, J.F. Ward, Optical harmonics and nonlinear phenomena, Rev. Mod. Phys., **35**, 1313 (1964)

[25] M. Yamada, N. Nada, M. Saitoh, K. Watanabe, First-order quasi-phase matched $LiNbO_3$ waveguide periodically poled by applying an external field for efficient blue second harmonic generation, Appl. Phys. Lett. **62**, 435 (1993)

[26] W.K. Burns, W. McElhanon, L. Goldberg, Second harmonic generation in field poled, quasi-phase matched, bulk $LiNbO_3$, IEEE Photon. Technol. Lett. **6**, 252 (1994)

[27] J. Webjörn, V, Pruneri, P.St.J. Russel, J.R.M. Barr, D.C. Hanna, Quasi-phase matched blue light generation in bulk lithium niobate, electrically poled via periodic liquid electrodes, Electron. Lett. **30**, 894 (1994)

[28] L.E. Myers, R.C. Eckhard, M.M. Fejer, R.L. Byer, E.R. Bosenberg, J.W. Pierce, Quasi-phase-matched optical parametric oscillators in bulk periodically poled $LiNbO_3$ J. Opt. Soc. Am. B **12**, 2102 (1995)

[29] Abschlußbericht, Verbundprojekt: Grundlagenuntersuchungenzur optischen Frequenzkonversion in Materialien mit Quasi-Phasenanpassung (QPM), Fachbereich Physik, Universit"at Kaiserslautern

[30] S.N. Zhu, Y.Y. Zhu, Z.Y. Zhang, H. Shu, H.F. Wang, J.F. Hong, C.Z. Ge, N.B. Ming, $LiTaO_3$ crystal periodically poled by applying an external pulsed field, J. Appl. Phys. **77**, 5481 (1995)

[31] J.-P. Meyn, M.M. Fejer, Tunable ultraviolet radiation by second-harmonic generation in periodically poled lithium tantalate, Opt. Lett. **22**, 1214 (1997)

[32] J.-P. Meyn, M.E. Klein, D. Woll, R. Wallenstein, D. Rytz, Periodically poled potassium niobate for second-harmonic generation at 463 nm, Opt. Lett. **24**, 1154 (1999)

[33] Q. Chen, W.P. Risk, Periodic poling of $KTiOPO_4$ using an applied electric field, Electron. Lett. **30**, 1516 (1994)

[34] H. Karlson, F. Laurell, P. Henrikson, G. Arvidsson, Electron. Lett. **32**, 556 (1996)

[35] G. Rosenman, A. Skliar, D. Eger, M. Oron, M. Katz, Low temperature periodic electrical poling of flux-grown $KTiOPO_4$ and isomorphic crystals, Appl. Phys. Lett., **73**, 3650 (1998)

[36] P. Urenski, G. Rosenman, Pyroelectric effect in $KTiOPO_4$ and family crystals with monodomain and domain patterned structures, J. Phys. D, **33**, 2069 (2000)

[37] C.B. Ebert, L.A. Eyres, M.M. Fejer, J.S. Harris, Jr., MBE growth of antiphase GaAs films using GaAs/Ge/GaAs heteroepitaxy, J. Cryst. Growth **201/201**, 187 (1999)

[38] L.A. Eyres, P.J. Tourreau, T.J. Pinguet, C.B. Ebert, J.S. Harris, M.M. Fejer, Quasi-phase-matched frequency conversion in thick all-epitaxial, orientation-patterned GaAs films, in Advanced Solid State Lasers, Trends in Optics and Photonics, T. Li, **34** OSA Proceedings Series, pp. 258-261

[39] S.C. Buchter, T.Y. Fan, V. Liberman, J.J. Zayhowski, M. Rothschild, A. Cassanho, H.P. Jenssen, E. Manson, J.H. Burnett, Periodically poled $BaMgF_4$ for ultraviolet frequency generation, Post deadline talk CPD23 on CLEO 2001

[40] G.D. Boyd, D.A. Kleinman, Parametric interaction of focused beams, J. Appl. Phys. **39**, 3597 (1968)

[41] A. Douillet, J.J. Zondy, A. Yelisseyev, S. Lobanov, L. Isaenko, Stability and frequency tuning of thermally loaded continuous-wave $AgGaS_2$ optical parametric oscillators, J. Opt. Soc. Am. B, **16**, 1481 (1999)

[42] D.H. Jundt, Temperature-dependent Sellmeier equation for the index of refraction, n_e, in congruent lithium niobate, Opt. Lett. **22**, 1553 (1997)

[43] V.G. Dimitriev, G.G. Gurzadyan, D.N. Nikogosyan, *Handbook of Nonlinear Optical Crystals*, 2nd ed. (Springer-Verlag, Berlin, 1997), pp. 107 – 125
Sellmeier equation for PPLN equivalent to
G.J. Edwards, M. Lawrence, A temperature-dependent dispersion equation for congruently grown lithium niobate, Opt. Quant. Electron. **16**, 373 (1984)

[44] W. Wiechmann, S. Kubota, T. Fukui, H. Masuda, Refractive-index temperature derivatives of potassium titanyl phosphate, Opt. Lett. **18**, 1208 (1993)

[45] J.D. Bierlein, H. Vanherzeele, Potassium titanyl phosphate: properties and new applications, J. Opt. Soc. Am. B **6**, 622 (1989)

[46] R.W.P. Drever, J.L. Hall, F.V. Kowalski, J. Hough, G.M. Ford, A.J. Munley, H. Ward, Laser Phase and Frequency Stabilisation Using an Optical Resonator, Appl. Phys. B **31**, 97 (1983)

[47] K. Fradkin, A. Arie, A. Skliar, G. Rosenman, Tunable midinfrared source by difference frequency generation in bulk periodically poled $KTiOPO_4$, Appl. Phys. Lett. **74**, 914 (1999);
K. Fradkin, A. Arie, A. Skliar, G. Rosenman, Erratum: “Tunable midinfrared . . . ”, Appl. Phys. Lett. **74**, 2723 (1999)

[48] K. Kato, Temperature insensitive SHG at 0.5321 μm in KTP, IEEE J. Quant. El. **28**, 1974 (1992)

[49] B. Boulanger, J.P. Feve, Y. Guillien, Thermo-optical effect and saturation of nonlinear absorption induced by gray tracking in a 532-nm-pumped KTP optical parametric oscillator, Opt. Lett. 25, 484 (2000)

[50] A. Fischer, private communication, July 2001

[51] J.C. Jacco, D.R. Rockafellow, E.E. Teppo, Bulk-darkening threshold of flux-grown $KTiOPO_4$ Opt. Lett. **16**, 1307 (1991)

[52] R.G. Batchko, G.D. Miller, A. Alexandrovski, M.M. Fejer, R.L. Byer, Limitations of high power visible wavelength periodically poled lithium niobate devices due to green induced infrared absorption and thermal lensing, talk CTuD6 on CLEO 1998

[53] A. Arie, G. Rosenman, V. Mahal, S. Skliar, M. Oron, M. Katz, D. Eger, Green and ultraviolet quasi-phase-matched second harmonic generation in bulk periodically-poled $KTiOPO_4$ Opt. Comm. **142**, 265 (1997)

[54] J.K. Tyminski, Photorefractive damage in KTP used as second-harmonic generator, J. Appl. Phys. **70**, 5570 (1991)

[55] B. Boulanger, M.M. Fejer, B. Blachmann, P.F. Bordui, Study of $KTiOPO_4$ gray-tracking at 1064, 532, and 355 nm, Appl Phys Lett **65**, 2401 (1994)

[56] R. Al-Tahtamouni, K. Bencheikh, R. Storz, K. Schneider, M. Lang, J. Mlynek, S. Schiller, Long term stable operation and frequency stabilization of a doubly resonant parametric oscillator, Appl. Phys. B **66**, 733 (1998)

[57] B. Scherrer, I. Ribet, A. Godard, E. Rosencher, M. Lefebvre, Dual-cavity doubly resonant optical parametric oscillators: demonstration of pulsed single-mode operation, J. Opt. Soc. Am. B, **17**, 1716 (2000)

[58] T. Hatanaka, K. Nakamura, T. Taniuchi, H. Ito, Y. Furukawa, K. Kitamura, Quasi-phase-matched optical parametric oscillation with periodically poled stoichiometric $LiTaO_3$, Opt. Lett. **25**, 651 (2000)

[59] K. Kitamura, S. Takekawa, M. Nakamura, Y. Furukawa, A. Alexandrovski, M.M. Fejer, Optical damage and light-induced absorption in near stoichiometric $LiTaO_3$ crystal, talk CTuI2 on CLEO (2000)

[60] C. Braxmeier, Fundamentale Tests der Physik mit ultrastabilen optischen Oszillatoren, Dissertation, University of Konstanz (2001)

[61] U. Strößner, A. Peters, J. Mlynek, S. Schiller, J.-P. Meyn, R. Wallenstein, Single-frequency continuous-wave radiation from 0.77 to 1.73 μm generated by a green-pumped optical parametric oscillator with periodically poled $LiTaO_3$, Opt. Lett. **24**, 1602 (1999)

[62] K. Schneider, S. Schiller, J. Mlynek, M. Bode, I. Freitag, 1.1 W cw single-frequency 532-nm radiation by second-harmonic generation of a miniature Nd:YAG ring laser, Opt. Lett. **21**, 1999 (1996)

[63] H. Karlsson and F. Laurell, Appl. Phys. Lett. **71**, 3474 (1997)

[64] D.R. Weise, U. Strößner, A. Peters, J. Mlynek, S. Schiller, A. Arie, A. Skliar, G. Rosenman, Continuous-wave 532-nm-pumped singly resonant optical parametric oscillator with periodically poled $KTiOPO_4$, Opt. Comm. **184**, 329 (2000)

[65] A. Arie, G. Rosenman, A. Korenfeld, A. Skliar, M. Oron, M. Katz, D. Eger, Efficient resonant frequency doubling of a cw Nd:YAG laser in bulk periodically poled $KTiOPO_4$, Opt. Lett. **23**, 28 (1998)

[66] I. Juwiler, A. Arie, A. Skliar, and G. Rosenman, Efficient quasi-phase-matched frequency doubling with phase compensation by a wedged crystal in a standing-wave external cavity, Opt. Lett. **24**, 1236 (1999)

[67] A. Garashi, A. Arie, A. Skliar, and G. Rosenman, Continuous-wave optical parametric oscillator based on periodically poled $KTiOPO_4$, Opt. Lett. **23**, 1739 (1998)

[68] M. Ebrahimzadeh, G.A. Turnbull, T.J. Edwards, D.J.M. Stothard, I.D. Lindsday, M.H. Dunn, Intracavity continuous-wave singly resonant optical parametric oscillators, J. Opt. Soc. Am. **B 16**, 1499 (1999)

[69] G.M. Gibson, M. Ebrahimzadeh, M.J. Padgett and M.H. Dunn, Continuous-wave optical parametric oscillator based on periodically poled $KTiOPO_4$ and its application to spectroscopy, Opt. Lett. **24**, 397 (1999)

[70] T.J. Edwards, G.A. Turnbull, M.H. Dunn, M. Ebrahimzadeh, Continuous-wave, singly-resonant, optical parametric oscillator based on periodically poled $KTiOPO_4$, Opt. Express. **6**, 58 (2000)

[71] J. Hellström, V. Pasiskevicius, F. Laurell, H. Karlsson, Efficient nanosecond optical parametric oscillators based on periodically poled KTP emitting in the 1.8 - 2.5 μm spectral region, Opt. Lett. **24**, 1233 (1999)

[72] T.Y. Fan, C.E. Huang, B.Q. Hu, R.C. Eckardt, Y.X. Fan, R.L. Byer, R.S. Feigelson, Second harmonic generation and accurate index of refraction measurements in flux-grown $KTiOPO_4$, Appl. Opt. **26**, 2390 (1987)

[73] B. Willke, N. Uehara, E.K. Gustafson, R.L. Byer, P.J. King, S.U. Seel, J.R.L. Savage, Spatial and temporal filtering of a 10-W Nd:YAG laser with a Fabry-Perot ring-cavity premode cleaner, Opt. Lett. **23**, 1704 (1998)

[74] D.R. Weise, Aufbau und effiziente Frequenzkonversion eines schmalbandigen Hochleistungs-Dauerstrich-Lasers, Diploma Thesis, University of Konstanz (1999)

[75] L. Myers, Laser Frequency Conversion with Periodically Poled Materials, invited talk QFD1 on CLEO-Europe (2000)

[76] D.D. Miller, R.G. Batchko, W.M. Tulloch, D.R. Weise, M.M. Fejer, R.L. Byer, 42 % efficient single-pass cw second harmonic generation in periodically poled lithium niobate, Opt. Lett. **22**, 1834 (1997)

[77] A. Hecker, C. Braxmaier, U. Strößner, M. Havenith, S. Schiller, A. Peters, High resolution Doppler-free spectroscopy of molecular iodine using a continuous wave optical parametric oscillator, in preparation for Physical Review A